Structural and Functional Studies of

Sensor Kinase RetS from *Pseudomonas aeruginosa*

and

Peptidoglycan Hydrolase SleB from *Bacillus anthracis*

Xing Jing

Dissertation submitted to the faculty of the Virginia Polytechnic Institute and State University in partial fulfillment of the requirements for the degree of

Doctor of Philosophy
In
Biological Sciences

Florian D. Schubot, Committee Chair
David R. Bevan
Daniel G. Capelluto
Zhaomin Yang

April 30, 2013

Blacksburg, Virginia

Keywords (PartI): *Pseudomonas aeruginosa,* biofilm formation, EPS, two-component systems, RetS, periplasmic sensory domain, GacS, dimer, phosphatase
Keywords (PartII): SleB, CwlJ, *Bacillus anthracis*, spore, germination, lytic transglycosylase, muramic-δ-lactam, peptidoglycan, cortex peptidoglycan

Structural and Functional Studies of Sensor Kinase RetS from *Pseudomonas aeruginosa* and Peptidoglycan Hydrolase SleB from *Bacillus anthracis*

Xing Jing

Abstract

Part I: The opportunistic human pathogen *Pseudomonas aeruginosa* causes both acute and chronic infections in predisposed individuals. Acute infections require a functional Type Three Secretion System (TTSS), which mediates the translocation of select cytotoxins into host cells. Chronic infections, the leading cause of death among cystic fibrosis patients, are characterized by drug-resistant biofilms formation. To regulate gene expression, *Pseudomonas aeruginosa* utilizes two-component regulatory systems (TCS). Specifically, we focus on the TCS signaling kinase RetS, which is a critical repressor of biofilm formation. The signaling mechanism of RetS is unusual. According to recent findings and one hypothesis, RetS employs a novel signaling mechanism involving direct binding to the signaling kinase GacS, thereby repressing the GacS-induced biofilm formation. RetS is believed to be regulated by the interaction of its periplasmic sensory domain ($RetS_{peri}$) with an unknown ligand. As such, $RetS_{peri}$ is a potential drug target. We hypothesized that ligand-binding shifts the equilibrium between the formation of a RetS homo-dimer and the RetS-GacS complex by tuning the homo-dimerization of the $RetS_{peri}$. While the molecular signal that regulates RetS is unknown, our structural studies of the sensory domain suggest that this ligand is a carbohydrate-based moiety. Unchanged biofilm-EPS production phenotype of $RetS_{peri}$ ligand binding site mutants indicates that the natural ligand is

not from *Pseudomonas aeruginosa.*

Additional experiments unambiguously determined that the sensory domain forms a stable homodimer. Adding to the complexity of the system, we have identified two possible dimer interfaces in our *in vitro* assays. However, inconsistent with the current model, elimination of $RetS_{peri}$ results in a slightly increased biofilm EPS production phenotype. Therefore, with the previous demonstration that RetS is able to dephosphorylate GacS, we propose an alternative hypothesis: the RetS kinase domain serves as a phosphatase for phosphorylated GacS; this phosphatase activity is tuned by signaling sensing on $RetS_{peri}$. Finally, to provide an important piece of information for understanding the molecular basis of RetS-GacS signaling, we have developed a crystallization-based structure determination strategy in order to reveal the precise RetS-GacS interaction pattern.

Part II: *Bacillus anthracis* produces metabolically inactive spores. Germination of these spores requires germination-specific lytic enzymes (GSLEs) that degrade the unique cortex peptidoglycan to permit resumption of metabolic activity and outgrowth. We report the first crystal structure of the catalytic domain of a GSLE, SleB. The structure revealed a transglycosylase fold with unique active site topology and permitted identification of the catalytic glutamate residue. Moreover, the structure provided insights into the molecular basis for the specificity of the enzyme for muramic-δ-lactam-containing cortex peptidoglycan. The protein also contains a metal-binding site that is positioned directly at the entrance of the substrate-binding cleft.

Acknowledgements

Foremost I want to thank my advisor Dr. Florian Schubot. You brought me into your lab and the protein-structure biology field with all exciting projects. You put a lot of energy and time in me which made me able to go further in research in the future. You have taught me not only about science but also about being ambitious and being precise. I benefited a lot from the communication skills and logical thinking that you passed on to me. Due to your mentoring during these five years, I have improved myself in many aspects.

I would also like to thank the other three members in my committee: Dr. David R. Bevan, Dr. Daniel G. Capelluto and Dr. Zhaomin Yang. Your suggestions have been invaluable to my research.

I really enjoyed Dr. David R. Bevan's class for protein structure-function study. Thank you for your recommendation letters for my application of 2010 National Summer School.

I thank Dr. Daniel G. Capelluto for your advice when I was applying to Virginia Tech.

I am grateful for Dr. Zhaomin Yang who let me join his pioneering research project. Your deep and precise understanding of signal transduction has been inspiring to me.

I also want to thank Dr. David Popham who provided me the opportunity to join the SleB project.

I also like to express appreciation for Dr. Birgit Scharf's kindness to me. Since you came to our program, I have obtained a lot of advice from you. You invited me to your thanksgiving party every year. You are a very kind person and friend.

To the Schubot lab, I thank all my labmates who I have worked with. I thank Robert Cory Bernhards, Yi Xiao, Jordan Mancl, Manisha Shrestha and all undergraduate students. I appreciate Jordan Mancl's editorial support to this dissertation.

I also want to thank my lovely girlfriend Dr. Ye Liu. You have brought a lot of happiness into my life.

To people in Microbiology program at Life Science I building, thank you all for constructing the friendly environment. Thank everybody who allowed me to borrow your reagents or to use your instruments.

Table of content

List of Figures

Part I

Chapter One

Chapter Two

Chapter Three

Chapter Four

List of Tables

Part I

Signaling Role of the Sensor Kinase RetS in Biofilm formation

Regulation of *Pseudomonas aeruginosa*

Chapter One

Introduction and Literature Review

Pseudomonas aeruginosa virulence mechanisms

Pseudomonas aeruginosa, the type species of the genus *Pseudomonas* (4), is an aerobic Gram-negative bacterium (87). Ubiquitous in nature, *P. aeruginosa* can be found in various environments such as soil, water, skin-flora and most man-made environments throughout the world, largely due to the fact that it is able to utilize a wide range of organic materials for nutrition (4). Because it grows on the surfaces of most materials, this human pathogen is found in many medical institutions (8, 56).

In plants, animals and humans, *P. aeruginosa* causes a broad range of opportunistic infections (44, 82, 89, 106). In humans, *P. aeruginosa* may cause chronic as well as acute infections in burn victims, and other immunocompromised patients (64). It has been estimated that the lungs of more than 80% of Cystic Fibrosis (CF) patients are infected by *Pseudomonas aeruginosa* (108). Therefore there is a strong interest in looking for effective therapies for this pathogen. The major challenge *Pseudomonas aeruginosa* brings to the medical community is its high antibiotic-resistance (64). Recent studies have shown that the environmental adaptability of *Pseudomonas aeruginosa* may be attributed to the complex regulation of gene expression, which controls the switch of specific virulence effector expression between chronic and acute infections (23, 39).

Pseudomonas aeruginosa has a relatively large genome (6-7Mb) encoding around 6000 (predicted) genes, among which, 5021 are conserved across at least five of the to date analyzed genomes with a minimum sequence identity of 70% (67). The pathogenesis of acute infections requires the expression of genes encoding the type III secretion system (TTSS), along with other effector proteins (115). The TTSS, a special toxin-translocating machinery found in a number of Gram-negative bacteria, is composed of a needle-like protein complex, which forms a channel to transport effector proteins into host cells. Four effectors have been identified for *Pseudomonas aeruginosa*: ExoS, ExoT, ExoU and ExoY (18, 113, 115). Responsible for virulence,

these toxins perform a wide range of functions, including inhibiting host cell phagocytosis, tuning of host inflammatory responses, and host cell killing (113). A three-protein set is required for translocation: hydrophobic proteins PopB and PopD act as translocators, inserting into host cells; while the hydrophilic protein PcrV, forms a complex at the end of the needle, which acts as a platform for the two translocators (16, 71). The whole set of machinery is constructed and activated by interaction with host eukaryotic cells and can also be induced *in vitro* under low-calcium conditions (24, 40).

Biofilm formation by *P. aeruginosa* is a serious problem for medical care in industrialized societies. The increased antimicrobial resistance of *P. aeruginosa* biofilms underlies the difficulties in treating of many chronic infections (81). *P. aeruginosa* biofilms may form on abiotic surfaces, such as catheters but are also the underlying cause of the chronic infections in Cystic Fibrosis patients' lungs (17). It has been shown that long term infections consist of a mixture of biofilm and planktonic *Pseudomonas aeruginosa* cells coexisting together (29). Biofilm communities are held together by a protective extracellular polymeric matrix. It has been demonstrated that biofilm formation involves the coordination of several sequential processes: beginning with surface attachment by planktonic bacteria followed by the formation of microcolonies and subsequent development of differentiated structures in which individual bacteria as well as the entire community are surrounded by exopolysaccharides (22, 33, 74, 76). Biofilms enable bacteria to be much more resistant to antibiotics compared to their planktonic counterparts. Many substances exist in the biofilm matrix, such as DNA, polysaccharides, cell debris such as flagella and pili, proteins, membrane vesicles (MV) and phage, which serves as a protective 'coating' for biofilm bacteria (43, 66). Current studies have shown that MVs are likely important in disease pathogenesis, possibly responsible for the antibiotic resistance of a biofilm. Different proteins are packaged into MVs to make it

like a ‘decoy’ or ‘sponge’ that would decrease the levels of harmful agents such as antibiotics and immune factors that penetrate the biofilm (90).

The sputum of CF patients, especially those with chronic infections, is rich in biofilm and planktonic *Pseudomonas aeruginosa* cells (34, 111). However, it is not a good source of this pathogen for pathobiology studies due to patients’ drug use and patient-to-patient variability (58, 93, 95). A variety of man-made media have been developed to simulate the CF lung environment. Most recently, an artificial CF sputum medium has been developed by using mucin, albumin and DNA, instead of CF sputum, to study the global transcription profile of *Pseudomonas aeruginosa*. Their results show that by using this special medium, 23 TTSS genes and a few anaerobic respiration genes were up-regulated in early exponential growth phase suggesting augmented virulence factor expression and priming biofilm formation. Under stationary growth phase, however, TTSS genes are down-regulated in this medium (27).

Two-Component Systems

There are many ways for bacteria to regulate virulence factor expression. The most commonly used signal transduction pathways are two-component sensor–regulator systems (TCSs) (20, 68). TCSs allow bacteria to modulate gene expression in response to environmental stimuli (38, 97). Most bacterial species contain dozens of TCSs, which regulate wide range of life activities such as fundamental metabolism and motility (28). TCSs are the most common multistep signaling pathways found in nature. Absent in mammalian cells, these systems are appealing targets for the development of antimicrobial agents against pathogens (28).

The conserved core structure of TCSs is composed of a membrane-associated sensor histidine kinase (HK) protein domain (the “sensor”) as well as a cognate receiver domain (the “response regulator”-RR) whose function is regulated by a phosphotransfer reaction from its cognate histidine kinase. The HK is responsible for

receiving the input environmental signal to regulate the signaling pathway followed by auto-phosphorylation at a conserved histidine residue. The RR then receives the phosphoryl group at a conserved Aspartate residue and subsequently induces a conformational change, which results in effective cellular responses (figure 1.1a) (79, 96).

The distinct trait of HKs phosphorylation is the formation of phosphoramidates rather than the phosphoesters formed in conventional Ser/Thr/Tyr kinases. The N-P bond in phosphor-Histidine between the phosphoryl group and the imidazole ring in Histidine is relatively unstable, and is thus more suitable as a phosphotransfer intermediate (28, 98). Like other signaling proteins, a HK has an input domain linked to a conserved catalytic kinase core in the cytoplasm composed of two domains: a dimeric Histidine phosphotransfer domain, which receives the phosphoryl group from ATP once it is hydrolyzed by a C-terminal ATPase domain (21). There are several conserved contiguous sequence motifs in the kinase cores of HKs. Based on their specific characteristic sequences they are named H, N, G1, F and G2 boxes (1, 79, 96). Most HKs also have phosphatase activity, which is often overlooked in phosphorylation assays. For regulatory purposes, the phosphorylation level of the RR is adjusted by tuning the balance between kinase and phosphatase activities via cellular signal sensing. This signal input often requires a distinct sensory domain that is linked to the N-terminus of the HK domain (2, 28). By virtue of having great sequence variability within the sensory domain, HKs are able to sense a wide range of environmental stimuli. The auto-phosphorylation of a HK domain occurs in “trans” mode, which requires homo-dimerization, however, this dimerization does not affect signal sensing induced HK signaling function (75, 78, 99, 100, 109, 114).

The RR is named based on its prototypical domain architecture: a phosphoryl receiver domain linked to a variable effecter (response) domain (28, 97). RR phosphorylation by HK at the Asp residue of the receiver generates a high-energy

acyl phosphate group, which causes a conformational change in the receiver domain (5, 48, 101). This change in turn shifts the equilibrium between activity on and off modes in the effecter domain. However, the lifetime of the phosphorylation state of Asp could vary from seconds to hours. The intrinsic phosphatase activity of many RRs shortens the lifetime of the aspartate site phosphorylation. But there are also a few cases that RRs stabilize the phospho-Asp (28, 47). The functions of activated RRs are usually associated with modulations of either DNA binding affinities of the RR (63% of the time) or enzymatic activities (59, 91, 92, 102). The presence of multiple homologous HK/RR pairs raises the possibility of cross-talk between structurally similar HK and receiver domains. Although the unwanted cross phosphorylation has been observed, the specific cognate HK/RR interactions are still strongly preferred kinetically (61, 94).

Besides the typical two-component organization, some multistep phosphor-relay systems possess and require individual histidine containing phosphotransfer proteins that are responsible for receiving phosphoryl group from first-step RRs and phosphorylating target aspartate residues in downstream RRs to achieve a three-step His-Asp-His-Asp phosphor-relay mechanism (figure 1.1b) (28, 97). This modular organization has been extensively investigated (54). Multistep phosphotransfer reactions can also take place within a single HK. These kinases contain additional phosphotransfer modules referred to as the R1 receiver and the HPt (histidine phosphotransfer) phosphotransfer domains that are attached to the C-terminal side of the kinase domain. These HKs are called hybrid kinases, representing about 25% of HKs (31).

In summary, 1) TCS signaling follows a highly conserved mechanism. 2) HK and RR interactions are highly conserved they are also highly specific, therefore unwanted cross-talk is rarely observed. 3) Irrespective of whether a TCS or phospho-relay system is employed, the input signal is transmitted via phosphate-transfer reactions

which ulitmately modulate gene expression by regulating the DNA binding affinity of a protein or altering its enzymatic activity.

Biofilm-a highly drug- resistant matrix

CF patients are frequently colonized by bacterial biofilms within a few years of their birth and the colonies can stay and survive throughout patients' lifetimes. The ability of *P. aeruginosa* to sustain decades-long chronic infections is thought to depend upon the regulated developmental process of biofilm formation (81). The interaction of *P. aeruginosa* with host cells can be described as a two-stage process: initially, colonizing bacteria regulate expression to cause an acute infection, while the subsequent persistent stage relies on the expression of adaptive factors that promote biofilm formation (31). In acute infection stage, *P. aeruginosa* is vulnerable to antibiotics. However, after successful colonization, this pathogen protects itself from the environment attack by biofilm formation. This highly drug- resistant matrix makes the clinical treatment for *P. aeruginosa* a challenge (19). The extracellular polysaccharides are the key attributes to the biofilm matrix and crucial for the architecture and antibiotic resistance of bacteria in biofilms (65). Different types of polysaccharides are synthesized to form biofilms depending on the environment. Nonmucoid *P. aeruginosa* strains initially colonize CF lungs, but over time, mucoid variants emerge and become predominant (33). Mucoid strains produce a capsular polysaccharide virulence factor called alginate, which is an acetylated polymer composed of nonrepetitive monomers of β-1,4 linked L-guluronic and D-mannuronic acid (33, 65). During the past decade, however, most *P. aeruginosa* strains being studied, such as PAO1 and PA14, are nonmucoid (88). These strains do not produce significant amount of alginate. Moreover, disruption of the alginate genes does not affect biofilm formation in PAO1 and PA14. However, the biofilms produced by these nonnucoid strains are still suggested to contain polysaccharide-material (112).

The exopolysaccharide synthesis locus (*psl*) and pellicle locus (*pel*)

Targeting nonmucoid *P. aeruginosa* strains, several groups initiated studies of non-alginate polysaccharide expression and identified two gene loci, *psl* and *pel* (112). The *pel* (pellicle) locus is a seven-gene locus, found to be responsible for pellicle formation in PA14 by screening a PA14 transposon library for pellicle-deficient mutants. Mutations in the *pel* locus do not affect PA14 biofilm initiation, however, the colony morphology is affected. Moreover, unlike wild type cells, *pel* mutants are not able to bind Congo red, which detects neutral polysaccharides (25). So far, the structure of *pel*-synthesized exopolysaccharide (called PEL) has not been chemically characterized (26). It has been demonstrated that PEL is a crucial component to maintaining cell-cell interactions in a PA14 biofilm, serving as a primary structural scaffold for the community. However, this function is strain specific because PEL is not required for biofilm cell attachment and development in a PAO1 strain (103). Instead, the *psl*-synthesized exopolysaccharide (PSL) has been proven to be the primary structural polysaccharide for biofilm maturity. 15 enzymes (PslA to PslO), encoded by the *psl* operon, are responsible for PSL biosynthesis. Mutational analysis in biofilm attachment assays indicated that PslH and PslI are two key enzymes (galactosyltransferase and mannosyltransferase respectively) for PSL biosynthesis. Deletion of either pslH or pslI also causes reduced biofilm formation (26, 46, 65). The Wozniak group has shown in their initial study that the exopolysaccharide PSL is mainly composed of galactose and mannose, as well as glucose and traces of rhamnose, xylose and GlcNAc (65). Later on, a more detailed biochemical analysis by the same group has demonstrated that PSL released from the cell is a polysaccharide with a pentasaccharide as the repeating unit, which contains D-mannose, D-glucose and L-rhamnose. Size-exclusion gel filtration of the isolated sample identified three fractions with different molecular weight, representing different degrees of polymerization (14). More studies are ongoing to uncover the detailed structures and

functional roles of biofilm matrix exopolysaccharides.

Virulence mechanisms associated with chronic and acute *P. aeruginosa* infections are reciprocally regulated

In early colonized CF lungs, *P. aeruginosa* is fully motile and features predominant expression of the TTSS for toxin injection into human cells and repression of the innate immune response. The gene expression of TTSS thusly plays a crucial role in early colonization, however as the bacterium transitions to a biofilm-assisted chronic infection, the TTSS is shut down, while exopolysaccharide production is greatly up-regulated (104). Initially the inactivity of the TTSS in *P. aeruginosa* biofilms was thought to be the result of mutations in key genes TTSS genes. However, recent studies have uncovered regulatory mechanisms that actively facilitate the transitions between planktonic and biofilm lifestyles.

Before translocating the four effector toxins from *P. aeruginosa* into host cells, the TTSS apparatus has to be structured and maintained for functional purpose. However, since assembling and maintenance of this needle-like machinery is very energy consuming, the bacteria tightly regulate the biosynthesis of the TTSS (105). In *P. aeruginosa*, the expression of all TTSS genes is perhaps most prominently regulated by ExsA, an AraC/XylS-type transcriptional activator. ExsA controls 10 promoters responsible for expression of toxin effectors and chaperones, secretion and translocation apparatus and TTSS gene expression regulators, including itself. Deletion of the *exsA* gene causes the loss of TTSS function and inability to cause acute infection. Three additional proteins ExsD, ExsC and ExsE form a signaling cascade that ties up-regulation of TTSS gene expression to host cell contact (55). However, whether or not the ExsACDE cascade also plays a role in the transition between acute and chronic infection modes is not clear.

Of the many other mechanisms that either directly or indirectly affect TTSS the signaling kinase RetS appears to play a key role in facilitating this transition.

The role of TCS in gene regulation in *P. aeruginosa*

In *P. aeruginosa*, at least 64 TCSs, representing 8% of transcriptional regulators, are utilized for the gene expression regulation in order to meet the needs of adaptation to the environment. This is the largest TCS population that has ever been found in a sequenced microbe (30, 85). One of the most studied TCSs in *P. aeruginosa*, for example, is the PilS/PilR system. This system is responsible for controlling the production of Type IV pili and biofilm formation (49, 77). In contrast, GacS/GacA TCS negatively regulates *ptrA* gene that positively regulates biofilm formation. These two systems represent good examples for regulatory networks that simultaneously control target gene expression for biofilm formation versus TTSS, in an antagonistic manner. This important concept has inspired more and more studies on the gene expression switch between TTSS-assisted acute infection and exopolysaccharide related biofilm formation to assist chronic infection. In this review I will emphasize the RetS/LadS/GacS(A)/RsmZ/RsmA system, which is the best characterized signal transduction pathway that reciprocally regulates TTSS and biofilm formation in *P. aeruginosa.*

RsmZ/RsmA regulatory system

The GacA/RsmZ/RsmA pathway is a conserved signal transduction system controlling a variety of functions in *P. aeruginosa* (51). RsmA (repressor of secondary metabolites), the homologue of which is called CsrA in *E. coli*, is a posttranscriptional regulatory protein, which belongs to CsrA/RsmA protein family found in many bacterial organisms (6, 86). This small protein (7kD) regulates gene expression by binding target mRNA to modulate mRNA stability. It recognizes an exposed stem-loop structure which contains a conserved GGA tri-nucleotide motif in the 5' side of target mRNA leader sequences. This protein-RNA interaction prevents ribosome binding and gene translation and promotes mRNA degradation, because the GGA motif always overlaps the ribosome binding site (11). But it has to be mentioned

that positive posttranscriptional regulation by CsrA has also been found in *E. coli* (86).

In 2006, Mulcahy and O'Gara demonstrated that RsmA plays a crucial role in the interaction between *P. aeruginosa* and human airway epithelial cells by positively regulating the TTSS. Loss of *rsmA* causes a severe defect in production of proteins required for TTSS machinery assembly and key toxin effectors to be injected into host cells and reduces the expression of positive regulators of TTSS genes (72). Through microarray analysis, Burrows and O'Gara were able to identify additional target genes that are controlled by RsmA in *P. aeruginosa.* Of 5570 screened genes, the expression of 9% was altered by the *rsmA* mutation in a PAO1 strain. This result indicates RsmA is a global regulatory protein, at least in *P. aeruginosa* (13). In 2008, a further detailed study by the same group demonstrated that mutation of *rsmA* in *P. aeruginosa* causes a significant defect in initial colonization of a mouse model of acute pneumonia and reduces the mortality in mice with chronic infection with *P. aeruginosa.* On the other hand, the PAO1 *rsmA* mutant displays increased adhesion to plastics and glass and increased air-liquid interface biofilm formation *in vitro* (72). Furthermore, higher persistence of *rsmA* mutants compared to the wild type PAO1 strain in lungs of chronically infected mice indicated that loss of RsmA promotes the development of chronic infection (73). In 2010, the Parsek group took a further step toward understanding the role of RsmA in biofilm-related gene expression regulation in *P. aeruginosa.* Using *psl* mRNA, they identified a large untranslated sequence which binds to RsmA. They also demonstrated that RsmA is a translational repressor of *psl* because psl translation, but not transcription, is increased in an *rsmA* deletion mutant of *P. aeruginosa* (45).

The activity of CsrA/RsmA proteins is regulated by noncoding small regulatory RNAs, which represent the other component of the Rsm/Csr system. In bacteria, these noncoding regulatory RNA molecules, also known as small RNAs (sRNAs), are a key

component in regulatory networks for gene expression regulation (6, 86). Even though most sRNAs in microorganisms function by base-pairing with mRNAs of target genes, several studies have been targeting their function of antagonizing CsrA/RsmA proteins (13, 63, 72). This important participation of sRNAs in the regulatory network was initially discovered from RNA-CsrA complexes that were isolated during CsrA protein purification (63). All known cognate sRNAs contain multiple repeated CsrA/RsmA binding sites and are capable of sequestering CsrA/RsmA proteins (11). Thus, the RsmA and the small RNA RsmZ which binds to RsmA, in most cases, have opposite effects on the expression of RsmA target genes.

GacS/GacA two-component system

Another common feature of sRNAs is that their transcription is activated by a TCS signal transduction system upon sensing of an environmental signal. In *P. aeruginosa*, the transcription of two small noncoding RNAs, RsmY and RsmZ, which are antagonists of the RsmA protein, is regulated by the well-defined GacS/GacA system (12).

The sensor kinase GacS was first characterized in *Pseudomonas syringae* strain B728A and initially called LemA, an essential factor for lesion manifestation (41, 57). The response regulator GacA was first defined as a global activator of antibiotic and cyanide production in *Pseudomonas fluorescens* strain CHAO (62). They were proposed as a putative pair of cognate sensor kinase and response regulator based on the first genetic study in *Pseudomonas syringae* and supported by later studies for many other organisms (36. 84). The interaction between GacS and GacA was eventually confirmed by experimentally demonstrating the phosphotransfer between GacS homologue BarA and GacA homologue UvrY in *E. coli* strain K-12 (80). The domain architecture of the GacS is highly conserved in many microorganisms. Its N-terminus has two transmembrance segments that are separated by a variable periplasmic loop region. The poor sequence conservation of this loop might explain

why the identification of the GacS signal has been unsuccessful (36). Following the N-terminus, the cytoplasmic part of GacS possesses a HAMP (present in histidine kinases, adenylate cyclases, methyl accepting proteins and phosphatases) domain, which serves as an amphipathic linker for signal transmission. The HAMP domain is followed by histidine kinase core containing a HisKA domain and an ATPase domain. The homodimerization of this kinase domain is a common and required feature for environmental signal triggered autophosphorylation in most histidine kinases (28). The phosphorylated HisKA domain is responsible for transferring the phosphoryl group to the following response regulator (receiver) domain and subsequently to a conserved aspartate residue in C-terminal Hpt domain (figure 1.2a) (28, 36, 97). The response regulator GacA is the last phosphoryl receiver at the end point of this phosphorelay. With a typical helix-turn-helix motif in the effecter domain, phosphorylated GacA binds to DNA and in turn controls target gene transcription (32, 36, 110).

Since its identification, the GacS/GacA family has been one of the best studied regulatory systems in many organisms, such as VarS/VarA in *Vibro cholerae*, BarA/UvrY in *E. coli* and LetS/LetA in *Legionella*. These global regulatory systems regulate the expression of a broad range of genes including those for various metabolic functions, secreted toxins, motility and quorum sensing (12). Moreover, GacS and GacA were also shown to be involved in the activation of multiple virulence genes including those related to biofilm formation (30). Consistent with this finding, GacA was shown to contribute to chronic *P. aeruginosa* infection in a murine CF model (30). A GacS mutant of *P. aeruginosa* also has a defect in swarming motility (30).

In many organisms the loss of the GacS/GacA system produces very similar phenotypes as sRNAs mutants. The reported cases include: *gacA* and *rsmY*/*rsmZ* mutants in *P. aeruginosa*, *uvrY* and *csrB*/*C* in *E. coli, gacA* and *rsmX*/*rsmY*/*rsmZ* in

Pseudomonas fluorescens (52, 53, 107). These cases provided an indication that GacS/GacA and RsmZ (or homologues) are concordant partners in signal transduction pathways. Even though it is possible that the GacS/GacA system directly controls other types of genes, there is enough evidence to suggest that GacS/GacA mainly regulates target gene expression through the regulation of Rsm systems. This hypothesis is also supported by Brencic's mutational analysis in *P. aeruginosa*, where a *gacA* mutant and an *rsmYZ* double mutant have almost indistinguishable gene expression patterns and reduced biofilm phenotypes. Furthermore, only two DNA fragments, which are located in the *rsmY* and *rsmZ* loci, were able to bind GacA protein in their genome-wide ChIP-on-chip analysis (12). In addition, at the upstream region of *rsmY* and *rsmZ* promoters there is a conserved sequence, which is highly conserved in many microorganisms. Deleting this sequence decreased transcription of both *rsmZ* and *rsmY*, similar to that of a *gacA* mutant in *P. aeruginosa* (12, 36, 53). Overall, these results demonstrate that this conserved DNA sequence upstream of *rsmY*/*rsmZ* is recognized by phosphorylated GacA and required for GacS-GacA dependent RsmY/RsmZ expression. In summary, all the previous analyses confirmed that the GacS/GacA TCS controls gene expression in *P. aeruginosa* primarily through modulating the expression levels of these two small RNAs, which in turn favor the Rsm-dependent gene expression for biofilm formation and control the TTSS in the opposite direction by sequestering RsmA (12).

The signaling kinase LadS enhances biofilm formation

Through microarray analysis of a transposon insertion library of the *P. aeruginosa* strain PAK, Ventre and Filloux identified another TCS gene that is associated with biofilm formation. Three transposon insertions that caused failure of biofilm formation were in the same gene, ORF PA3974 in the *P. aeruginosa* PAO1 genome. Amino acid sequence analysis suggested that this ORF codes for a putative two-component sensor kinase, which was designated as "*ladS*" (lost adhesion sensor)

because its deletion resulted in a defect of biofilm formation and expression of LadS in a PAK *ladS* mutant restored the wild-type biofilm phenotype (104). The predicted LadS domain architecture shows that it contains a putative periplasmic N-terminal 7TMR-DISMED2 (7-transmembrane-receptor with diverse intracellular signaling modules extracellular domain 2) followed by a 7TMR-DISM_7TM domain (7 transmembrane segments found adjacent to 7TMR-DISM domains). In the cytoplasmic portion, the 7TMR-DISM_7TM domain is followed by a histidine kinase domain and a response regulator domain, which makes LadS a hybrid sensor kinase (figure 1.2b) (3, 37, 104).

The identification of LadS was later applied to explain the deficiency of biofilm formation and enhanced cytotoxicity of the PA14 strain, which contains an out-of-frame mutation in the *ladS* gene (37). These phenotypes in PA14 are consistent with Ventre and Filloux's transcriptome analysis wherein a PAK *ladS* mutant displayed repression of the biofilm associated *pel* (pellicle locus) genes but activation of TTSS genes. Ventre and Filloux further found that overexpression of LadS could not restore the pellicle formation of a *pelF* deletion mutant of PAK, indicating that LadS activates pellicle formation in a *pel*-dependent manner, and in turn induces biofilm formation (104). On the other hand, deletion of the *ladS* gene dramatically increased the ExoS expression and secretion, which are strong indicators of TTSS activation in *P. aeruginosa.* LadS has also been connected to the Gac/Rsm system. The effects of the *ladS* gene on *pel* expression and TTSS activation are likely the result of the negative impact this protein has on in a RsmZ expression (35, 104). But exactly how LadS interacts with this system remains unknown.

The non-canonical sensor kinase RetS inhibits GacS/GacA signaling

Another essential TCS protein that critically controls virulence factor expression in *P. aeruginosa* and attracts intense interest among the medical community is RetS. RetS was initially named RtsM by Laskowski in 2004 because it was found to be a

crucial Regulator of Type three secretion System (59). Using a PA103 transposon insertion library for mutational analysis Laskowski found that deletion of this gene, located at locus PA4856 in the PAO1 genome, resulted in remarkably reduced *P. aeruginosa* cytotoxicity. They further demonstrated that this altered phenotype is due to the loss of TTSS activity. First of all, RetS is required for the production and secretion of toxin effectors that are translocated into host cells by a functional TTSS; secondly, RetS is required for transcription of the TTSS machinery (31, 105); finally, RetS controls the transcription of *exsA* and *exsD*, which encode the transcriptional activator and anti-activator of TTSS respectively (55). In addition, the restoration of TTSS effector production and secretion in the *rtsM* mutant by overexpression of ExsA also suggests that RtsM controls TTSS in an ExsA-dependent manner (9, 55). Shortly after its identification, this putative TCS sensor was shown to be a global pathogenesis regulator. From a 39-mutant library in the strain PAK, Andrew Goodman found that single mutation in *rtsM* (PA4856) could dramatically raise biofilm formation and activate a number of biofilm related genes including the *psl* and *pel* operons which encode biofilm matrix-required exopolysaccharides (112). He also found that, consistent with Laskowski's results, deletion of PA4856 causes the loss of cytotoxicity due to the defect of the TTSS gene expression, which in turn abates the virulence of *P. aeruginosa* in a murine acute pneumonia model. Goodman, therefore designated RtsM (PA4856) as RetS (Regulator of Exopolysaccharide and Type III secretion), which became the commonly used name from then on (31, 59).

Sequence analysis shows that RetS is a putative hybrid TCS kinase (31, 59, 116). Resembling LadS, RetS also contains a 7-segment transmembrane domain that belongs to the 7TM-DISM family (3). The integration of these 7 helices into the inner membrane is presumbly assisted by the Sec translocation system because a Sec-dependent leader sequence is located at the amino-terminal end of RetS (amino acids 1-27), which will be removed during or after protein translocation (15). In the

periplasm between the leader sequence and the transmembrane segments, there is a putative signal sensing domain which makes RetS a "sensor" kinase and sequence conservation places it in the 7TMR-DISMED2 family (3). Interestingly, the sensory domains of RetS and LadS share a 35% sequence identity, suggesting they receive similar but nonidentical environmental signals (31, 37, 59, 104). We were the first group that solved the crystal structure of the sensory domain of RetS ($RetS_{peri}$), which is the first determined structure in 7TMR-DISMED2 family. Consistent with the prediction for this family, we have demonstrated that it is indeed a carbohydrate binding domain (50). In the cytoplasm, following the transmembrane segments, RetS possesses a conventional histidine kinase domain and two response regulator domains in tandem. This is an unusual feature compared to other identified hybrid sensor kinases which only have one response regulator domain, suggesting a complex cellular communication network or multiple functional roles for RetS. The importance of RetS was demonstrated by a transcriptome analysis, which showed that RetS controls at least 400 genes in *P. aeruginosa* (28, 31, 97). Deletion of the *retS* gene causes downregulation of several essential genes for a functional type II secretion system (31). A *retS* mutant also exhibits the repressed expression of type IV pili which are required for acute infection with *P. aeruginosa* in several animal models (116). RetS is also connected to signaling of c-di-GMP which is utilized as a secondary messenger for the transition between the planktonic and sessile lifestyles of *P. aeruginosa* (70). In addition, the RetS orthologue in *Pseudomonas syringae* has been shown to regulate genes for EPS production and represses type VI secretion system and controls several virulence-associated activities (83).

The most notable functional role of RetS is its participation in the Gac/Rsm regulatory pathway, which was proposed based on the repressed TTSS and hyperbiofilm phenotypes of a *retS* mutant of *P. aeruginosa* (31, 59). After identifying and changing the nomenclature of RetS, Goodman applied a transposon insertion

derived mutagenesis experiment to identify additional genes that are connected to RetS signaling transduction. Targeting the transposon insertion mutants that failed to show a hyperbiofilm phenotype and repressed TTSS activity, they identified genes in the Gac/Rsm pathway such as *gacS*, *gacA* and *rsmZ* (31). This discovery implied that RetS controls the GacS/GacA/RsmZ regulatory system. In addition, deletion of *ladS*, which is the gene favoring biofilm formation, also exhibits high *rsmZ* expression level in the *retS* mutant background (104). This finding indicates that RetS and LadS signaling are antagonistic and RetS is downstream of LadS, even though the signaling mechanism between these two sensor kinases is still unknown. As a result, a model for reciprocal regulation of genes required for chronic and acute infections by RetS and LadS sensors converging on sRNA regulation has been proposed: LadS and GacS/GacA favor biofilm gene expression and repress the TTSS through activation of the *rsmZ* gene; on the other hand, RetS stimulates the TTSS and suppresses biofilm formation by blocking the Gac/Rsm system. Due to its central role in regulating virulence gene expression in *P. aeruginosa* this signal transduction pathway has been the focus of subsequent studies aimed at revealing the molecular basis for the choice between TTSS expression and biofilm formation (7, 31, 104).

Even though it possesses conserved histidine and aspartate residues in the kinase and response regulator domains respectively, RetS does not have detectable kinase activity (32, 42). This unexpected characteristic of RetS aroused the interest in its exact signaling task in signal transduction pathways. Laskowski and Kazmierczak took the first step toward uncovering the functional role of each putative signaling domain in RetS. They found that deletion of the putative periplasmic sensory domain did not cause a defect in TTSS activity and acute infection in the mouse model, indicating the sensory domain is not required for TTSS-inducing function of RetS in PA103 strain, which is a biofilm-deficient strain. By mutational analysis targeting the conserved phosphorylation residues in kinase domain (HK) and two response

regulator domains (RR1 and RR2), they further showed that single mutations in the HK and RR2 domains, but not the RR1 domain, cause a significant decrease in TTSS activity. The slightly greater TTSS activity of the HK/RR1 double mutant compared to that of the HK single mutant also suggests that RR1 might inhibit RetS function. Interestingly, only the RR2 domain is required for RetS activity *in vivo* (60). Although the strain (PA103) used in that study is naturally deficient in biofilm formation, the presence of a conserved RetS/Gac/Rsm pathway suggests that the mutations described above should have the opposite effect on biofilm genes (60, 104). Surprisingly, this expected gene expression pattern was not observed by Goodman who showed that mutations on neither HK domain nor RR1/RR2 domains impacted RsmZ expression level in PAK strain (32). Therefore, whether RetS functions as a typical bacterial sensor kinase is still controversial.

Lacking a Hpt domain, RetS requires an Hpt protein to execute its cellular phosphorelay activity (28, 97). There are three Hpt proteins identified in *P. aeruginosa* by Hsu and colleagues in 2008, annotated as HptA, HptB and HptC. They demonstrated that only HptB can interact with RetS by both *in vitro* phosphorelay assay and *in vivo* bacterial two-hybrid assay (42). Bordi, Filloux and colleagues have subsequently shown that an *hptB* mutant has a *pel*-dependent hyperbiofilm phenotype, similar to that of a *retS* mutant. Furthermore, similar to RetS, HptB favors TTSS expression and represses biofilm formation through GacS/GacA/RsmZ regulatory system. However, although the HptB regulon is entirely included in the RetS regulon, RetS regulates many other genes that are not controlled by HptB (10). Finally, the reversible phosphorylation between RetS and HptB suggests these two TCS proteins could participate in other unknown signaling pathways (10, 42).

RetS-GacS Signaling mechanism

The demonstration that a *retS* and *gacS*/*gacA* double mutant has the same biofilm-deficient phenotype as that of a *gacS* or *gacA* single mutant implies that RetS

represses biofilm formation by inhibiting the GacS/GacA system (10, 12). This inhibition mechanism remained a mystery until a novel model was proposed by Goodman and Lory (32). After excluding the possibility that RetS controls the transcription or translation of GacS or GacA, they demonstrated that RetS and GacS are able to interact physically. This interaction can be observed *in vitro* or *in vivo* by co-purification from *P. aeruginosa* and by a two-hybrid experiment. They also found that the kinase domains of RetS and GacS are sufficient for this interaction. Furthermore, they have shown that RetS, despite lacking detectable kinase activity, can inhibit GacS phosphorylation with its kinase domain. This discovery, along with the fact that most histidine kinases require homo-dimerization for autophosphorylation, allowed Goodman and Lory to hypothesize a model for RetS-GacS signaling wherein the competitive binding of RetS with GacS disrupts the GacS homo-dimer thus blocking the GacS trans-autophosphorylation needed to induce the GacS/GacA system (28, 32, 97).

Hypothesis and objectives of the study

Possessing a periplasmic sensory domain ($RetS_{peri}$), RetS is believed to represent one of the sensors responsible for sensing an extracellular signal that allows *P. aeruginosa* to adapt to environmental change (28, 31, 97). Uncovering the specific functional role of $RetS_{peri}$ can provide invaluable information to gain a full understanding of the RetS signaling mechanism for biofilm formation regulation. Considering the absence of TCS in mammalian cells and crucial participation of RetS in pathogenesis regulation, $RetS_{peri}$ is an appealing drug target to assist clinical therapy for patients infected by *P. aeruginosa* (28).

The objective of this study is to uncover the specific functional role of $RetS_{peri}$ in biofilm formation. Based on the current published RetS-GacS signaling model and the role of RetS in repressing biofilm formation, we proposed an alternative hypothesis which is described in chapter two: signal sensing by $RetS_{peri}$ disrupts dimerization in

the periplasmic domain and in turn causes disruption of a RetS homo-dimer to permit binding of GacS and blocking of GacS trans-autophosphorylation. Another aim of this chapter is to provide initial characterization of $RetS_{peri}$ ligand binding and homo-dimerization activities. The analyses and discoveries were used for subsequent studies with the aim to reveal the exact functional roles of ligand binding and dimerization of $RetS_{peri}$, which are described in chapter three. To test the current RetS-GacS model and our hypothesis and uncover the molecular basis of the RetS-GacS interaction and signaling mechanism, chapter four describes a mutational analysis targeting conserved cytoplasmic phosphorylation residues on RetS. Overall, this chapter aims to resolve the ambiguity in the current literature regarding the question whether RetS phosphorylation activity is required for RetS-GacS signaling and biofilm regulation. Moreover, the interaction pattern and the signaling mechanism for RetS-GacS complex are discussed.

Part II of this dissertation focuses on the structural studies aimed at understanding substrate recognition and ligand binding in another carbohydrate binding protein, the germination specific lytic peptidoglycan hydrolysis enzyme called SleB from *Bacillus anthracis*.

Reference

1. Alex LA, Simon MI. Protein histidine kinases and signal transduction in prokaryotes and eukaryotes. 1994. Trends Genet.10:133–38.
2. Alves R, Savageau MA. 2003. Comparative analysis of prototype two-component systems with either bifunctional or monofunctional sensors: differences in molecular structure and physiological function. Mol. Microbiol. 48:25–51.
3. Anantharaman V, Aravind L. 2003. Application of comparative genomics in the identification and analysis of novel families of membrane-associated receptors in bacteria. BMC Genomics. 4: 34.
4. Anzai; Kim, H; Park, JY; Wakabayashi, H; Oyaizu, H. 2000. Phylogenetic affiliation of the pseudomonads based on 16S rRNA sequence. Int J Syst Evol Microbiol. 50: 1563–89.
5. Aravind L, Galperin MY, Koonin EV. 1998. The catalytic domain of the P-type ATPase has the haloacid dehalogenase fold. Trends Biochem Sci. 23:127–29.
6. Paul Babitzke, Tony Romeo. 2007. CsrB sRNA family: sequestration of RNA-binding regulatory proteins. Current Opinion in Microbiology. 10: 156-163
7. Balasubramanian D, Schneper L, Kumari H, Mathee K. 2013. A dynamic and intricate regulatory network determines Pseudomonas aeruginosa virulence. Nucleic Acids Res. 41:1-20.
8. Bayram Y, Parlak M, Aypak C, Bayram I. 2012. Three-year review of bacteriological profile and antibiogram of burn wound isolates in Van, Turkey. Int J Med Sci. 10:19-23.
9. Bernhards RC, Jing X, Vogelaar NJ, Robinson H, Schubot FD. 2009. Structural evidence suggests that antiactivator ExsD from Pseudomonas aerugin osa is a DNA binding protein. Protein Sci. 18:503-13.
10. Bordi C, Lamy MC, Ventre I, Termine E, Hachani A, Fillet S, Roche B, Bleves S, Méjean V, Lazdunski A, Filloux A. 2010. Regulatory RNAs and the HptB/RetS signalling pathways fine-tune Pseudomonas aeruginosa pathogenesis. Mol Microbiol. 76:1427-43.
11. Brencic A, Lory S. 2009. Determination of the regulon and identification of novel mRNA targets of Pseudomonas aeruginosa RsmA. Molecular Microbiol. 72:612-32.
12. Brencic A, McFarland KA, McManus HR, Castang S, Mogno I, Dove SL, Lory S. 2009. The GacS/GacA signal transduction system of Pseudomonas aeruginosa acts exclusively through its control over the transcription of the RsmY and RsmZ regulatory small RNAs. Mol Microbiol. 73:434-45.
13. Burrowes E, Baysse C, Adams C, O'Gara F. 2006. Influence of the regulatory protein RsmA on cellular functions in Pseudomonas aeruginosa PAO1, as revealed by transcriptome analysis. Microbiology. 152:405-18.
14. Byrd MS, Sadovskaya I, Vinogradov E, Lu H, Sprinkle AB, Richardson SH, Ma L, Ralston B, Parsek MR, Anderson EM, Lam JS, Wozniak DJ. 2009. Genetic

and biochemical analyses of the Pseudomonas aeruginosa Psl exopolysaccharide reveal overlapping roles for polysaccharide synthesis enzymes in Psl and LPS production. Mol Microbiol. 73:622-38.
15. Chatzi KE, Sardis MF, Karamanou S, Economou A. 2013. Breaking on through to the other side: protein export through the bacterial Sec system. Biochem J. 449:25-37.
16. Cornelis, G., and Van Gijsegem, F. 2000. Assembly and function of type III secretory systems. Annu Rev Microbiol. 54**:**735–774.
17. Cornelis P (editor). 2008. Pseudomonas: Genomics and Molecular Biology (1st edition). Caister Academic Press.
18. Dean P. 2011. Functional domains and motifs of bacterial type III effector proteins and their roles in infection. FEMS Microbiol Rev. 3:1100-25.
19. Drenkard E. 2003. Antimicrobial resistance of Pseudomonas aeruginosa biofilms. Microbes Infect. 5:1213-9.
20. M. Dziejman, J.J. Mekalanos. 1995. Two-component signal transduction and its role in the expression of bacterial virulence factors, in: J.A. Hoch, T.J. Sihavy (Eds.), Two-Component Signal Transduction, Vol. ASM Press, Washington, DC.
21. Finn RD, Tate J, Mistry J, Coggill PC, Sammut SJ, et al. 2008. The Pfam protein families database. Nucleic Acids Res. 36:281–88
22. Fletcher, E. L., Weissman, B. A., Efron, N., Fleiszig, S. M., Curcio, A. J. & Brennan, N. A. 1993. The role of pili in the attachment of Pseudomonas aeruginosa to unworn hydrogel contact lenses. Curr. Eye Res. 12:1067–1071.
23. Folkesson A, Jelsbak L, Yang L, Johansen HK, Ciofu O, Hoiby N, Molin S. 2012. Adaptation of Pseudomonas aeruginosa to the cystic fibrosis airway: an evolutionary perspective. Nat Rev Microbiol. 10:841-51.
24. Frank, D.W. 1997. The exoenzyme S regulon of Pseudomonas aeruginosa. Mol Microbiol. 4**:**621–629.
25. Friedman L, Kolter R. 2004. Genes involved in matrix formation in Pseudomonas aeruginosa PA14 biofilms. Mol Microbiol. 51:675–690.
26. Friedman L, Kolter R. 2004. Two genetic loci produce distinct carbohydrate-rich structural components of the Pseudomonas aerguinosa biofilm matrix. J Bacteriol. 186:4457–4465.
27. Fung C, Naughton S, Turnbull L, Tingpej P, Rose B, Arthur J, Hu H, Harmer C, Harbour C, Hassett DJ, Whitchurch CB, Manos J. 2010. Gene expression of Pseudomonas aeruginosa in a mucin-containing synthetic growth medium mimicking cystic fibrosis lung sputum. J Med Microbiol. 59: 1089-100.
28. Gao R, Stock AM. 2009. Biological insights from structures of two-component proteins. Annu Rev Microbiol. 63:133-54.
29. Garcia-Medina, R., Dunne, W. M., Singh, P. K. & Brody, S. L. 2005. Pseudomonas aeruginosa acquires biofilm-like properties within airway epithelial cells. Infect Immun. 73:8298–8305.
30. Gooderham WJ, Hancock RE. 2009. Regulation of virulence and antibiotic resistance by two-component regulatory systems in Pseudomonas aeruginosa.

FEMS Microbiol Rev. 33:279-94.
31. Andrew L. Goodman, Bridget Kulasekara, Arne Rietsch, Dana Boyd, Roger S. Smith, and Stephen Lory. 2004. A Signaling Network Reciprocally Regulates Genes Associated with Acute Infection and Chronic Persistence in Pseudomonas aeruginosa. Developmental Cell. 7:745–754.
32. Goodman AL, Merighi M, Hyodo M, Ventre I, Filloux A, Lory S. 2009. Direct interaction between sensor kinase proteins mediates acute and chronic disease phenotypes in a bacterial pathogen. Genes Dev. 23:249-59.
33. Govan, J. R. & Deretic, V. 1996. Microbial pathogenesis in cystic fibrosis: mucoid Pseudomonas aeruginosa and Burkholderia cepacia. Microbiol. Rev. 60:539–574.
34. Hassett, D. J., Cuppoletti, J., Trapnell, B., Lymar, S. V., Rowe, J. J., Yoon, S. S., Hilliard, G. M., Parvatiyar, K., Kamani, M. C. & other authors. 2002. Anaerobic metabolism and quorum sensing by Pseudomonas aeruginosa biofilms in chronically infected cystic fibrosis airways: rethinking antibiotic treatment strategies and drug targets. Adv Drug Deliv Rev. 54:1425–1443
35. Heeb S, Blumer C, Haas D. 2002. Regulatory RNA as mediator in GacA/RsmA-dependent global control of exoproduct formation in Pseudomonas fluorescens CHA0. J Bacteriol. 184:1046-56
36. Heeb S, Haas D. 2001. Regulatory Roles of the GacS/GacA Two-Component System in Plant-Associated and Other Gram-Negative Bacteria. Mol Plant Microbe Interact. 14:1351-63.
37. Helga Mikkelsen, Rachel McMullan, Alain Filloux. 2011. The Pseudomonas aeruginosa Reference Strain PA14 Displays Increased Virulence Due to a Mutation in lads. PLoS One. 6:29113.
38. Hoch JA, Silhavy TJ. 1995. Two-Component Signal Transduction.Washington, DC: Am. Soc. Microbiol. Press. 488 pp. eds.
39. Hogardt M, Heesemann J. 2010. Adaptation of Pseudomonas aeruginosa during persistence in the cystic fibrosis lung. Int J Med Microbiol. 300:557-62.
40. Hornef, M.W., Roggenkamp, A., Geiger, A.M., Hogardt, M., Jacobi, C.A., and Heesemann, J. 2000. Triggering the ExoS regulon of Pseudomonas aeruginos*a*: a GFPreporter analysis of exoenzyme (Exo) S, ExoT and ExoU synthesis. Microb Pathog. 29:329–343.
41. Hrabak, E. M., and Willis, D. K. 1992. The lemA gene required for pathogenicity of Pseudomonas syringae pv. syringae on bean is a member of a family of two-component regulators. J. Bacteriol. 174:3011-3020.
42. Hsu JL, Chen HC, Peng HL, Chang HY. 2008. Characterization of the histidine-containing phosphotransfer protein B-mediated multistep phosphorelay system in Pseudomonas aeruginosa PAO1. J Biol Chem. 283:9933-44.
43. Hunter RC, Beveridge TJ. 2005. High-resolution visualization of Pseudomonas aeruginosa PAO1 biofilms by freeze-substitution transmission electron microscopy. Journal of Bacteriology. 187:7619–7630
44. Iglewski BH. 1996. Pseudomonas. In: Baron's Medical Microbiology (Baron S et al., eds.) (4th ed.). Univ of Texas Medical Branch.

45. Irie Y, Starkey M, Edwards AN, Wozniak DJ, Romeo T, Parsek MR. 2010. Pseudomonas aeruginosa biofilm matrix polysaccharide Psl is regulated transcriptionally by RpoS and post-transcriptionally by RsmA. Mol Microbiol. 78:158-72.
46. Jackson KD, Starkey M, Kremer S, Parsek MR, Wozniak DJ. 2004. Identification of psl, a locus encoding a potential exopolysaccharide that is essential for Pseudomonas aeruginosa PAO1 biofilm formation. J Bacteriol. 186:4466–4475.
47. Janiak-Spens F, Sparling JM, Gurfinkel M, West AH. 1999. Differential stabilities of phosphorylated response regulator domains reflect functional roles of the yeast osmoregulatory SLN1 and SSK1 proteins. J. Bacteriol. 181:411–17
48. Jencks WP. 1980. The utilization of binding energy in coupled vectorial processes. Adv. Enzymol. 51: 75–106
49. Jin S, Ishimoto KS, Lory S. 1994. PilR, a transcriptional regulator of piliation in Pseudomonas aeruginosa, binds to a cis-acting sequence upstream of the pilin gene promoter. Mol Microbiol. 14:1049-57.
50. Jing X, Jaw J, Robinson HH, Schubot FD. 2010. Crystal structure and oligomeric state of the RetS signaling kinase sensory domain. Proteins. 78:1631-40.
51. Karin Heurlier, Faye Williams, Stephan Heeb, Corinne Dormond, Gabriella Pessi, Dustin Singer, Miguel Cámara, Paul Williams, Dieter Haas. 2004. Positive control of swarming, rhamnolipid synthesis, and lipase production by the posttranscriptional RsmA/RsmZ system in Pseudomonas aeruginosa PAO1. J Bacteriol. 186:2936–2945.
52. Kay E, Dubuis C, Haas D. 2005. Three small RNAs jointly ensure secondary metabolism and biocontrol in Pseudomonas fluorescens CHA0. Proc Natl Acad Sci U S A. 102:17136-41.
53. Kay E, Humair B, Dénervaud V, Riedel K, Spahr S, Eberl L, Valverde C, Haas D. 2006. Two GacA-dependent small RNAs modulate the quorum-sensing response in Pseudomonas aeruginosa. J Bacteriol. 188:6026-33.
54. Dong-jin Kim and Steven Forst. 2001. Genomic analysis of the histidine kinase family in bacteria and archaea Microbiology. 147:1197–1212
55. King JM, Brutinel ED, Marsden AE, Schubot FD, Yahr TL. 2012. Orientation of Pseudomonas aeruginosa ExsA monomers bound to promoter DNA and base-specific contacts with the P(exoT) promoter. J Bacteriol. 194:2573-85.
56. King EO, Ward MK, Raney DE. 1954. Two simple media for the demonstration of pyocyanin and fluorescein. J Lab Clin Med. 44:301–7
57. Kitten, T., Kinscherf, T. G., McEvoy, J. L., and Willis, D. K. 1998. A newly identified regulator is required for virulence and toxin production in Pseudomonas syringae. Mol. Microbiol. 28:917-929.
58. Klausen, M., Heydorn, A., Ragas, P., Lambertsen, L., Aaes-Jorgensen, A., Molin, S. & Tolker-Nielsen, T. 2003. Biofilm formation by Pseudomonas aeruginosa wild type, flagella and type IV pili mutants. Mol Microbiol. 48:1511–1524.

59. Michelle A. Laskowski, Ellice Osborn and Barbara I. Kazmierczak. 2004. A novel sensor kinase–response regulator hybrid regulates type III secretion and is required for virulence in Pseudomonas aeruginosa. Molecular Microbiology. 54:1090–1103.
60. Michelle A. Laskowski and Barbara I. Kazmierczak. 2006. Mutational Analysis of RetS, an Unusual Sensor Kinase-Response Regulator Hybrid Required for Pseudomonas aeruginosa Virulence. Infection and Immunity. 74:4462–4473.
61. Laub MT, Goulian M. 2007. Specificity in two-component signal transduction pathways. Annu. Rev. Genet. 41:121–45
62. Laville, J., Voisard, C., Keel, C., Maurhofer, M., Défago, G., and Haas, D. 1992. Global control in Pseudomonas fluorescens mediating antibiotic synthesis and suppression of black root rot of tobacco. Proc. Natl. Acad. Sci. U.S.A. 89:1562-1566.
63. Liu MY, Gui G, Wei B, Preston JF 3rd, Oakford L, Yüksel U, Giedroc DP, Romeo T. 1997. The RNA molecule CsrB binds to the global regulatory protein CsrA and antagonizes its activity in Escherichia coli. J Biol Chem. 272:17502-10.
64. Lyczak, J. B., C. L. Cannon, and G. B. Pier. 2000. Establishment of Pseudomonas aeruginosa infection: lessons from a versatile opportunist. Microbes Infect. 2:1051–1060.
65. Ma L-Y, Jackson K, Landry RM, Parsek MR, Wozniak DJ. 2006. Analysis of Pseudomonas aeruginosa conditional Psl variants reveals roles for the Psl polysaccharide in adhesion and maintaining biofilm structure postattachment. J Bacteriol. 188:8213–8221.
66. L. Mashburn-Warren, R. J. C. Mclean and M. Whiteley. 2008. Gram-negative outer membrane vesicles: beyond the cell surface. Geobiology. 6:214–219
67. Mathee, K., Narasimhan, G.; Valdes, C., Qiu, X., Matewish, J. M., Koehrsen, M., Rokas, A., Yandava, C. N. et al. 2008. Dynamics of Pseudomonas aeruginosa genome evolution. Proceedings of the National Academy of Sciences. 105: 3100–3105
68. J.J. Mekalanos. 1992. Environmental signals controlling expression of virulence determinants in bacteria. J. Bacteriol. 174:1–7.
69. Mizuno T. 1997. Compilation of all genes encoding two-component phosphotransfer signal transducers in the genome of Escherichia coli. DNA Res. 4:161–68.
70. Moscoso JA, Mikkelsen H, Heeb S, Williams P, Filloux A. 2011. The Pseudomonas aeruginosa sensor RetS switches type III and type VI secretion via c-di-GMP signalling. Environ Microbiol. 13:3128-38.
71. C. A. Mueller, P. Broz and G. R. Cornelis. 2008. The type III secretion system tip complex and ranslocon. Molecular Microbiology. 68:1085–1095
72. Mulcahy H, O'Callaghan J, O'Grady EP, Adams C, O'Gara F. 2006. The posttranscriptional regulator RsmA plays a role in the interaction between Pseudomonas aeruginosa and human airway epithelial cells by positively regulating the type III secretion system. Infect Immun. 74:3012-5.

73. Mulcahy H, O'Callaghan J, O'Grady EP, Maciá MD, Borrell N, Gómez C, Casey PG, Hill C, Adams C, Gahan CG, Oliver A, O'Gara F. 2008. Pseudomonas aeruginosa RsmA plays an important role during murine infection by influencing colonization, virulence, persistence, and pulmonary inflammation. Infect Immun. 76:632-8.
74. Nickel, J. C., Downey, J. A. & Costerton, J. W. 1989. Ultrastructural study of microbiologic colonization of urinary catheters. Urology. 34:284–291.
75. Ninfa EG, Atkinson MR, Kamberov ES, Ninfa AJ. 1993. Mechanism of autophosphorylation of Escherichia coli nitrogen regulator II (NRII or NtrB): trans-phosphorylation between subunits. J. Bacteriol. 175:7024–32.
76. O'Toole, G., Kaplan, H. B.and Kolter, R. 2000. Biofilm formation as microbial development. Annu. Rev. Microbiol. 54:49–79.
77. O'Toole GA, Kolter R. 1998. Flagellar and twitching motility are necessary for Pseudomonas aeruginosa biofilm development. Mol Microbiol. 30:295-304.
78. Pan SQ, Charles T, Jin S, Wu Z-L, Nester EW. 1993. Preformed dimeric state of the sensor protein VirA is involved in plant--Agrobacterium signal transduction. Proc. Natl. Acad. Sci. USA. 90:9939–43.
79. Parkinson JS, Kofoid EC. 1992. Communication Modules in Bacterial Signaling Proteins. Annu. Rev. Genet. 26:71–112.
80. Pernestig, A. K., Melefors, O., and Georgellis, D. 2001. Identification of UvrY as the cognate response regulator for the BarA sensor kinase in Escherichia coli. J. Biol. Chem. 276:225-231.
81. Poole, K. 2004. Efflux-mediated multiresistance in Gram-negative bacteria. Clinical Microbiology and Infection. 10:12–26.
82. Rahme LG, Stevens EJ, Wolfort SF, Shao J, Tompkins RG, Ausubel FM. 1995. Common virulence factors for bacterial pathogenicity in plants and animals. Science. 268:1899–1902.
83. Records AR, Gross DC. 2010. Sensor kinases RetS and LadS regulate Pseudomonas syringae type VI secretion and virulence factors. J Bacteriol. 192:3584-96.
84. Rich, J. J., Kinscherf, T. G., Kitten, T., and Willis, D. K. 1994. Genetic evidence that the *gacA* gene encodes the cognate response regulator for the lemA sensor in Pseudomonas syringae. J. Bacteriol. 176:7468-7475.
85. Rodrigue, A., Quentin, Y., Lazdunski, A., Mejean, V., and Foglino, M. 2000. Two-component systems in Pseudomonas aeruginosa: why so many? Trends Microbiol. 8:498–504.
86. Romeo T. 1998. Global regulation by the small RNA-binding protein CsrA and the non-coding RNA molecule CsrB. Mol Microbiol. 29:1321-30.
87. Ryan KJ, Ray CG (editors). 2004. Sherris Medical Microbiology (4th ed.). McGraw Hill.
88. Ryder C, Byrd M, Wozniak DJ. 2007. Role of polysaccharides in Pseudomonas aeruginosa biofilm development. Curr Opin Microbiol. 10:644-8.

89. Sadikot RT, Blackwell TS, Christman JW, Prince AS. 2005. Pathogen-host interactions in Pseudomonas aeruginos*a* pneumonia. Am J Respir Crit Care Med. 171:1209–1223.
90. Schooling SR, Beveridge TJ. 2006. Membrane vesicles: an overlooked component of the matrices of biofilms. Journal of Bacteriology. 188:5945–5957.
91. Shaulsky G, Escalante R, Loomis WF. 1996. Developmental signal transduction pathways uncovered by genetic suppressors. Proc. Natl. Acad. Sci. USA 93: 15260–65.
92. Shaulsky G, Fuller D, Loomis WF. 1998. A cAMP-phosphodiesterase controls PKA-dependent differentiation. Development. 125:691–99.
93. Shrout, J. D., Chopp, D. L., Just, C. L., Hentzer, M., Givskov, M. & Parsek, M. R. 2006. The impact of quorum sensing and swarming motility on Pseudomonas aeruginosa biofilm formation is nutritionally conditional. Mol Microbiol. 62: 1264–1277.
94. Skerker JM, Prasol MS, Perchuk BS, Biondi EG, Laub MT. 2005. Two-component signal transduction pathways regulating growth and cell cycle progression in a bacterium: a system-level analysis. PLoS Biol. 3:1770–88.
95. Sriramulu, D. D., Lunsdorf, H., Lam, J. S. & Romling, U. 2005. Microcolony formation: a novel biofilm model of Pseudomonas aeruginosa for the cystic fibrosis lung. J Med Microbiol 54:667–676.
96. J B Stock, A J Ninfa and A M Stock. 1989. Protein phosphorylation and regulation of adaptive responses in bacteria. Microbiol Rev. 53:450–490.
97. Stock AM, Robinson VL, Goudreau PN. 2000. Two-component signal transduction. Annu. Rev. Biochem. 69:183–215.
98. Stock JB, Stock AM, Mottonen JM. 1990. Signal transduction in bacteria. Nature. 344:395–400.
99. Surette MG, Levit M, Liu Y, Lukat G, Ninfa EG, et al. 1996. Dimerization is required for the activity of the protein histidine kinase CheA that mediates signal transduction in bacterial chemotaxis. J. Biol. Chem. 271: 939–45.
100. Swanson RV, Bourret RB, Simon MI. 1993. Intermolecular complementation of the kinase activity of CheA. Mol. Microbiol. 8:435–41.
101. Tanford C. 1984. Twenty questions concerning the reaction cycle of the sarcoplasmic reticulum calcium pump. CRC Crit. Rev. Biochem. 17:123–51.
102. Thomason PA, Traynor D, Cavet G, ChangW-T, Harwood AJ, Kay RR. 1998. An intersection of the cAMP/PKA and two-component signal transduction systems in Dictyostelium. EMBO J. 17:2838–45.
103. Vasseur P, Vallet-Gely I, Soscia C, Genin S, Filloux A. 2005. The pel genes of the Pseudomonas aeruginosa PAK strain are involved at early and late stages of biofilm formation. Microbiology. 151:985–997.
104. Ventre I, Goodman AL, Vallet-Gely I, Vasseur P, Soscia C, Molin S, Bleves S, Lazdunski A, Lory S, Filloux A. 2006. Multiple sensors control reciprocal expression of Pseudomonas aeruginosa regulatory RNA and virulence genes. Proc Natl Acad Sci U S A. 103:171-6.

105. Vogelaar NJ, Jing X, Robinson HH, Schubot FD. 2010. Analysis of the crystal structure of the ExsC.ExsE complex reveals distinctive binding interactions of the Pseudomonas aeruginosa type III secretion chaperone ExsC with ExsE and ExsD. Biochemistry. 49:5870-9.
106. Walker TS; Bais HP; Déziel E; Schweizer, HP; Rahme, LG; Fall, R; Vivanco, JM. 2004. Pseudomonas aeruginosa-plant root interactions. Pathogenicity, biofilm formation, and root exudation. Plant Physiol. 134:320–331.
107. Weilbacher T, Suzuki K, Dubey AK, Wang X, Gudapaty S, Morozov I, Baker CS, Georgellis D, Babitzke P, Romeo T. 2003. A novel sRNA component of the carbon storage regulatory system of Escherichia coli. Mol Microbiol. 48:657-70.
108. M. D. P. Willcox, et, al. 2008. Role of quorum sensing by Pseudomonas aeruginosa in microbial keratitis and cystic fibrosis. Microbiology. 154:2184–2194.
109. Wolfe AJ, Stewart RC. 1993. The short form of the CheA protein restores kinase activity and chemotactic ability to kinase-deficient mutants. Proc. Natl. Acad. Sci. USA. 90:1518–22.
110. Workentine ML, Chang L, Ceri H, Turner RJ. 2009. The GacS-GacA two-component regulatory system of Pseudomonas fluorescens: a bacterial two-hybrid analysis. FEMS Microbiol Lett. 292:50-6.
111. Worlitzsch, D., Tarran, R., Ulrich, M., Schwab, U., Cekici, A., Meyer, K. C., Birrer, P., Bellon, G., Berger, J. & other authors. 2002. Effects of reduced mucus oxygen concentration in airway Pseudomonas infections of cystic fibrosis patients. J Clin Invest 109:317–325.
112. Wozniak DJ, Wyckoff TJ, Starkey M, Keyser R, Azadi P, O'Toole GA, Parsek MR. 2003. Alginate is not a significant component of the extracellular polysaccharide matrix of PA14 and PAO1 Pseudomonas aeruginosa biofilms. Proc Natl Acad Sci U S A. 100:7907-12.
113. Yahr, T. L., and E. P. Greenberg. 2004. The genetic basis for the commitment to chronic versus acute infection in Pseudomonas aeruginosa. Mol. Cell. 16:497–498.
114. Yang Y, Park H, Inouye M. 1993. J. Mol. Biol. 232:493–98.
115. Zigangirova NA, Nesterenko LN, Tiganova IG, Kost EA. 2012. The role of the type-three secretion system of the gram-negative bacteria in regulation of chronic infections. Mol Gen Mikrobiol Virusol. 3:3-13.
116. Zolfaghar I, Angus AA, Kang PJ, To A, Evans DJ, Fleiszig SM. 2005. Mutation of retS, encoding a putative hybrid two-component regulatory protein in Pseudomonas aeruginosa, attenuates multiple virulence mechanisms. Microbes Infect. 7:1305-16.

a)

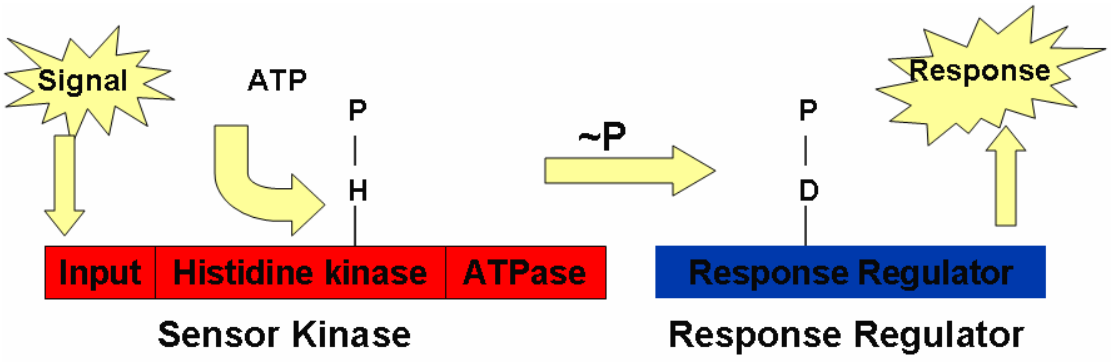

b)

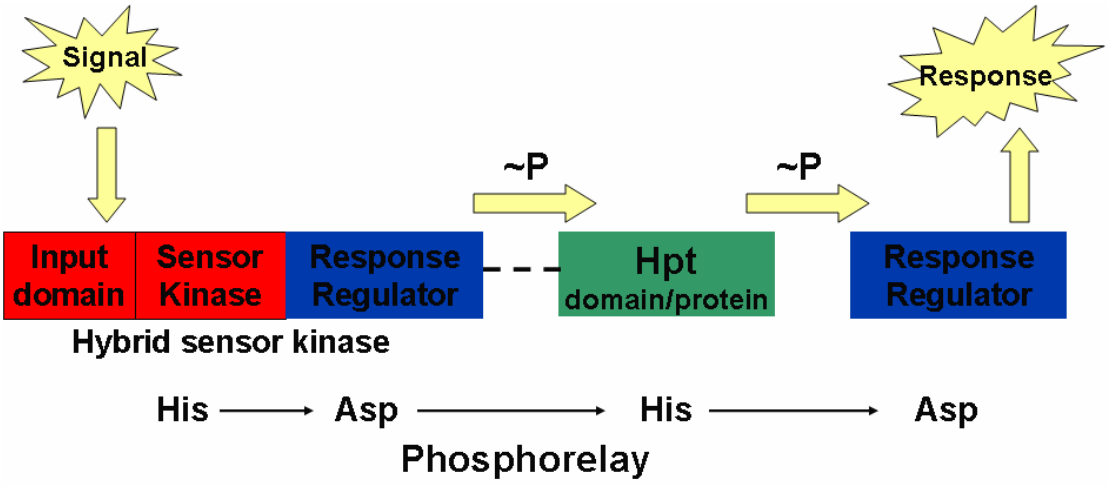

Figure 1.1 Schematic diagrams of two-component systems (TCSs). **(a)** The typical TCS pathway features a conserved phosphor-transfer between the highly conserved histidine kinase and response regulator domain to couple extracellular signal input and output responses. **(b)** A conserved phosphorelay mechanism is employed by hybrid sensor histidine kinase and a histidine phosphotransfer (Hpt) domain. The intermediate Hpt domain can either be an independent protein or a domain linked to the hybrid sensor kinase (28, 97).

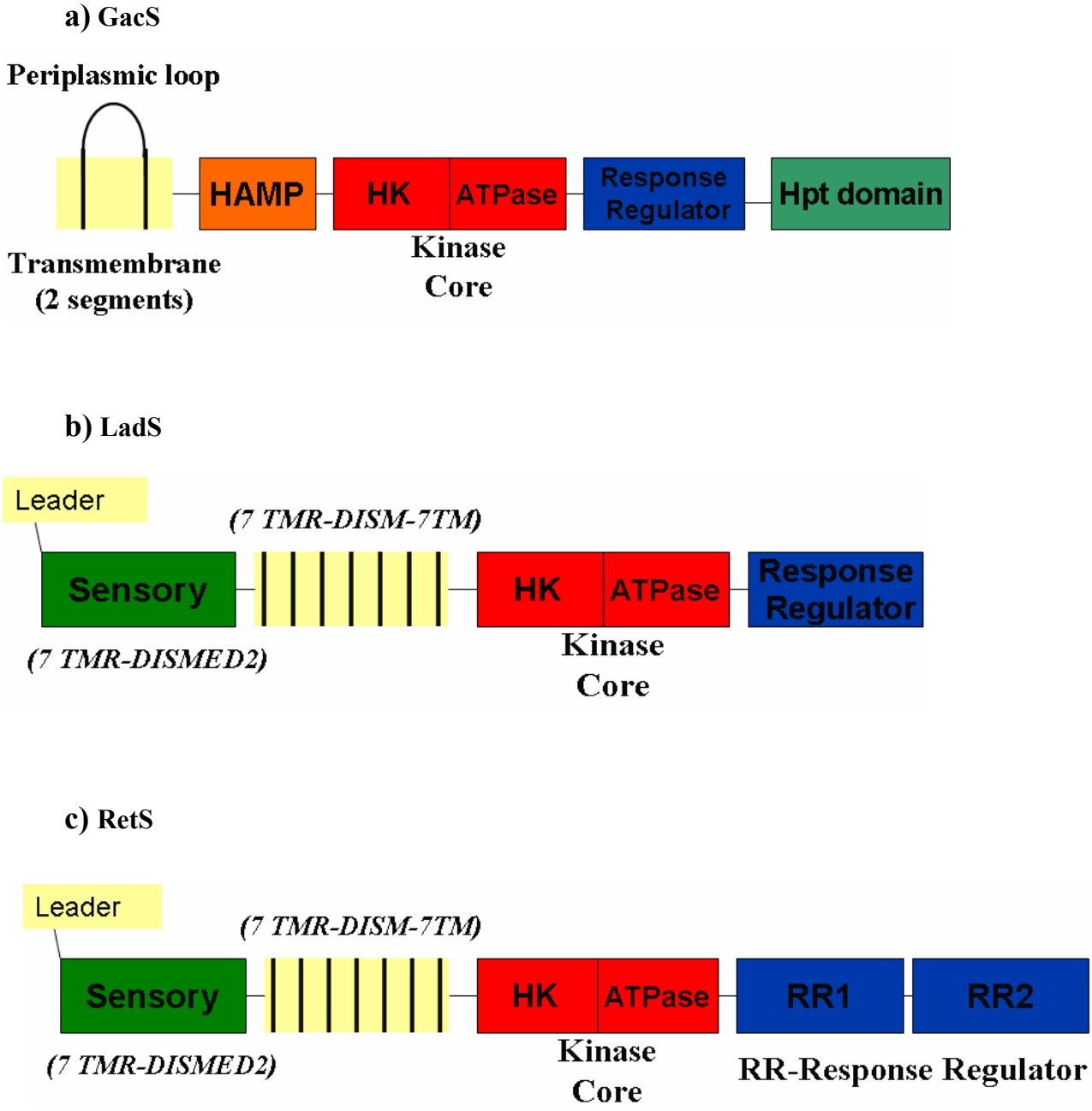

Figure 1.2 Schematic diagrams of domain organizations of GacS, LadS and RetS based on sequence analysis. (a) Hybrid sensor kinase GacS (36). **(b)** Hybrid sensor kinase LadS (37, 104). **(c)** Hybrid sensor kinase RetS (31, 59. 116). **HK:** histidine kinase domain; **RR:** response regulator domain; **Sensory:** periplasmic signal sensing domain; **Leader**: leader sequence, which will be removed after protein translocation; **7TMR-DISMED2:** 7-transmembrane-receptor with diverse intracellular signaling modules extracellular domain 2 (3); **7TMR-DISM_7TM:** 7 transmembrane segments found adjacent to 7TMR-DISM domains (3).

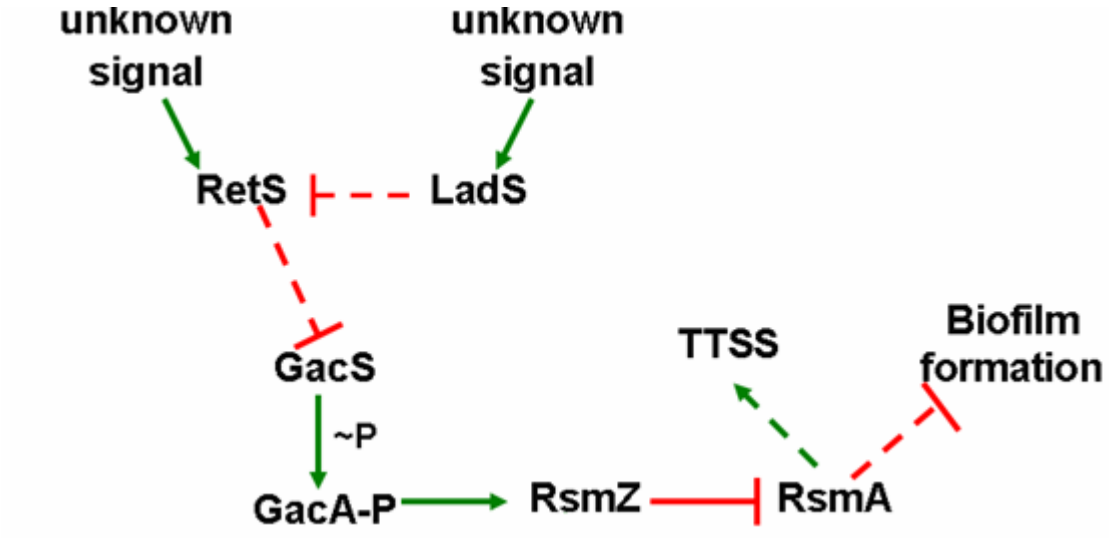

Figure 1.3 Schematic representation summarizing the current model of the signal transduction pathway for the reciprocal regulation of genes associated with chronic and acute infections, respectively. RetS and LadS have similar modular architecture. However, while RetS acts to suppress the synthesis of the small regulatory RNA rsmZ through block GacS/GacS system, LadS and GacS promote rsmZ synthesis (7, 31, 32, 104).

Chapter Two

Crystal structure and oligomeric state of the RetS signaling kinase sensory domain

Xing Jing[1], Jessica Jaw[1], Howard H. Robinson[2] and Florian David Schubot[1]. 2010. Proteins Journal. (15)78:1631-40

[1] Department of Biological Sciences, Life Science I, Virginia Polytechnic Institute and State University, Blacksburg, Virginia 24060
[2] Biology Department, Brookhaven National Laboratory, Upton, New York 11973-5000

Keywords: RetS; type III secretion; biofilm formation; sensor kinase; sensory domain; carbohydrate binding; signal transduction; two-component system; periplasmic domain.

Abstract

The opportunistic pathogen *Pseudomonas aeruginosa* may cause both acute and chronic-persistent infections in predisposed individuals. Acute infections require the presence of a functional type III secretion system (T3SS), whereas chronic *P. aeruginosa* infections are characterized by the formation of drug-resistant biofilms. The T3SS and biofilm formation are reciprocally regulated by the signaling kinases LadS, RetS, and GacS. RetS downregulates biofilm formation and upregulates expression of the T3SS through a unique mechanism. RetS forms a heterodimeric complex with GacS and thus prevents GacS autophosphorylation and downstream signaling. The signals that regulate RetS are not known but RetS possesses a distinctive periplasmic sensor domain that is believed to serve as receptor for the regulatory ligand. We have determined the crystal structure of the RetS sensory domain at 2.0 Å resolution. The structure closely resembles those of carbohydrate binding modules of other proteins, suggesting that the elusive ligands are likely carbohydrate moieties. In addition to the conserved beta-sandwich structure, the sensory domain features two alpha helices which create a unique surface topology. Protein–protein crosslinking and fluorescence energy transfer experiments also revealed that the sensory domain dimerizes with a dissociation constant of $K_d = 580 \pm 50$ n*M*, a result with interesting implications for our understanding of the underlying signaling mechanism.

Introduction

The Gram-negative bacterium *Pseudomonas aeruginosa* poses a major challenge to the medical community. Antibiotic-resistant strains of this pathogen may cause chronic-persistent as well as acute infections in transplant patients and other immunocompromised individuals (6, 12, 7, 22, 31). Most prominently, chronic *P. aeruginosa*-associated lung infections are the leading cause of mortality among people with cystic fibrosis (27).

Beyond its ability to colonize human tissues *P. aeruginosa* can persist in a variety of other milieus including plants and soil. This remarkable versatility may be attributed to a diverse array of virulence mechanisms, which enable the bacterium to adapt to vastly different environmental challenges. Expression and activation of these virulence mechanisms are carefully controlled by complex regulatory networks to ensure an optimal adaptive response. The type III secretion system (T3SS), for instance, is a hallmark of acute infections but is not active in chronic infections (11, 33), which are instead characterized by the formation of antibiotic-resistant biofilms (35).

The two-component signaling system (TCS) is the primary means of bacteria to translate complex environmental cues into adaptive gene expression patterns. A canonical TCS is composed of a histidine kinase (HK) and a cognate receiver response regulator (RR). Signaling in response to a stimulus involves HK autophosphorylation and subsequent transfer of the phosphate group to a cognate RR. Frequently the receiver proteins are transcription factors where the RR domains are coupled with DNA binding domains. Phosphorylation and dephosphorylation control gene expression by modulating the affinity of these transcription factors for their DNA binding sites.

P. aeruginosa harbors a particularly broad array of over 60 TCSs to modulate its gene expression (15), including the expression of genes related to the T3SS and biofilm

formation. Remarkably, T3SS and biofilm formation are regulated in a coordinated but reciprocal fashion by the signaling kinases RetS, LadS, and GacS (18, 23, 39). RetS and LadS are hybrid sensor kinases, combining both HK and RR domains in a single polypepetide, whereas GacS is a canonical signaling kinase requiring the RR GacA for downstream signaling. RetS is pivotal for the transcription of genes associated with cytotoxicity and acute infections, including the T3SS. On the other hand, a *retS* mutant displayed a hyperadhesive phenotype and showed elevated levels of transcription for the *psl* and *pel* operons, which are associated with the synthesis of biofilm oligosaccharides, suggesting that RetS downregulates biofilm formation in the wild-type strain (15, 39). RetS accomplishes its task by blocking the synthesis of RsmZ, a small regulatory RNA. RsmZ had previously been shown to bind to and sequester the translational repressor RsmA. Free RsmA blocks biofilm formation and favors the expression of the T3SS (3, 25). The kinases LadS and GacS, on the other hand, directly counteract RetS, as they stimulate the expression of the *psl* and *pel* operons by upregulating the expression of the RsmA-antagonist RsmZ (21, 39). Underlying this reciprocal regulation of the T3SS and biofilm formation is an entirely novel regulatory mechanism that was uncovered in a recent study by Goodman *et al*. and involves direct contacts between RetS and GacS (16). Signaling kinases are usually homodimeric and autophosphorylation occurs almost always *in trans*. According to the proposed model, an unknown environmental signal causes the RetS homodimer to dissociate to form a heterodimeric RetS-GacS complex. The asymmetric geometry of the heterodimer is thought to block RsmZ biosynthesis by preventing GacS trans-autophosphorylation. Remarkably, neither the kinase activity nor the RR domains of RetS are required for its unusual interactions with GacS (16).

Although the signal that causes RetS-GacS heterodimer formation is unknown, the periplasmic RetS sensory domain is believed to serve as the receptor for the elusive ligand. The sensory domain encompasses about 160 amino acids and belongs

to the large but poorly characterized 7TM-DISM2 domain family, which has been hypothesized to constitute a new class of carbohydrate binding proteins (2). However, experimental support for this model is lacking. The crystal structure of the RetS sensory domain reported here not only offers insights into the nature of the molecular signal but also represents the first reported structure for any member of this domain family. Dimerization of the sensory domain and the stability of the dimer were also examined because the currently held model assumes a mechanism where ligand binding shifts the equilibrium from RetS and GacS homodimers to a RetS-GacS complex.

Materials and Methods

Cloning, expression, and purification of the RetS sensory domain

The boundaries of the RetS sensory domain, containing amino acids 27–185, are defined by two transmembrane helices. The gene fragment coding for the entire periplasmic domain (RetS27–185) was PCR-amplified from *P. aeruginosa* genomic DNA (ATCC 17933D). During PCR, a tobacco etch virus (TEV) protease recognition site and the appropriate recombination sites (*attB1* and *attB2*) were added to RetS27–185. Subsequently, the amplicon was recombined into pDONR201 (Invitrogen) to produce the plasmid pDONR201-RetS27–185. After verifying the nucleotide sequence via DNA sequencing, RetS27–185 was recombined into the destination vector pDEST-HisMBP (28) to create the expression vector pDEST-HMBP-RetS27–185. This vector is designed to produce RetS27–185 fused to the carboxy-terminal end of amino-terminally hexahistidine-tagged *E. coli* maltose binding protein (MBP).

Vector pDONR201-RetS41–185, containing a shortened segment of the sensory domain, was generated via PCR with the appropriate primer and using pDONR201-RetS27–185 as a template. Following sequence verification, RetS41–185 was recombined into pDEST-HisMBP to create the expression vector pDEST-HMBP-RetS41–185. The RetS41–185–S45C variant used for the dimerization studies was generated via site-directed mutagenesis with pDONR201-RetS41–185 serving as template. Subsequent recombination yielded the pDESTHMBP-RetS41–185–S45C vector.

The protein expression and purification protocols for RetS27–185, RetS41–185 ($RetS_{peri}$), and RetS41–185–S45C ($RetS_{peri}$-S45C) were identical. Single colonies of *E. coli* BL21(DE3) CodonPlus RIL cells (Stratagene, La Jolla, CA) containing the expression plasmid were used to inoculate 100 mL of Luria broth supplemented with glucose at 2 g/L, 100 μg/mL ampicillin, and 30 μg/mL chloramphenicol. The cell

culture was grown with shaking (225*g*) to saturation overnight at 37°C and then diluted 66-fold into 6 L of fresh medium. When the cell density reached midlog phase (OD_{600} = 0.5), the temperature was reduced to 30°C and isopropyl-β-D-thiogalacto-pyranoside (IPTG) was added to a final concentration of 1 mM. After 4 h, cells were harvested by centrifugation at 5000*g* for 15 min.

All of the following steps were carried out at 4°C. Cells were resuspended using a buffer containing 50 mM Tris-HCl, 150 mM NaCl, and 25 mM imidazole, pH 7.4 (buffer A) and 5 μL EDTA-free protease inhibitor cocktail (Sigma P8849) per milliliter of buffer (10 mL of buffer per gram of cell mass). Cells were lyzed through sonication and insoluble debris removed by centrifuging the cell extract at 40,000*g* for 30 min. The supernatant was filtered through a 0.45 μm polyethersulfone membrane and loaded onto to a 30 mL Ni-NTA chromatography column (Qiagen, Valencia, CA) pre-equilibrated in buffer A. The column was washed to baseline with buffer A and eluted with a linear imidazole gradient to 250 mM over 10 column volumes. Peak elution fractions were combined and His-TEV (S219V)-Arg (1 mg/100 mg of total protein) was added to effect the cleavage of His-MBP. The TEV protease-digest reaction mixture was dialyzed overnight against buffer A. After dialysis, the protein solution was filtered and applied to a 40-mL Ni-NTA Superflow column (Qiagen) pre-equilibrated with buffer A. Flow-through fractions containing the sensory domain were pooled and dialyzed overnight into buffer of 50 mM MES, 50 mM NaCl, pH 6.0 (buffer B). The sample was then applied to a 5 mL Heparin column (GE Healthcare,) pre-equilibrated with buffer B and was eluted with a linear salt gradient to 1M NaCl. Peak fractions were concentrated and loaded onto a HiPrep 26/60 Sephacryl S-200 HR column (GE Healthcare), pre-equilibrated in a buffer of 25 mM Tris-HCl, 150 mM NaCl, pH 7.4 (buffer C). The protein was judged to be >95% pure by sodium dodecyl sulfate-polyacrylamide gel electrophoresis (SDS-PAGE).

Preparation of selenomethionine- labeled $RetS_{peri}$

Selenomethionine-substituted $RetS_{peri}$ (SeMet-$RetS_{peri}$) was produced in the same nonauxotrophic strain of *E. coli* as used for routine protein production. The incorporation of externally added selenomethionine into the recombinant protein was accomplished by suppressing methionine biosynthesis (9). Initially, a 1 L overnight culture of the expression strain was grown in LB medium also containing 100 μg/mL ampicillin and 30 μg/mL chloramphenicol. The cells were washed twice in 100 mL of M9 selenomethionine growth media (Medicilon, Chicago, IL). The cells were resuspended in 100 mL of M9 selenomethionine growth media and used to inoculate four 1 L cultures containing M9 selenomethionine growth media and antibiotics. These cultures were grown with agitation at 37°C until the OD_{600nm} reading reached 0.2. At this point IPTG was added to a final concentration of 1 mM and the temperature lowered to 30°C. Cells were harvested the following morning. The purification of selenomethione-containing protein followed the same protocols as that for the native protein with the exception that 2 mM DTT was added to all but final buffer, which contained 1 mM tris (2-carboxyethyl) phosphine (TCEP) instead.

Limited proteolysis of the RetS sensory domain

A 1 mg/mL stock solution of thermolysin (Roche Molecular Biochemicals) in thermolysin buffer (10 mM Tris-HCl, 0.2M NaCl, and 2 m*M*$CaCl_2$, pH 8.0) was used for the limited proteolysis experiments. The RetS27–185 stock solution consisted of the protein at 1 mg/mL in buffer C. The five individual reactions were composed of 25 μL of RetS27–185 stock solution, 25 μL of 2X thermolysin buffer, and 0.5 μL of serial 1:4 dilutions of the thermolysin stock solution. The reactions were allowed to proceed for 1 h at 37°C before the protease was inactivated by the addition of 0.5 μL of 0.5*M* EDTA. Reaction products were initially visualized by SDS-PAGE. The precise molecular weights of select fragments were determined using LC-electrospray

ionization mass spectrometry. The peptide fragments that corresponded to the observed molecular masses were determined using the FindPep program (13).

Crystallization of $RetS_{peri}$ and SeMet-$RetS_{peri}$

High-throughput crystallization screening was conducted in the sitting-drop format by combining a solution of 17 mg/mL $RetS_{peri}$ in buffer C with commercially available crystallization matrices at volume ratios of 3:1, 1:1, and 1:3, where the protein solution was maintained at a constant volume of 0.3 μL throughout. Preliminary crystals were obtained from condition D4 of the IndexHT screen (Hampton Research). Hit optimization was carried out using the hanging drop vapor diffusion method at 18°C. In the optimized conditions crystals for both the native protein and SeMet-$RetS_{peri}$ were obtained from drops containing a 1:1 mixture of 17 mg/mL proteins in their respective storage buffers and a crystallization solution composed of 0.1M citric acid, 22.5% w/v polyethylene glycol 3350 and 10% v/v glycerol.

Data collection, structure solution, and refinement

Crystals of $RetS_{peri}$ were loop-mounted and flash-frozen in liquid nitrogen. Data sets were collected at beamline X-29A of the National Synchrotron Light Source using an ADSC Q315 CCD detector. Data were processed at the beamline using the HKL2000 program suite (29). Details of data collection and processing are provided in Table 2.1. The SeMet-$RetS_{peri}$ structure was determined using the single-wavelength anomalous dispersion (SAD) method. The location of heavy atoms, initial phase calculations, phase improvement through density modification, initial maps, and automated model building steps were all completed in the PHENIX program suite (41). PHENIX built nearly complete models for both molecules in the asymmetric unit. Iterative cycles of manual model adjustment using COOT2 (10) followed by refinement in PHENIX rapidly converged to produce the final structures. Model quality was assessed with PROCHECK2 (24) and the atomic

coordinates and structure factors have been deposited in the protein data bank (PDB) (37) with accession code 3JYB.

Protein–protein crosslinking

$RetS_{peri}$ was dialyzed into a buffer of 20 mM NaH_2PO_4 and 30 mM NaCl, pH 7.4. A 2 mM stock solution of bis (sulfosuccinimidyl) suberate (BS3) was prepared in water. The 50 µL reaction mixtures contained 10 µM $RetS_{peri}$ and 500 µM BS3. Crosslinking reactions were quenched by adding 20 µL of each reaction to 10 µL 150 mM Tris-HCl, pH 7.4. Crosslinking reactions containing MBP instead of $RetS_{peri}$were used as negative controls. Crosslinked samples were analyzed via SDS-PAGE.

Quantitative oligomerization assay

The $RetS_{peri}$-S45C variant was fluorescently labeled with Alexa Fluor 488 and Alexa Fluor 555 (Invitrogen) according to the manufacturer's instructions. Following overnight labeling, the modified proteins were separated from the unincorporated dye molecules through buffer exchange into a buffer of 20 mM Tris-HCl and 150 mM NaCl, pH 7.4. The degree of labeling of both the AlexaFluor 555-labeled form of the $RetS_{peri}$ variant ($RetS_{peri\text{-}555}$) and the Alexa Fluor 488-labeled form of the $RetS_{peri}$ variant ($RetS_{peri\text{-}488}$) were near 100% as assessed by UV-spectroscopy in conjunction with the estimated molar extinction coefficients of $RetS_{peri}$ and the respective fluorophores.

The fluorescence resonance energy transfer (FRET) measurements involved titrating a solution of 3 nM $RetS_{peri\text{-}488}$ with $RetS_{peri\text{-}555}$. Triplicate setups of 80 µL reactions containing 3 nM $RetS_{peri\text{-}488}$ and 0–100 µM $RetS_{peri\text{-}555}$ were transferred to a 96-well half area black polystyrene assay plate (Corning). Background fluorescence produced by $RetS_{peri\text{-}555}$ was accounted for by measuring and subtracting the signal of solutions that did not contain $RetS_{peri\text{-}488}$ but identical concentrations of $RetS_{peri\text{-}555}$.

A TECAN infinite M200 fluorescence intensity scanner (Tecan) was used for the experiment. The excitation wavelength was set to 430 nm, whereas the emission

spectrum was recorded in between in the wavelength range between 510 and 646 nm using a 4 nm step-size. The integration time was set to 20 μs and all scans were carried out at a room temperature of 24°C. Dimer formation was monitored by recording the decrease in the peak fluorescence of $RetS_{peri\text{-}488}$ at λ = 522 nm. Data were fit to Equation I (figure 2.1a) using *Matlab* (The MathWorks).

R_{5T} and R_{4T} are the total concentrations of $RetS_{peri\text{-}555}$ and $RetS_{peri\text{-}488,}$ respectively, F is the fluorescence measured at λ = 522 nm,F_{max} is the fluorescence measured at λ = 522 nm in absence of $RetS_{peri\text{-}555}$, F_{min} the residual fluorescence of $RetS_{peri\text{-}488}$ due to incomplete quenching even when all $RetS_{peri\text{-}488}$ is bound to $RetS_{peri\text{-}555}$, and K_d is the dissociation constant of the $RetS_{peri}$ dimer.

Results

The RetS sensory domain assumes a beta-sandwich fold reminiscent of carbohydrate binding proteins

To ensure that the complete sensory domain was contained in the cloned construct, the entire periplasmic region of RetS encompassing residues 27–185 was initially cloned and overexpressed. Subsequently, the domain boundaries were more precisely mapped through limited proteolysis of RetS27–185 to facilitate crystallization. Mass spectrometric analysis of the obtained fragments identified a relatively stable fragment comprising RetS residues 41–185 ($RetS_{peri}$). $RetS_{peri}$, overexpressed from a newly engineered plasmid, readily crystallized. SeMet-$RetS_{peri}$ crystals, while very small (~0.05 × 0.02 × 0.01 mm^3), produced X-ray diffraction to a resolution of 2.0 Å.

Forming an asymmetric dimer, there are two independent $RetS_{peri}$ molecules in asymmetric unit of the crystal. The structural differences between the backbone atoms of the two molecules are small as reflected in a root-mean-square-deviation (RMSD) of 0.4 Å. The electron density throughout the structure was excellent. However, the amino-terminal regions ranging from Ala-41 to Asn-47 are disordered and produced no discernable electron density in either molecule. All nonglycine residues of the final model reside either in the most favorable or in the allowed regions of the Ramachandran plot; and the overall geometry was comparable to other structures solved at the same resolution.

A cartoon drawing of the final $RetS_{peri}$ structure model is depicted in figure 2.2a, while the correlation between protein sequence and tertiary structure is visualized in figure 2.2b. The sensory domain of RetS adopts β-sandwich or jelly-roll fold formed by two opposing antiparallel β-sheets. The two sheets have a β1-β3-β8-β5-β6 and a β2-β9-β4-β7 topology, respectively. The β-sandwich structure is augmented by two alpha-helices, α-1 follows strand β-1 and the short α-2 helix is formed by the

carboxy-terminal residues of $RetS_{peri}$. The observed fold is characteristic of carbohydrate binding modules (CBMs). Consistent with this notion, a DALI-guided3 (20) search of the PDB identified CBMs and enzymes involved in carbohydrate degradation as the closest structural homologs of $RetS_{peri}$. While the structural conservation extends to both beta sheets, helix α-1 appears to be unique to $RetS_{peri}$. The position of this helix directly above the β1-β3-β8-β5-β6 sheet is interesting because in most of the related CBMs the equivalent β-sheets form the carbohydrate binding sites. We examined the temperature factors as well as intermolecular and intramolecular contacts of helix α-1 to evaluate whether or not this helix might be conformationally flexible and its conspicuous position perhaps the result of packing contacts. However, we found no intermolecular contacts involving α-1 within a 5 Å radius. On the other hand, α-1 forms a total of 18 intramolecular contacts with neighboring residues if a 4 Å distance cutoff is applied, burying a surface area of 525 $Å^2$. Furthermore, the positions of the two α-1 helices are identical for both molecules in the asymmetric unit and the average temperature factor of ~20 $Å^2$ for the main chain atoms also suggest a stable conformation. Therefore, the unique topology of this region suggests that the 7TM-DISM2 domains constitute a novel class of carbohydrate binding proteins.

Qualitative and quantitative evidence for $RetS_{peri}$ dimerization

The reversible oligomerization of RetS is believed to play a pivotal role in the regulation of RetS function. Consequently, we sought to establish whether or not $RetS_{peri}$ dimerization contributes to the stability of the RetS homodimer. Intuitively, we would have expected to observe a symmetric dimer in the crystal, but the two molecules that form the asymmetric unit display no twofold symmetry. While unusual this asymmetric dimer could nevertheless represent a biologically relevant dimer. However, when we compared the intermolecular contacts within the asymmetric unit to packing contacts between symmetry-related asymmetric units in the crystal, we

found them to be very similar. These packing arrangements are visualized in figure 2.2c, where molecules A and B represent the original asymmetric unit and B′ a molecule from a symmetry-related asymmetric unit. The buried surface area of the A·B and A·B′ interfaces are very similar at 610 and 629 $Å^2$, respectively. There are 21 interacting residue pairs at A·B interface and 23 such pairs at the A·B′ interface when a 4 Å distance cutoff is applied (this cutoff was chosen because it represents the default value in programs such as Ligplot3 (40) that are designed to analyze intermolecular contacts). Twenty of these interactions are found at both interfaces. Distances for the four contacts that did not match ranged between 3.7 and 4 Å, suggesting that they make only small contributions to the stability of the respective intermolecular interactions. These similarities suggest that the dimer observed in the asymmetric unit arose due to crystal packing contacts and does not represent the biological unit of the protein. Otherwise, if the interactions in the asymmetric unit were indeed representative of the solution state then $RetS_{peri}$ should be forming higher order oligomers or even polymerize in solution. This was not observed in the crosslinking experiments described later.

Since the nonphysiological pH of 3.0 of the crystallization conditions could have caused a biological $RetS_{peri}$ oligomer to dissociate, protein–protein crosslinking using chemical BS3 was employed to probe for dimer formation at neutral pH. Monomeric *E. coli* MBP served as negative control. After crosslinking MBP still migrated as a monomer on an SDS-polyacrylamide gel, while a substantial portion of $RetS_{peri}$ had shifted to a higher band corresponding to the molecular weight of a $RetS_{peri}$ dimer (figure 2.3a). Higher order oligomers were not observed.

Although the crosslinking result demonstrates $RetS_{peri}$ dimerization, a substantial fraction of $RetS_{peri}$ failed to crosslink even when large excess of crosslinking agent and extended reaction times were used. This finding is consistent with the presence of monomer-dimer equilibrium rather than a purely dimeric state. A FRET-based assay

was developed to validate this hypothesis and quantify the strength of the $RetS_{peri}$-$RetS_{peri}$ interactions. A low concentration of Alexa-Fluor-488-labeled $RetS_{peri}$-S45C ($RetS_{peri-488}$) was titrated with an Alexa-Fluor-555-labeled form of the same $RetS_{peri}$ variant ($RetS_{peri-555}$). Dimerization was monitored by observing the quenching of the Alexa Fluor 488 fluorescence at λ = 522 nm. The concentration of the $RetS_{peri-488}$ was maintained more than a 100-fold below the dissociation constant (K_d) for $RetS_{peri}$ dimer formation because here virtually all of the protein should be monomeric. This optimal concentration of $RetS_{peri-488}$ was determined in an iterative process where titration experiments were carried out at concentrations of 50, 10, and finally 3 nM of $RetS_{peri-488}$ and fit to Equation I (figure 2.1a). The two higher concentrations of the protein resulted in a poor fit and a K_d value that suggested that a substantial proportion of $RetS_{peri-488}$ was dimeric at the outset of the experiment. A second important consideration relates to the fact that, as the concentration of $RetS_{peri-555}$ is increased during the titration experiment, a large fraction of this protein is already dimeric and therefore not available for binding to $RetS_{peri-488}$. To properly model $RetS_{peri}$ dimerization, it was therefore necessary to express the concentration of the $RetS_{peri-555}$ monomer as a function of the total concentration of $RetS_{peri-555}$ and the K_d. Usually, equations for binding isotherms are arranged to express the amount of complex formed in terms of the variable concentration of one of the binding partners. However, when this was done for the modified isotherm the resulting cubic equation was solvable but the obtained solution was awkwardly long (figure 2.1b). Therefore, the data were fit to the rearranged and thus simpler Equation I (figure 2.1a). This equation is valid under the assumption that the fluorescent labels do not influence the monomer-dimer equilibrium, which is based on the observation that the S45C mutation used to mediate thiol-based labeling is located in a structurally disordered region that does not appear to constitute a pivotal part of the sensory domain. Background-corrected example graphs are presented in figure 2.3b. The resulting

FRET data are plotted in figure 2.3c; and fitting Equation I to these data yielded a dissociation constant of K_d = 580 ± 50 nM for $RetS_{peri}$ dimerization. If $RetS_{peri\text{-}555}$ dimerization is not taken into consideration and the data are simply fit to a conventional isotherm, the fit is poor and the obtained K_d incorrect (dashed line in figure 2.3c).

Discussion

The putative ligand binding site of $RetS_{peri}$

The crystal structure suggests that RetS is regulated by a carbohydrate-based moiety. However, since the natural ligand of RetS is currently not known, the common strategy for mapping the ligand binding site involving a mutational analysis coupled with *in vitro* binding studies could not be employed. Nevertheless, insights could be obtained by comparing $RetS_{peri}$ to the altogether eight structurally homologous proteins, where the positions of the ligand binding sites are known. Protein–carbohydrate complexes have been reported for the related family 4 CBM of Lam16A from *Thermotoga maritima* (*Tm*CBM4-2, PDB code 1gui) (4), the family 6 CBM *Sd*Aga16B-CBM6-2 of the β-agarase Aga16B from *Saccharophagus degradans* (PDB code: 2CDO) (5), and the family 15 CBM of the *Cellvibrio japonicas*Xylanase 10C, (*Cj*Xyn10C-m, PDB code: 1US2) (30). In addition, the binding sites of the following proteins have also been mapped and were therefore included in the analysis: the carbohydrate-recognition domain of the human glycoprotein sorting receptor p58/ERGIC-53 (PDB code: 1R1Z) (38) the carbohydrate recognition domain of the cargo receptor Emp46p from *Saccharomyces cerevisiae* (PDB code: 2A6W) (32), the carbohydrate binding module of xylanase 10A from the thermophilic bacterium *Rhodothermus marinus* (*Rm*Xyn10A-CBM4-2, PDB code: 1K42) (34), the catalytic domain of the endoglucanase CelB from *Streptomyces lividans*, (*Sl*CelB-2, PDB code: 1NLR) (36), and family 32 carbohydrate-binding protein *Ye*CBM32 from *Yersinia enterolitica* (PDB code: 2JDA) (1). Although all eight proteins share the same fold, their ligand binding sites cluster to not one but two regions when superimposed. In *Ye*CBM32 and *Sd*Aga16B-CBM6-2, the ligand binding sites are located between the two beta sheets, involving residues equivalent to the carboxy-terminal end of β-2, the amino-terminal end of β-9, and residues from the two connected loop regions in

$RetS_{peri}$. This pocket is not present in $RetS_{peri}$ suggesting that its binding cleft is located elsewhere.

In the other six homologous structures, the critical residues map to structurally conserved section of the proteins that corresponds to the β1-β3-β8-β5-β6 sheet in $RetS_{peri}$. In the *Tm*CBM4-2 and *Cj*Xyn10C-m complexes, the entire beta-sheet forms an extended cleft, where their respective oligosaccharide ligands are bound, while the ligand binding site in the other four proteins are smaller, covering only part of the beta-sheet. In $RetS_{peri}$ helix α-1 alters the topology of this the corresponding surface area. In fact, α-1 effectively occupies the same space as the bound ligands in *Tm*CBM4-2 and *Cj*Xyn10C-m (figure 2.4a). However, together with residues from the beta sheet and several surrounding loops α-1 does create three large grooves that appear well-suited for ligand binding. The pocket that most closely coincides with the prevalent binding pockets observed in the related proteins is formed by the loop connecting β-1 and α-1, the amino terminal regions of strands β3 and β5, the carboxy-terminal ends of strands β1, β8, and β6 and the loop regions between β-2 and β-3 as well as those between β-8 and β-9 (figure 2.4b,c).

The hypothesis that this site indeed constitutes the ligand binding pocket may be evaluated from two additional angles. The solvent-accessible surface area of $RetS_{peri}$ was color-coded according to the degree of sequence conservation using the ConSurf (14). Those regions with the three highest conservation scores were colored brightly, while the remainder of the surface was kept white (figure 2.4b,c). Remarkably, 7 of the 10 amino acids that received the highest conservation scores map to the β1-β3-β8-β5-β6 beta sheet. Four of these seven residues, Trp-90, Tyr-117, Arg-162, and Ser-164 are part of the pocket that was identified from the structural comparison with other binding sites. Trp-90 is one of only two amino acids that are strictly conserved in all 32 of the homologous protein sequences that were used for this analysis.

Finally, the predicted binding site may also be assessed by analyzing the types of amino acids that form this pocket. Tryptophan, arginine, asparagine, glutamic acid, tyrosine, and histidine display the highest propensities for participating in carbohydrate binding (26). The highly conserved Trp-90, Tyr-117, and Arg-162 fall into this category. Other residues in the binding pocket also feature prominently in carbohydrate binding sites: Gln-59, Arg-61, Gln-112, Arg-134, and Asn-166, and the aromatic residues Tyr-113 and His-129. Pro-86 and Thr-164 constitute the only unusual residues among the amino acids that are form the putative ligand binding site (Figure 2.4b,c). In summary, three independent indicators—structural conservation, sequence conservation, and composition of the putative binding pocket—all point toward the same location of the ligand binding site and suggest that the elusive ligand is a carbohydrate moiety. Ultimate confirmation of these findings, however, will require the identification of the natural ligand of RetS.

Implications of $RetS_{peri}$ dimerization for the RetS-GacS signaling mechanism

RetS is an unusual sensor kinase because at least one of its signaling modes does not require its kinase activity but relies on direct interactions with GacS kinase to prevent phosphate transfer in the GacS/GacA TCS (16). The kinase domains of both enzymes appear to be sufficient for this interaction. The model assumes ligand binding to the periplasmic sensory domain disrupts the RetS dimer, but how is this signal communicated across the inner cell membrane? The hypothesis that the RetS sensory domain mediates the upregulation of T3SS-related gene expression also appears to be at odds with a previous study, where deletion of the sensory domain did not cause a decrease but a slight increase in virulence associated with the T3SS (23). Our finding that $RetS_{peri}$ alone is capable of dimer formation offers a possible explanation for this apparent contradiction as it suggests that the sensory domain is required for repression as well as activation of the T3SS. Ligand-free $RetS_{peri}$ likely dimerizes and prevents RetS-GacS interactions by stabilizing the RetS homodimer.

The unknown ligand could act by disrupting the interface between the two sensory domains, and thus favor RetS-GacS heterodimer formation. Consistent with the previously published results this model would explain why a deletion of the sensory domain did not result in a repression of the T3SS, since such a deletion, just as ligand binding, would favor a RetS-GacS complex.

Conclusions

The crystal structure of the RetS sensory domain, the first representative structure for the 7TM-DISM2 domain family, revealed a fold closely related to carbohydrate binding modules, suggesting that RetS function is regulated by a carbohydrate-based ligand. While the crystal structure does not unambiguously reveal the ligand binding site, structural homology, sequence conservation, and amino acid composition suggest that the ligand likely binds to a pocket formed by one of the two beta sheets and helix α-1. $RetS_{peri}$ dimerizes with a submicromolar dissociation constant, suggesting that dimerization of the RetS sensory domain plays a role in both stabilizing the RetS homodimer and, on ligand binding, in shifting the equilibrium toward RetS-GacS heterodimer formation.

Acknowledgements

The authors thank Dr. Keith Ray for his assistance with the mass spectrometry work.

References

1. Abbott DW, Hrynuik S, Boraston AB. 2007. Identification and characterization of a novel periplasmic polygalacturonic acid binding protein from Yersinia enterolitica. J Mol Biol. 367:1023–1033.
2. Anantharaman V, Aravind L. 2003. Application of comparative genomics in the identification and analysis of novel families of membrane-associated receptors in bacteria. BMC Genomics. 4:34.
3. Ang S, Horng YT, Shu JC, Soo PC, Liu JH, Yi WC, Lai HC, Luh KT, Ho SW, Swift S. 2001. The role of RsmA in the regulation of swarming motility in Serratia marcescens. J Biomed Sci. 8:160–169.
4. Boraston AB, Nurizzo D, Notenboom V, Ducros V, Rose DR, Kilburn DG, Davies GJ. 2002. Differential oligosaccharide recognition by evolutionarily-related beta-1,4 and beta-1,3 glucan-binding modules. J Mol Biol. 319:1143–1156.
5. Brunger AT. 1992. Free R value: a novel statistical quantity for assessing the accuracy of crystal structures. Nature. 355:472–475.
6. Cheng KH, Leung SL, Hoekman HW, Beekhuis WH, Mulder PG, Geerards AJ, Kijlstra A. 1999. Incidence of contact-lens-associated microbial keratitis and its related morbidity. Lancet. 354:181–185.
7. Crouch Brewer S, Wunderink RG, Jones CB, Leeper KV, Jr. 1996. Ventilator-associated pneumonia due to Pseudomonas aeruginosa. Chest. 109:1019–1029.
8. DeLano WL. 2001. The PyMOL molecular graphics system. San Carlos, CA: DeLano Scientific LLC.
9. Doublie S. 2007. Production of selenomethionyl proteins in prokaryotic and eukaryotic expression systems. Methods Mol Biol. 363:91–108.
10. Emsley P, Cowtan K. 2004. Coot: model-building tools for molecular graphics. Acta Crystallogr D Biol Crystallogr. 60: 2126–2132.
11. Feltman H, Schulert G, Khan S, Jain M, Peterson L, Hauser AR. 2001. Prevalence of type III secretion genes in clinical and environmental isolates of Pseudomonas aeruginosa. Microbiology (Reading England). 147: 2659–2669.
12. Garau J, Gomez L. 2003. Pseudomonas aeruginosa pneumonia. Curr Opin Infect Dis. 16:135–143.
13. Gattiker A, Bienvenut WV, Bairoch A, Gasteiger E. FindPept, a tool to identify unmatched masses in peptide mass finger printing protein identification. Proteomics 2002; 2: 1435–1444.
14. Goldenberg O, Erez E, Nimrod G, Ben-Tal N. 2009. The ConSurf-DB: pre-calculated evolutionary conservation profiles of protein structures. Nucleic Acids Res. 37:323– D327.

15. Goodman AL, Kulasekara B, Rietsch A, Boyd D, Smith RS, Lory S. 2004. A signaling network reciprocally regulates genes associated with acute infection and chronic persistence in Pseudomonas aeruginosa. Dev Cell. 7:745–754.
16. Goodman AL, Merighi M, Hyodo M, Ventre I, Filloux A, Lory S. 2009. Direct interaction between sensor kinase proteins mediates acute and chronic disease phenotypes in a bacterial pathogen. Genes Dev. 23:249–259.
17. Gouet P, Robert X, Courcelle E. 2003. ESPript/ENDscript: extracting and rendering sequence and 3D information from atomic structures of proteins. Nucleic Acids Res. 31:3320–3323.
18. Heeb S, Blumer C, Haas D. 2002. Regulatory RNA as mediator in GacA/RsmA-dependent global control of exoproduct formation inPseudomonas fluorescens CHA0. J Bacteriol. 184:1046–1056.
19. Henshaw J, Horne-Bitschy A, van Bueren AL, Money VA, Bolam DN, Czjzek M, Ekborg NA, Weiner RM, Hutcheson SW, Davies GJ,Boraston AB, Gilbert HJ. 2006. Family 6 carbohydrate binding modules in beta-agarases display exquisite selectivity for the non-reducing termini of agarose chains. J Biol Chem. 281:17099–17107.
20. Holm L, Kaariainen S, Wilton C, Plewczynski D. 2006. Using Dali for structural comparison of proteins. Curr Protoc Bioinformatics. Chapter 5:Unit 5.5.
21. Kay E, Humair B, Denervaud V, Riedel K,Spahr S, Eberl L, Valverde C, Haas D. 2006. Two GacA-dependent small RNAs modulate the quorum-sensing response in Pseudomonas aeruginosa. J Bacteriol. 188:6026–6033.
22. Labrec EH, Schneider H, Magnani TJ, Formal SB. 1964. Epithelial cell penetration as an essential step in the pathogenesis of bacillary dysentery. J Bacteriol. 88:1503–1518.
23. Laskowski MA, Kazmierczak BI. 2006. Mutational analysis of RetS, an unusual sensor kinase-response regulator hybrid required forPseudomonas aeruginosa virulence. Infect Immun. 74:4462–4473.
24. Laskowski RA, MacArthur MW, Moss DS, Thornton JM. 1993. PROCHECK: a program to check the steriochemical quality of protein structures. J Appl Cryst. 26:282–291.
25. Liaw SJ, Lai HC, Ho SW, Luh KT, Wang WB. 2003. Role of RsmA in the regulation of swarming motility and virulence factor expression inProteus mirabilis. J Med Microbiol. 52:19–28.
26. Malik A, Ahmad S. 2007. Sequence and structural features of carbohydrate binding in proteins and assessment of predictability using a neural network. BMC Struct Biol. 7:1
27. Mulcahy H, O'Callaghan J, O'Grady EP, Macia MD, Borrell N, Gomez C, Casey PG, Hill C, Adams C, Gahan CG, Oliver A, O'Gara F. 2008. Pseudomonas aeruginosa RsmA plays an important role during murine infection by

influencing colonization, virulence, persistence, and pulmonary inflammation. Infect Immun. 76:632–638.
28. Nallamsetty S, Austin BP, Penrose KJ, Waugh DS. 2005. Gateway vectors for the production of combinatorially-tagged His6-MBP fusion proteins in the cytoplasm and periplasm of Escherichia coli. Protein Sci. 14:2964–2971.
29. Otwinowski ZM, W. 1997. HKL2000. Methods Enzymol. 276:307–326.
30. Pell G, Szabo L, Charnock SJ, Xie H, Gloster TM, Davies GJ, Gilbert HJ. 2004. Structural and biochemical analysis of Cellvibrio japonicusxylanase 10C: how variation in substrate-binding cleft influences the catalytic profile of family GH-10 xylanases. J Biol Chem. 279:11777–11788.
31. Richards MJ, Edwards JR, Culver DH, Gaynes RP. 1999. Nosocomial infections in medical intensive care units in the United States. National Nosocomial Infections Surveillance System. Crit Care Med. 27:887–892.
32. Satoh T, Sato K, Kanoh A, Yamashita K, Yamada Y, Igarashi N, Kato R, Nakano A, Wakatsuki S. 2006. Structures of the carbohydrate recognition domain of Ca^{2+}-independent cargo receptors Emp46p and Emp47p. J Biol Chem. 281:10410–10419.
33. Shaver CM, Hauser AR. 2004. Relative contributions of Pseudomonas aeruginosa ExoU, Exo S, and Exo T to virulence in the lung Infect Immun. 72:6969–6977.
34. Simpson PJ, Jamieson SJ, Abou-Hachem M, Karlsson EN, Gilbert HJ, Holst O, Williamson MP. 2002. The solution structure of the CBM4–2 carbohydrate binding module from a thermostable Rhodothermus marinus xylanase. Biochemistry. 41:5712–5719.
35. Singh PK, Schaefer AL, Parsek MR, Moninger TO, Welsh MJ, Greenberg EP. 2000. Quorum-sensing signals indicate that cystic fibrosis lungs are infected with bacterial biofilms. Nature. 407:762–764.
36. Sulzenbacher G, Shareck F, Morosoli R, Dupont C, Davies GJ. 1997. The Streptomyces lividans family 12 endoglucanase: construction of the catalytic cre, expression, and X-ray structure at 1.75 Å resolution. Biochemistry. 36:16032–16039.
37. Sussman JL, Lin D, Jiang J, Manning NO, Prilusky J, Ritter O, Abola EE. 1998. Protein data bank (PDB): database of three-dimensional structural information of biological macromolecules. Acta Crystallogr D Biol Crystallogr. 54:1078–1084.
38. Velloso LM, Svensson K, Pettersson RF, Lindqvist Y. 2003. The crystal structure of the carbohydrate-recognition domain of the glycoprotein sorting receptor p58/ERGIC-53 reveals an unpredicted metal-binding site and conformational changes associated with calcium ion binding. J Mol Biol. 334:845–851.

39. Ventre I, Goodman AL, Vallet-Gely I, Vasseur P, Soscia C, Molin S, Bleves S, Lazdunski A, Lory S, Filloux A. 2006. Multiple sensors control reciprocal expression of Pseudomonas aeruginosa regulatory RNA and virulence genes. Proc Natl Acad Sci USA. 103:171–176.
40. Wallace AC, Laskowski RA, Thornton JM. 1995. LIGPLOT: a program to generate schematic diagrams of protein-ligand interactions.Protein Eng. 8:127–134.
41. Zwart PH, Afonine PV, Grosse-Kunstleve RW, Hung LW, Ioerger TR, McCoy AJ,McKee E, Moriarty NW, Read RJ,Sacchettini JC, Sauter NK, Storoni LC, Terwilliger TC, Adams PD. 2008. Automated structure solution with the PHENIX suite. Methods Mol Biol. 426:419–435.

Table 2.1 Data Collection and Refinement Statistics for the SeMet-RetS$_{peri}$ Crystal

Data collection statistics	
Wavelength (Å)	0.97900
Space group	$P2_12_12_1$
Unit cell parameters (Å)	a = 51.164; b = 67.193; c = 86.214
Molecules/asymmetric unit	2
Resolution (Å) (last shell 2.11–2.04)	30.00–2.04
Total reflections	255,128
Unique reflections	19,459
Completeness (%)	99.9 (99.2)[a]
I/σ	26.3 (3.40)
R_{merge} (%)[b]	9.0 (39.5)
Refinement	
Resolution (highest resolution shell) (Å)	29.62–2.04 (2.1–2.04)
No. reflections	17870 (1265)
R_{work}[c]/R_{free}[d] (%)	19.9 (20.1)/23.5 (27.5)
No. total atoms	2403
No. protein atoms	2298
No. water atoms	105
Overall mean B factor value (Å^2)	18.747
RMSD bond lengths (Å)	0.007
RMSD bond angles (°)	1.119

a. The values in parentheses relate to the highest resolution shell.

b. $R_{merge} = \Sigma |I - \langle I \rangle| / \Sigma I$, where I is the observed intensity and ‹I› is the average intensity obtained from multiple observations of symmetry-related reflections after the rejection of significant outliers.

c. $R = \Sigma ||Fo| - |Fc|| / \Sigma |Fo|$, where F_o and F_c are the observed and calculated structure factors, respectively.

d. R_{free} defined by Brunger (5).

a) $$R_{5T} = \frac{K_d(F_{max} - F_{min})}{F - F_{min}}[\frac{2(F_{max} - F_{min})}{F - F_{min}} - 3] + R_{4T}\frac{F_{max} - F}{F_{max} - F_{min}} + K_d \qquad \textbf{(Equation I)}$$

b)
$$\Delta F = -\frac{K_d - 2R_{4T} - R_{5T}}{3R_{4T}} - (2^{1/3}(-(K_d - 2R_{4T} - R_{5T})^2 + 3R_{4T}(K_d + R_{4T} + 2R_{5T})))/(3R_{4T}(-2K_d^3 + 21K_d^2R_{4T} - 33K_dR_{4T}^2 - 2R_{4T}^3 + 6K_d^2R_{5T} -$$
$$15K_dR_{4T}R_{5T} + 6R_{4T}^2R_{5T} - 6K_dR_{5T}^2 - 6R_{4T}R_{5T}^2 + 2R_{5T}^3 +$$
$$3\sqrt{3}\sqrt{-K_d^4R_{4T}^2 + 6R_{4T}^3K_d^3 + 15K_d^2R_{4T}^4 + 8K_dR_{4T}^5 - 6K_d^3R_{4T}^2R_{5T} + 78K_d^2R_{4T}^3R_{5T} - 24K_dR_{4T}^4R_{5T} + 15K_d^2R_{4T}^2R_{5T}^2 + 24K_dR_{4T}^3R_{5T}^2 - 8K_dR_{4T}^2R_{5T}^3})^{1/3}) +$$
$$\frac{1}{32^{1/3}R_{4T}}(-2K_d^3 + 21K_d^2R_{4T} - 33K_dR_{4T}^2 - 2R_{4T}^3 + 6K_d^2R_{5T} - 15K_dR_{4T}R_{5T} + 6R_{4T}^2R_{5T} - 6K_dR_{5T}^2 - 6R_{4T}R_{5T}^2 + 2R_{5T}^3 +$$
$$3\sqrt{3}\sqrt{-K_d^4R_{4T}^2 + 6R_{4T}^3K_d^3 + 15K_d^2R_{4T}^4 + 8K_dR_{4T}^5 - 6K_d^3R_{4T}^2R_{5T} + 78K_d^2R_{4T}^3R_{5T} - 24K_dR_{4T}^4R_{5T} + 15K_d^2R_{4T}^2R_{5T}^2 + 24K_dR_{4T}^3R_{5T}^2 - 8K_dR_{4T}^2R_{5T}^3})^{1/3}$$

c) $$\Delta F = \frac{1}{2R_{4T}}(K_d + R_{4T} + R_{5T} - \sqrt{(K_d + R_{4T} + R_{5T})^2 - 4R_{4T}R_{5T}})$$

Definitions

R_4, R_5 - concentration of monomeric $RetS_{peri\text{-}488}$ and $RetS_{peri\text{-}555}$, respectively.

R_{4d}, R_{5d} - concentration of homo-dimeric $RetS_{peri\text{-}488}$ and $RetS_{peri\text{-}555}$, respectively.

R_{4T}, R_{5T} - total concentration of $RetS_{peri\text{-}488}$ and $RetS_{peri\text{-}555}$, respectively.

R_{45} - concentration of $RetS_{peri\text{-}488}$-$RetS_{peri\text{-}555}$ "hetero-dimer".

F - fluorescence at λ=522 nm.

F_{max} - fluorescence at λ=522 nm in absence of $RetS_{peri\text{-}555}$.

F_{min} - residual fluorescence of $RetS_{peri\text{-}488}$ due a transfer efficiency to $RetS_{peri\text{-}555}$ of less than 100%.

$$\Delta F = \frac{F_{max} - F}{F_{max} - F_{min}}$$

Figure 2.1 The final equations to fit the FRET data

a) Equation I
b) Alternative equation but mathematically equivalent to Equation I
c) Equation for the standard binding isotherm solved for ΔF

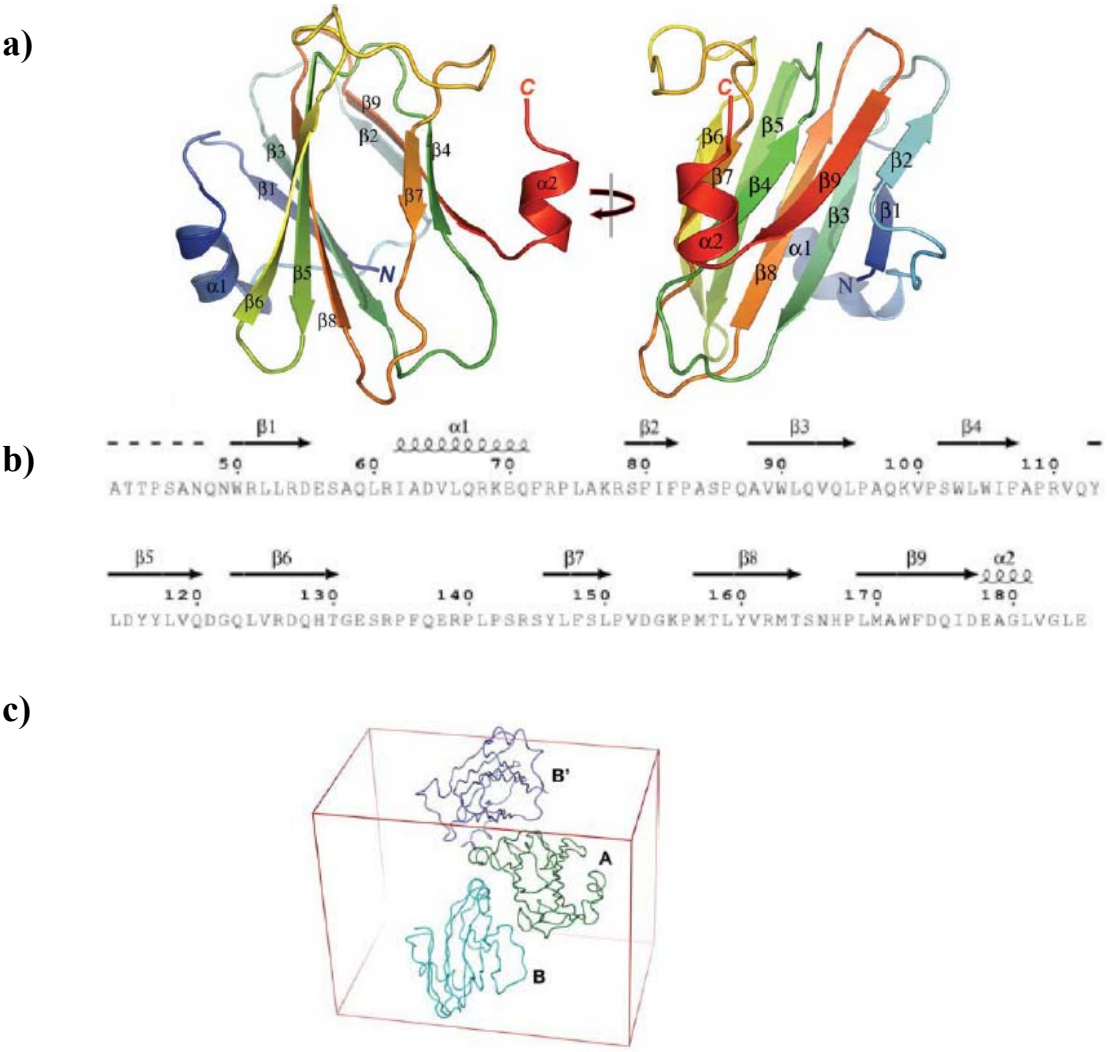

Figure 2.2 Structural determination and analysis of $RetS_{peri}$

a) Two orthogonal views of the PYMOL29-generated cartoon representation of the $RetS_{peri}$ structure. All secondary structure elements are labeled. b) Alignment of the secondary structure elements identified from the crystal structure with the primary structure $RetS_{peri}$. This figure was generated with ESPript.30 c) The asymmetric unit of the crystal consists of molecules A and B. The contacts between A and B closely resemble the packing contacts between A and the symmetry-related B' molecule, suggesting that the dimer in the asymmetric unit arose from crystal packingcontacts.

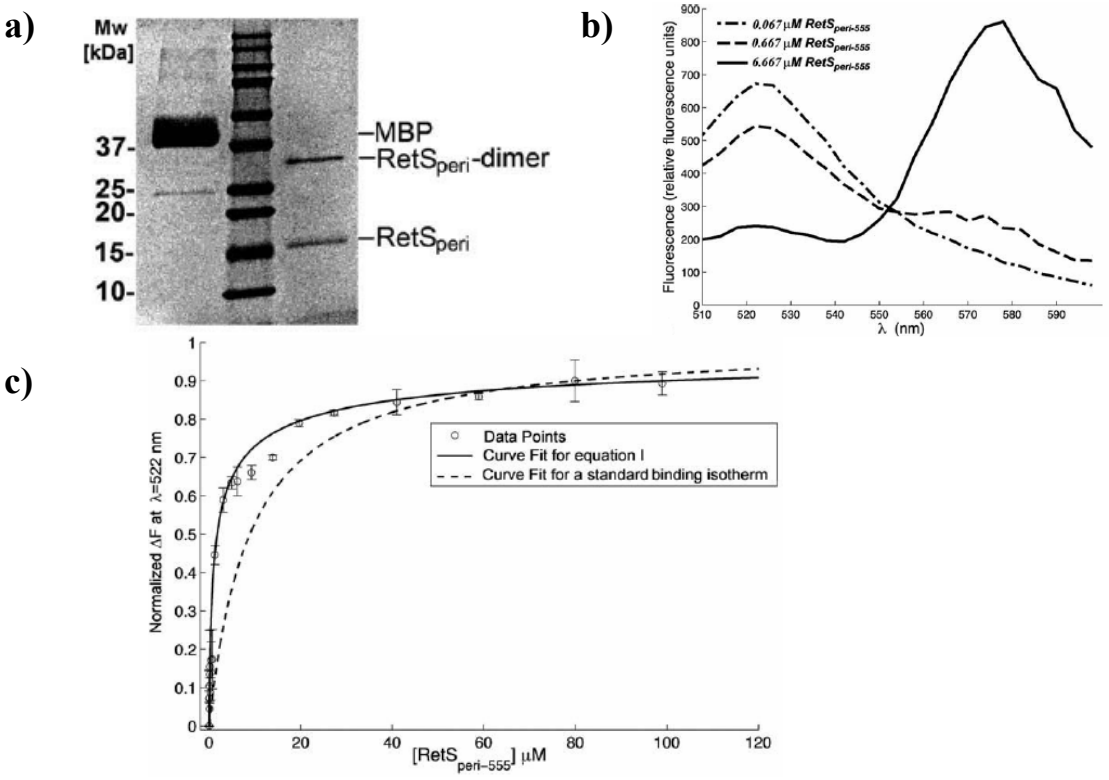

Figure 2.3 Demonstration and quantification of $RetS_{peri}$ dimerizatioin

(a) SDS-PAGE analysis of the BS3-mediated crosslinking experiment with $RetS_{peri}$. Shown in the lanes are from left to right: MBP, the molecular weight makers, and $RetS_{peri}$. (b) Sample plots of fluorescence spectra obtained during the FRET-based dimerization assay at three different concentrations of $RetS_{peri\text{-}555}$. The spectra are generated by subtracting the background fluorescence produced by the same concentrations of $RetS_{peri\text{-}555}$ in the absence of $RetS_{peri\text{-}488}$ from the raw data. (c) Shown is the resulting curve when Equation I is fit to the FRET data where $\Delta F = \frac{F_{max} - F}{F_{max} - F_{min}}$. The error bars signify the standard deviation of the ΔF calculated from the readings obtained from triplicate setups. For comparative purposes, the data were also fit to the conventional binding isotherm (figure 2.1c), which does not consider the increasing amounts $RetS_{peri\text{-}555}$ dimer. This fit is shown as a dashed line.

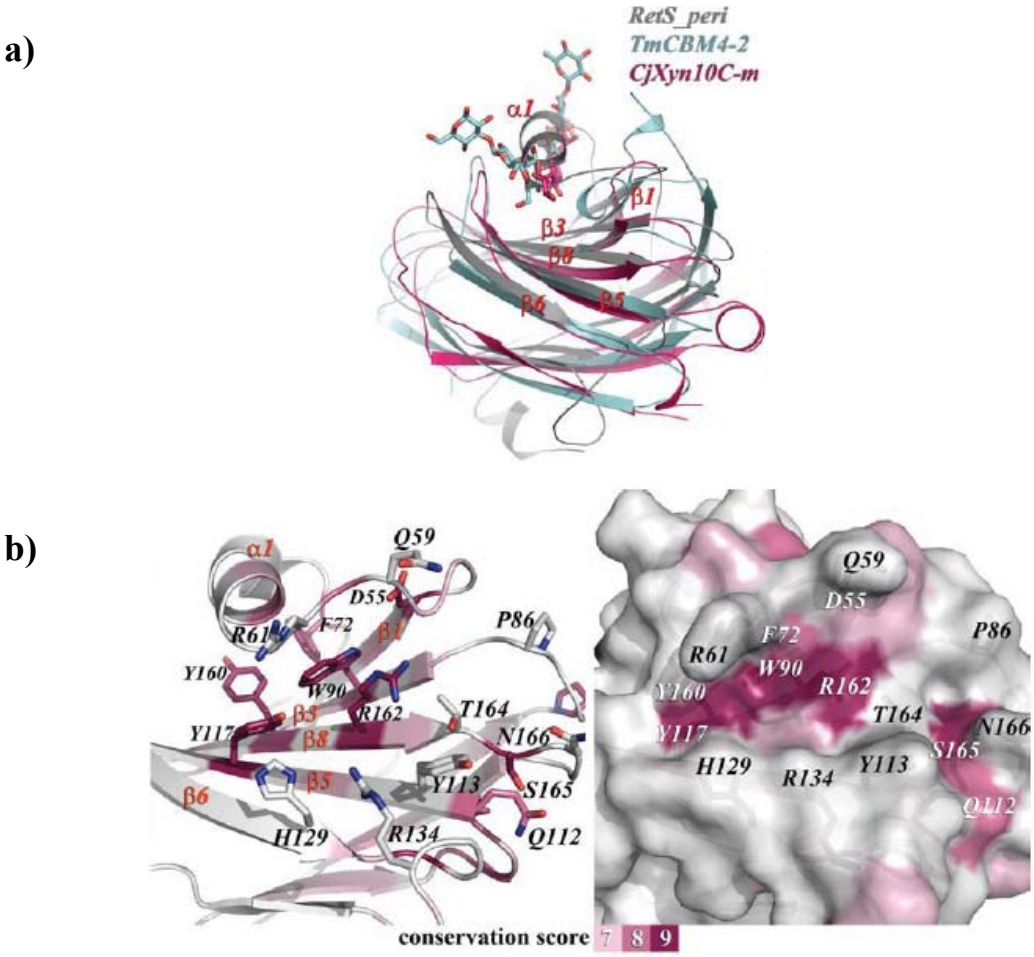

Figure 2.4 Structural analysis for RetSperi ligand binding site prediction
(a) Superposition of $RetS_{peri}$, TmCBM4-2, and CjXyn10C-m. TmCBM4-2 and CjXyn10C-m have both been crystallized in complex with xylopentaose. The positions of the ligands in the latter complexes coincide with helix a-1 in $RetS_{peri}$. (b) Left: the backbone structure of $RetS_{peri}$ has been colored according to the level of sequence conservation among proteins with related 7TM-DISM2 domains. Also, shown are side chains and labels of the seven broadly conserved amino acids that are concentrated in this section of the protein and of those amino acids that form the putative binding site. (b) Right: the solvent-accessible surface area of $RetS_{peri}$, viewed from the same perspective and also color-coded according to the level of sequence conservation, reveals a large cavity that is proposed to constitute the ligand binding site.

Chapter Three

Characterization of the Ligand Binding and Dimerization of RetS Periplasmic Sensory Domain *In vitro* and *In vivo*

ABSTRACT

To regulate gene expression for TTSS and biofilm formation in *P. aeruginosa*, the two-component system sensor kinase RetS participates in Gac/Rsm signaling pathway. The complexity in the domain architecture of RetS implies that this hybrid sensor kinase might be involved in additional signaling pathways and intermolecular cross-talk with other upstream or downstream TCS proteins. However, all to date attempts to detect RetS intrinsic kinase activity have failed. The mechanism whereby RetS executes its cellular signal transduction task remains unclear. To bring to light to the signaling mechanism of RetS, we focus on the periplasmic sensory domain ($RetS_{peri}$) which is a presumed starting point of RetS signaling. Being a potential drug target, $RetS_{peri}$ is putatively a trigger that turns on RetS cellular signaling activity. The only reported functional study targeting this domain suggests it might inhibit RetS-induced TTSS expression. However, the specific functional role of $RetS_{peri}$ in biofilm formation regulation has not yet been examined. Except for testing the current GacS-RetS signaling model and our hypothesis, the objective of this chapter is to resolve the precise mechanism where the ligand binding and dimerization activities of $RetS_{peri}$ regulate RetS-controlled biofilm formation. Another aim of this work is to identify the natural ligand of $RetS_{peri}$ or a synthetic compound that could affect biofilm formation through $RetS_{peri}$ mediated signaling.

Introduction

One remarkable trait of *P. aeruginosa* is its high drug-resistance assisted by the biofilm formation on abiotic and biotic surfaces, especially in CF patient's lungs (4). Like many other bacterial pathogens, *P. aeruginosa* utilizes two-component systems (TCSs) for gene expression regulation (7, 20). TCSs act by sensing extracellular signals and subsequently transducing these signals to mediate target gene expression. RetS is one of the crucial TCS proteins that regulate TTSS and biofilm assisted pathogenesis (8, 17), Influencing the expression of more than 400 genes, RetS has been demonstrated to be a critical negative regulator of biofilm formation (8). Different from typical sensor kinases, RetS does not have detectable kinase activity (9, 10). In addition, unlike other TCS hybrid sensors, RetS possesses two distinct response regulator domains implying that RetS might be part of a complex regulatory network involving communication with other TCSs (8). However, whether the conserved phosphorylation residues (histidine and aspartate) are required for RetS signaling function is under debate (8, 16). Our study focused on the $RetS_{peri}$ domain, which is a putative starting point for RetS signaling (6). Solving the mystery of the role of this signal sensing domain will provide invaluable information to build up our understanding of the RetS signal transduction mechanism.

Based on the RetS-GacS signaling model, we have proposed that the functional role of signal sensing by $RetS_{peri}$ is to disrupt the homo-dimerization of RetS and in turn to promote RetS-GacS hetero-dimerization in the cytoplasm (8, 12). In this study our objectives are to test the current hypothesis as well as mapping of the ligand binding site and dimer interface of $RetS_{peri}$. Firstly, we demonstrate that both predicted dimerization sites exist *in vitro*. Furthermore, we developed different experimental strategies to either eliminate or enhance $RetS_{peri}$ dimerization and examine the resulting changes in biofilm-related gene expression and phenotype. Secondly, targeting the two putative ligand binding pockets (12, 23), we carried out

mutational analyses combined with an *in vivo* functional assay with the goal of uncovering the signaling role of signal sensing capability of $RetS_{peri}$.

Finally, $RetS_{peri}$ is a potential target for the development of antimicrobial agents against biofilm gene expression in *P. aeruginosa*. Therefore, we aim to identify the natural or synthetic ligands that are able to affect biofilm formation specifically through interaction with $RetS_{peri}$ in *P. aeruginosa.* The crystal structure of $RetS_{peri}$, which we determined and characterized, suggests that the mystery ligand is a carbohydrate moiety. This notion is very appealing because RetS regulates the production of biofilm-related exopolysaccharides. But whether the source of the ligand is the host or *P. aeruginosa* itself is still unknown. High throughput ligand screening of human made carbohydrate compounds did not reveal any potential leads for the RetS ligand. So we sought to identify a possible carbohydrate-like ligand from the biofilm matrix which is rich in exopolysaccharides (EPS) (24). RetS regulates the expression of the *psl* and *pel* operons which are responsible for the biosynthesis of PSL and PEL, which are major exopolysaccharide components of the biofilm matrix of nonmucoid *Pseudomonas* strains such as PAO1 (15, 24). Our preliminary tests suggest that PSL, but not PEL, binds to $RetS_{peri}$. Thus, we purified the previously characterized PSL polysaccharides to conduct further tests (2). In addition, we tested if any of the compounds identified from a whole cell screen for inhibition of biofilm formation in *P. aeruginosa* are acting through RetS (13).

Materials and Methods

PSL overexpression and isolation from *Pseudomonas aeruginosa*

To over-express PSL, the Wozniak group has generated a *psl*-inducible *P. aeruginosa* PAO1 strain (Δ*psl*/p*BAD-psl*) WFPA801 by replacing the *psl* promoter region with *araC*-p*BAD* which can be controlled by arabinose. We have obtained this strain kindly provided by the Wozniak group. For PSL over-production and isolation, we strictly followed the protocol which Wozniak group has developed (2). Briefly, 5 ml stationary phase overnight LB culture of WFPA801 was inoculated into 0.5L of M63 minimal medium (3L per batch) for 48 hours with slow agitation (250 rpm) at 37°C. To overexpress PSL, the cultures were supplemented with 0.4% (w/v) arabinose (15). Cells and cell-associated matrix material were separated from the viscous growth media by centrifugation (5000g, 4°C, 30 min). The pellets were resuspended in saline (0.9% NaCl, 50ml/L cell culture) and the cell surface-associated polymers were detached by mild sonication (4 × 20 s, 50% cycle, intensity 0.5). The pellet was then removed by centrifugation (same parameters) and resuspended with fresh saline. This procedure was repeated twice in order to extract as much biofilm matrix extract as possible. After that, this extract and the 3L growth medium were treated the same way. To precipitate DNA and proteins, TCA was added to a final concentration of 5% (w/v). The precipitation and any insoluble components were removed by centrifugation (10,000g, 10 minutes). The collected supernatant was then dialyzed in pure water and lyophilized. The obtained residue was resuspended in pure water and was centrifuged (10000g, 10 minutes) to remove insoluble materials. The supernatant was further deproteinated by extracting with equivalent volume of phenol twice and finally with phenol-chloroform (1:1 volume ratio). This crude polysaccharide sample was then fractionated by gel filtraction in pure water using a Sephadex G-50 size-exclusion column (16mm x 60cm).

A colorimetric assay was performed to quantify the sample in each fraction (19).

Briefly, each 50 µl polysaccharide or mono-mannose sample was mixed with 10µl 20% phenol and 250 µl sulphuric acid. The absorbance at 485nm was measured for all mixtures using a 96-well transparent plate. The final concentration of PSL was determined by comparing to a standard curve for a mono-mannose sample.

Differential Scanning Fluorimetry (DSF) assay for $RetS_{peri}$ ligand binding study

5µM $RetS_{peri}$ in either Tris buffer or sodium phosphate buffer (pH7.4) containing 50mM NaCl was incubated with or without 100µM ligand. 5X SYPRO Orange (5000X commercial stock) was also included in all 30µl samples. Protein melting (unfolding) was assessed by continuous thermal monitoring using the RT-PCR thermocycler instrument to detect increases in the fluorescence of the fluorophor. Samples were heated from 11 °C to 70 °C, with fluorescence acquisition in 0.5 °C increments. Fluorescence intensities were plotted versus temperature. The stability of $RetS_{peri}$ with or without ligands was indicated by the melting temperatures which are represented by the inflecion points of the sigmoidally-shaped melt curves (18).

Circular Dichroism

Far-UV CD spectra were generated using $RetS_{peri}$ protein (10µM) with or without purified PSL samples on a Jasco J-815 spectropolarimeter equipped with a Jasco PFD-425 S temperature-control unit. Spectra were collected in a 1-mm path-length quartz cell at 4°C. Spectra were obtained from three accumulated scans from 240 to 190 nm using a bandwidth of 1 nm and a response time of 1 s at a scan speed of 100 nm/min. Buffer (described in chapter two) backgrounds with or without PSL-A were used to subtract from the protein spectra with or without PSL-A (14).

Construction of expression plasmids for *retS* and *retS* mutant genes

The *retS* gene including its native promoter sequence (258bp) was amplified by *FailSave* PCR (Epicentre Biotechnologies) using PAO1 genomic DNA as the template with the primers containing restriction enzyme sites (SacI/EcoRI) (table 3.2) (16). The PCR product was then cloned into the pBluescript II SK (pSK) plasmid, which was

used for expression of RetS or RetS variant proteins (table 3.1). To transform all the plasmids carrying either *retS* or *retS* mutant gene into the PAO1 *retS* transposon insertion mutant strain (PAO1Δ*retS*) (22), the competent cell preparation and transformation steps followed a well developed protocol (3). Briefly, PAO1Δ*retS* cells were harvested from an overnight LB culture (supplemented with 15μg/ml tetracycline) by centrifugation (16000g) and washed with fresh 0.3M sucrose twice at room temperature. Cell pellets were resuspended into 50μl aliquots. Plasmids were individually transformed to the competent cells by electroporation. All the mutant *retS* genes were generated by PCR assisted site-directed mutagenesis (5) using pSK containing wild type *retS* gene as the PCR template.

$RetS_{peri}$ cysteine variant preparation for *in vitro* crosslinking experiments

The $RetS_{peri}$ cysteine mutation variants were generated by site-directed mutagenesis using an entry clone followed by Gateway cloning (Invitrogen) into an expression plasmid. Protein expression and purification followed the same procedures for wild type $RetS_{peri}$ with only the exception that DTT was included in all protein buffers during purification (12). All of mutation primers are listed in Table 3.2.

Before crosslinking experiments, every protein sample was buffer exchanged to 0.1M Na_2HPO_4 (pH 7.2), 50mM NaCl and 5mM EDTA using a HiPrep^{TM} 26/10 desalting column (GE Healthcare). To assist crosslinking, two commercial crosslinkers were individually used: bis(maleimido)ethane (BMOE) (8Å spacer) and 1,11-bismaleimidotriethyleneglycol ($BM[PEG]_3$) (17.8Å spacer) (ThermoScientific) which were dissolved in 50% DMSO at 1.4mM stock. Each reaction mixture containing 5μM crosslinker and 2μM $RetS_{peri}$ variant was incubated in 4°C for 2 hours. Each 75μl crosslinking reaction was quenched by adding 5μl 1M DTT. The reaction set-up with wild type $RetS_{peri}$ was used as a negative control. Crosslinked samples were analyzed via SDS-PAGE.

Bacterial strains and growth

PAO1 and PAO1 mutants used for all the *in vivo* experiments are listed in table 3.1 (22). Except during cloning, all strains were grown in chemically defined Jensen's minimal medium which was prepared according to a published protocol (11). For the overnight cultures: PAO1 was grown in the presence of 5µg/ml triclosan; PAO1Δ*retS* was grown in the presence of 15µg/ml tetracycline; all the strains containg a pSK plasmid were grown in the presence of 300µg/ml carbenicillin. For the congo red experiments, all the cultures were set up without antibiotics. For the growth of psl overexpression strain WFPA801, the growth cultures were also supplemented with or without (for control) arabinose.

Reverse transcription-PCR and quantitative real-time PCR (qRT-PCR)

To isolate RNA, all used strains were grown at 37°C in Jensen's minimal medium with appropriate antibiotics. Each overnight culture was then subcultured 1:25 into fresh medium and grown at 37°C to mid-logarithmic phase (optical density at 600 nm ($O.D._{600}$) of 0.6). Bacteria were then pelleted by centrifugation and used for RNA isolation using Trizole as instructed by the manufacturer (5 PRIME). The RNA samples were treated with DNase to remove bacterial chromosomal DNA. The concentrations of all finally obtained RNA samples were determined by UV-260nm absorbance measurements. 1µg of each RNA sample was used for cDNA synthesis with the reverse transcription kit (Invitrogen).

For quantitative real-time PCR, 1 µl of cDNA synthesized from RNA isolated from each strain was added to the iQ SYBR Green Supermix (Bio-Rad). The primer concentration was 50nM. The constitutively expressed *rpoD* gene was used as an endogenous control to normalize quantification of the mRNA target. Real-time PCR data were analyzed, validated, and calculated according to the instructions of the manufacturer.

Congo red biofilm assay to detect biofilm exopolysaccharides (EPS) production

All target strains were grown at 37°C in Jensen's minimal medium with appropiate antibiotics. The cell densities of overnight cultures were then measured at 600nm and then subcultured in fresh medium starting with $O.D._{600}$ reading of 0.05. After all strains arrived in stationary phase, the cultures were normalized again to $O.D._{600}$ reading of 0.03 in 3ml fresh medium supplemented with 10µl of filtered 50mg/ml Congo red dye. All the final cultures with Congo red (CR) were grown in glass tubes at 37°C with 150rpm shaking for different time periods. To achieve *in vivo* crosslinking, the crosslinker BMOE was also added to the two cysteine mutant stains at time zero.

The following day, a 200µl culture was removed in order to determine the $O.D._{600}$ before the bacterial cells were pelleted by centrifugation at 14,000g. For quantification of CR binding, the A_{490} of the supernatant of each sample was determined. Each strain was assayed in duplicate to generate a mean and standard error. All the samples to be measured were loaded onto a 96-well plate and the measurements were done by a TECAN infinite M200 fluorescence intensity scanner (Tecan).

Results and Discussion

Ligand titration into $RetS_{peri}$ causes a decreased melting temperature (Tm) and only PSL-A (not B or C) could shift the Tm of $RetS_{peri}$

The crystal structure of $RetS_{peri}$ and structural alignment with other CBMs unquestionably indicate that it binds to carbohydrate molecules (1, 12). To preliminarily test this hypothesis, we carried out DSF assay for a small-scale ligand screening using carbohydrate-like compounds. We found that the polymerized galacturonic acid, but not mono-galacturonic acid, causes a decreased melting temperature of $RetS_{peri}$ (figure 3.2). Considering the protein stabilization by ligands, a decreased melting temperature implies suggests an oligmerization disruption of $RetS_{peri}$ by ligand binding. This indication is consistent with our hypothesis that $RetS_{peri}$ signal sensing favors RetS-GacS hetero-dimer formation (9, 12).

More interestingly, the ligand that caused the most significant Tm shift is a crude biofilm matrix material. This is a very alluring result because RetS regulates biofilm-polysaccharide expression. Using the same assay to test the effect of biofilm PEL polysaccharides on $RetS_{peri}$ stability, we couldn't detect a change of Tm. So we ask the question that if biofilm-PSL could be a ligand of $RetS_{peri}$ (15). The previous study has shown that PSL is a mixture of polysaccharides with the same repeating unit but different degrees of polymerization and can be separated in three fractionations: PSLA, B and C (2). Following the published protocol, we isolated PSL-A, B and C (figure 3.3a). Each fraction was tested for $RetS_{peri}$ binding by DSF experiments. As shown by figure 3.3b, only PSL-A, which is the high molecular weight fraction, could cause a Tm shift of $RetS_{peri}$. However, when applying circular dichoism experiment to confirm the DSF result, we could not detect a change of far-UV spectrum of $RetS_{peri}$ by titrating either PSL-A or PSL-C into the protein sample (figure 3.4a).

PSL-A has no signaling role in RetS-involved biofilm formation regulation

Since the *in vitro* DSF and CD experiments could not lead a conclusion that

whether PSL-A binds to $RetS_{peri}$ or not, we wondered if this putative interaction takes place *in vivo* and in turn affects biofilm formation through RetS signaling. To test this hypothesis, we employed a real-time PCR based examination targeting the expression of the *rsmZ* gene, which is part of the RetS signal transduction pathway to regulate biofilm formation. The expression of PSL was controlled by adjusting the concentration of arabinose in the growing cultures. As shown in figure 3.4b, we could not detect an effect of PSL overexpression on RsmZ expression.

Previously identified synthetic biofilm inhibitors do not affect RetS signaling

Junker and Clardy have identified 30 compounds that inhibited biofilm formation in *P. aeruginosa* PAO1 strain using a high throughput screening of over 60,000 compounds. To examine if any of these compounds regulates biofilm formation by signaling through $RetS_{peri}$, we tested 21 of the 30 compounds in an *in vitro* DSF-based protein ligand binding assay as well as our *in vivo* congo red biofilm assay. One of these compounds (compound ID: 34600076) caused a shift of $RetS_{peri}$ melting temperature in the DSF assay (figure 3.5a). This compound also caused a slightly decreased of biofilm exopolysaccharide production in the PAO1 wild type strain. However, as shown by figure 3.5b, this compound also had the same effect in the $retS_{peri}$ deletion mutant. This result indicates that this compound does not act through binding to $RetS_{peri}$.

Deletion of $RetS_{peri}$ causes moderately increased biofilm EPS production

Previous studies have shown that $RetS_{peri}$ is not required for RetS activity to induce the expression of TTSS and might mediate RetS autoinhibition *in vivo* (16). However, the role of $RetS_{peri}$ in the regulation of biofilm formation was not examined. To fill this gap, we transformed a PAO1Δ*retS* mutant strain with the high copy number plasmid pSK containing either the wild-type *retS* gene or a *retS* gene lacking the sensory domain (*retS*41-185). In both cases, the expression of the proteins is controlled by native *retS* promoter (16). For *in vivo* functional studies, the congo red

biofilm assay was carried out (15). As shown by figure 3.1, the PAO1 Δ*retS* shows a hyperbiofilm-EPS production and hyperbiofilm-attachment phenotypes as expected (8). Expression of full length RetS protein restored wild type PAO1 with respect to biofilm EPS production. The slightly lower EPS production by the complemented strain compared to wild type PAO1 is probably due to a higher expression level of RetS using the high copy number plasmid pSK (16). On the other hand, the mutant complementation strain expressing truncated RetS (Δ41-185) shows a moderately increased biofilm EPS production phenotype compared to the complemented and the wild type strains. It has been demonstrated that this truncation does not impact the expression or steady-state stability of RetS (16). To confirm that these phenotypes are controlled by RetS involved signaling through Gac/Rsm regulatory system, the transcription levels of the sRNA *rsmZ* in the mutants were examined by real-time PCR. Consistent with the result of congo red biofilm assay, the RsmZ expression level of the strain complmented with *retS* (Δ41-185) is between those of the *retS* mutant and the complementation strain. These results indicate that $RetS_{peri}$ does appear to inhibit, but not sufficiently repress, RetS-controlled biofilm formation (figure 3.1). However, in the context of the current hypothesis that $RetS_{peri}$ favors homo-dimerization of RetS and GacS and in turn biofilm formation, this result is unexpected as we would have predicted a decrease in biofilm formation as the result of $retS_{peri}$ deletion (9, 12).

Both putative dimer interfaces assist *in vitro* cysteine-cysteine crosslinking

Our hypothesis postulates that ligand binding disrupts $RetS_{peri}$ dimerization. Accordingly, we predicted that the $RetS_{peri}$ dimer interface would be close to the alpha-helix 1 and the predicted ligand binding site (figure 3.6a) (12). After our prediction, another dimer interface and ligand binding site were hypothesized, which located the pocket close to alpha-helix 2 (figure 3.6a) (23). We have demonstrated $RetS_{peri}$ dimerization via an *in vitro* lysine-lysine (amine) crosslinking assay (12).

However, the involvement of the N-terminus of the protein in amine crosslinking made it difficult to locate the dimer interface with this strategy. Therefore, targeting these two putative dimer interfaces, we applied a cysteine-cysteine based crosslinking strategy. To this end, two single cysteine mutations were introduced in each of the two putative dimer interfaces. Each $RetS_{peri}$ cysteine variant was successfully purified and applied to the crosslinking experiment. Crosslinking for the wild type $RetS_{peri}$, which was used for a negative control, yielded no dimers. Interestingly, all four cysteine variants could be crosslinked by either of the two crosslinkers (BMOE and $BM[PEG]_3$) as shown by figure 3.6b. This result is not too surprising because it has been shown by small angle scattering data that there are 7% tetramers of $RetS_{peri}$ in solution (23).

Introduction of single cysteine mutations to $RetS_{peri}$ do not affect *in vivo* biofilm EPS production phenotype

It has been proposed that there is a functional role of $RetS_{peri}$ dimerization in biofilm formation regulation. Disruption of $RetS_{peri}$ dimerization is hypothesized to promote RetS-GacS interaction and in turn biofilm repression (9, 12). Here we are also interested in the effect of an enhanced $RetS_{peri}$ dimerization on RetS signaling. Since we have shown that both putative dimer interfaces could assist *in vitro* dimerization in our cysteine-based crosslinking assay, we accordingly introduced single cysteine mutations to periplasmic domain of RetS, which is expressed in the PAO1Δ*retS* mutant in order to achieve irreversible dimerization of RetS. One cysteine residue was introduced to each dimer interface by site-directed mutagenesis method (glutamin67 and isolusine176). Congo red biofilm *in vivo* assay was applied to check the complementation phenotypes of the single cysteine mutants. As shown by figure 3.7a, each cysteine mutant shows the same biofilm phenotype as that of the full complementation strain.

One explanation for this result is that irreversible dimerization of $RetS_{peri}$ *in vivo* requires the presence of a crosslinker despite that the periplasm is an oxidizing

environment (21). Thus, the membrane-permeable cysteine crosslinker BMOE (8Å arm space) was introduced into the congo red biofilm experiments. Unfortunately, there is no phenotype difference between the cysteine mutants and the complementation strain in terms of biofilm formation (figure 3.8).

Single Mutations on either putative ligand binding site do not affect biofilm EPS production

The proposed functional role of $RetS_{peri}$ ligand binding in RetS signaling is to disrupt $RetS_{peri}$ dimerization, thus promoting RetS-GacS interaction, which in turn inactivates biofilm gene expression. Hence, increased biofilm formation is expected if th $RetS_{peri}$ ligand binding site is disrupted. Based on our crystal structure, we have predicted the first putative $RetS_{peri}$ ligand binding site, which is close to the alpha-helix1. This site meets all the requirements for the common features of ligand binding sites in CBM and is structurally conserved in closest structural homologues of $RetS_{peri}$ (12). However, we could not exclude another putative binding pocket located close to alpha-helix2 (23). Targeting the critical residues in these two sites, we employed a mutational analysis combined with *in vivo* congo red biofilm assay. To this end, single mutations on two putative $RetS_{peri}$ ligand binding sites were introduced by site-directed mutagenesis. Corresponding RetS variants were expressed in PAO1Δ*retS* mutant strain. Surprisingly, as shown by figure 3.9, none of these single mutations was able to affect biofilm EPS production.

Conclusion and Discussion

The DSF and CD data indicate that PSL-A might bind $RetS_{peri}$ *in vitro*. Having the same sugar composition and repeating unit as those of PSL-A, PSL-B and PSL-C could not show binding to $RetS_{peri}$. One explanation for this finding is that except for the difference in the degrees of polymerization, PSL-A is not identical to PSL-B and PSL-C (2). Another possibility is that the observations in *in vitro* DSF and CD experiments are not due to $RetS_{peri}$-PSL-A binding. This explanation is more likely

true because the qPCR experiment shows that PSL overexpression was not able to affect RsmZ expression. Additionally, the two identified synthetic biofilm inhibitors, which could shift the melting temperature of $RetS_{peri}$, did not impact RetS signaling to regulate biofilm formation. In summary, our attempt to identify a $RetS_{peri}$ ligand that could affect biofilm formation through RetS signaling has been unsuccessful.

The current hypothesis states that ligand binding of $RetS_{peri}$ tunes the homo-dimerization of RetS and RetS-GacS hetero-dimerization (9, 12). Thus, the deficiency of $RetS_{peri}$ ligand binding is expected to cause an increased biofilm formation. However, all the single mutations targeting putative $RetS_{peri}$ ligand binding sites was unable to affect biofilm phenotype. One explanation for this particular result is that the $RetS_{peri}$ ligand in the congo red assay might be absent. On the other hand, a down-regulated biofilm phenotype by deletion of $RetS_{peri}$, which is proposed to promote RetS-GacS heterodimer formation, was expected (12). However, we observed the opposite phenomenon. In addition, introduction of single cysteine residues, which could assist irreversible $RetS_{peri}$ dimerization *in vitro*, did not impact biofilm phenotype related exopolysaccharide production through RetS signaling. Therefore, targeting $RetS_{peri}$-controlled RetS signaling mechanism as well as the specific functional role(s) of RetS-GacS interaction, alternative explanations have to be examined.

Acknowledgements

I thank the first year graduate student Jordan Mancl who has been assisting in the congo red biofilm assay. I thank Dr. Webster Santos for kindly allowing us to use the circular dichroism instrument in his lab. This work is funded by the Jeffress Memorial Trust, the American Heart Association, and the DOE/DER, NIH/NCRR.

References

1. Boraston AB, Bolam DN, Gilbert HJ, Davies GJ. 2004. Carbohydrate-binding modules: fine-tuning polysaccharide recognition. Biochem J. 38:769-81.
2. Byrd MS, Sadovskaya I, Vinogradov E, Lu H, Sprinkle AB, Richardson SH, Ma L, Ralston B, Parsek MR, Anderson EM, Lam JS, Wozniak DJ. 2009. Genetic and biochemical analyses of the Pseudomonas aeruginosa Psl exopolysaccharide reveal overlapping roles for polysaccharide synthesis enzymes in Psl and LPS production. Mol Microbiol. 73:622-38.
3. Choi KH, Kumar A, Schweizer HP. 2006. A 10-min method for preparation of highly electrocompetent Pseudomonas aeruginosa cells: Application for DNA fragment transfer between chromosomes and plasmid transformationJ Microbiol Methods. 64:391-7.
4. Cornelis P (editor). 2008. Pseudomonas: Genomics and Molecular Biology (1st edition.). Caister Academic Press.
5. Costa GL, Bauer JC, McGowan B, Angert M, Weiner MP. 1996. Site-Directed Mutagenesis Using a Rapid PCR-Based Method. Methods Mol Biol. 57:239-48.
6. Gao R, Stock AM. 2009. Biological insights from structures of two-component proteins. Annu Rev Microbiol. 63:133-54.
7. Gooderham WJ, Hancock RE. 2009. Regulation of virulence and antibiotic resistance by two-component regulatory systems in Pseudomonas aeruginosa. FEMS Microbiol Rev. 33:279-94.
8. Andrew L. Goodman, Bridget Kulasekara, Arne Rietsch, Dana Boyd, Roger S. Smith, and Stephen Lory. 2004. A Signaling Network Reciprocally Regulates Genes Associated with Acute Infection and Chronic Persistence in Pseudomonas aeruginosa, Developmental Cell. 7:745–754.
9. Goodman AL, Merighi M, Hyodo M, Ventre I, Filloux A, Lory S. 2009. Direct interaction between sensor kinase proteins mediates acute and chronic disease phenotypes in a bacterial pathogen. Genes Dev. 23:249-59.
10. Hsu JL, Chen HC, Peng HL, Chang HY. 2008. Characterization of the histidine-containing phosphotransfer protein B-mediated multistep phosphorelay system in Pseudomonas aeruginosa PAO1. J Biol Chem. 283:9933-44.
11. Jensen, S. E., I. T. Facycz, and J. N. Campbell. 1980. Nutritional factors controlling exocellular protease production by Pseudomonas aeruginosa. J. Bacteriol. 144**:**844-847.
12. Jing X, Jaw J, Robinson HH, Schubot FD. 2010. Crystal structure and oligomeric state of the RetS signaling kinase sensory domain. Proteins. 78:1631-40.
13. Junker LM, Clardy J. 2007. High-Throughput Screens for Small-Molecule Inhibitors of Pseudomonas aeruginosa Biofilm Development. Antimicrob Agents Chemother. 51:3582-90.
14. Kelly SM, Jess TJ, Price NC. 2005. How to study proteins by circular dichroism.

Biochim Biophys Acta. 1751:119-39.
15. Ma L-Y, Jackson K, Landry RM, Parsek MR, Wozniak DJ. 2006. Analysis of Pseudomonas aeruginosa conditional Psl variants reveals roles for the Psl polysaccharide in adhesion and maintaining biofilm structure postattachment. J Bacteriol. 188:8213–8221.
16. Michelle A. Laskowski, and Barbara I. Kazmierczak. 2006. Mutational Analysis of RetS, an Unusual Sensor Kinase-Response Regulator Hybrid Required for Pseudomonas aeruginosa Virulence. Infection and Immunity. 74:4462–4473.
17. Michelle A. Laskowski, Ellice Osborn and Barbara I. Kazmierczak. 2004. A novel sensor kinase–response regulator hybrid regulates type III secretion and is required for virulence in Pseudomonas aeruginosa. Molecular Microbiology. 54:1090–1103.
18. Niesen FH, Berglund H, Vedadi M. 2007. The use of differential scanning fluorimetry to detect ligand interactions that promote protein stability. Nat Protoc. 2:2212-21.
19. Petrakova E, Glaudemans CP. 1995. Synthesis of the methyl cu-glycosides of some isomalto-oligosaccharides specifically deoxygenated at position C-4 Carbohydr Res. 279:133-50.
20. Rodrigue, A., Quentin, Y., Lazdunski, A., Mejean, V., and Foglino, M. 2000. Two-component systems in Pseudomonas aeruginosa: why so many? Trends Microbiol. 8:498–504.
21. Schlapschy M, Skerra A. 2011. Periplasmic Chaperones Used to Enhance Functional Secretion of Proteins in E. coli. Methods Mol Biol. 705:211-24.
22. Shawn Lewenza, et. al. 2005. Construction of a mini-Tn5-luxCDABE mutant library in Pseudomonas aeruginosa PAO1: A toll for identifying differentially regulated genes. Genome Research. 15:583-589.
23. Vincent F, Round A, Reynaud A, Bordi C, Filloux A, Bourne Y. 2010. Distinct oligomeric forms of the Pseudomonas aeruginosa RetS sensor domain modulate accessibility to the ligand binding site. Environ Microbiol. 12:1775-86.
24. Wozniak DJ, Wyckoff TJ, Starkey M, Keyser R, Azadi P, O'Toole GA, Parsek MR. 2003. Alginate is not a significant component of the extracellular polysaccharide matrix of PA14 and PAO1 Pseudomonas aeruginosa biofilms. Proc Natl Acad Sci U S A. 100:7907-12.

Table 3.1 Bacterial cells and plasmids

Stain or plasmid	Relevant information	Source/ Reference
***E. coli* strains:**		
BL21	DE3 CodonPlus RIL cells	Stratagene
DH5α	Only for cloning procedures	This study
***P. aeruginosa* cells:**		
PAO1	Wild type strain	22
PAO1Δ *retS*	PAO1 *retS* transposon insertion mutant	22
WFPA801	PAO1 PSL-overexpression mutant	15
PAO1Δ *retS*+ *retS*_pSK	PAO1 *retS* complementation strain	This study
PAO1Δ*retS*+ *retS*Q67C_pSK	PAO1 *retS* complementation strain with cysteine mutation on Gln67	This study
PAO1Δ *retS*+ *retS*I176C_pSK	PAO1 *retS* complementation strain with cysteine mutation on Ile176	This study
PAO1Δ *retS* +*retS*Y117A_pSK	For RetS ligand binding site mutation	This study
PAO1Δ *retS* +*retS*R162A_pSK		This study
PAO1Δ *retS* +*retS*D115A_pSK		This study
PAO1Δ *retS* +*retS*F107A_pSK		This study
PAO1Δ *retS* +*retS*W103A_pSK		This study
PAO1Δ *retS* +*retS*W105A_pSK		This study
PAO1Δ *retS* +*retS*Δperi_pSK	$RetS_{peri}$ deletion mutant	This study
PAO1+ pSK	PAO1 with empty pSK vector	This study
PAO1Δ *retS* +pSK	*retS* mutant with empty pSK vector	This study

Plasmids:

$RetS_{peri}$Q67C/I176C/W105C/T158C_pDONR201	Donor vectors in Gateway cloning for purification of $RetS_{peri}$ cysteine variants	This study
$RetS_{peri}$Q67C/I176C/W105C/T158C_His_6MBPpDEST	Expression vectors in Gateway cloning for purification of $RetS_{peri}$ cysteine variants	This study
pSK	Empty vector in cloning procedures for *in vivo* studies	Stratagene
pSK_*retS*	pSK carrying wild type *retS* gene	This study
pSK_*retS*Δ*peri*	pSK carrying retS *ret*SΔ*peri*	This study
pSK_*retS*Q67C	pSK carrying $retS_{peri}$ cysteine mutation	This study
pSK_*retS*I176C	pSK carrying $retS_{peri}$ cysteine mutation	This study
pSK_*retS*W105A		This study
pSK_*retS*T117A		This study
pSK_*retS*R162A	pSK carrying $retS_{peri}$ binding site mutation	This study
pSK_*retS*D115A		This study
pSK_*retS*F107A		This study
pSK_*retS*W105A		This study

Table 3.2 Primers (underlined sequences correspond to unique restriction sites utilized for cloning)

Primer	Sequence (5' to 3')	Source/ Reference
RetSD121-555	GTTCCCCTGCAAACCACCGAGAAGCCCGCCTACGCC	This study
RetSD121-555-r	GGCGTAGGCGGGCTTCTCGGTGGTTTGCAGGGGAAC	This study
-258retS_SacI-F	ATCAGTGCGGAGCTCGTGCTCTGTGCCACCGCCATC	This study
+1006retS_AscI-re	CGATCAGGCGCGCCGGCTGGTAGCCG	This study
RetSEndEcorRI_R	ATCAGTGAATTCTCAGGAGGGCAGGGCGTCG	This study
Q67Cys_F	CGACGTCCTCTGCCGCAAGGAGCAGTTCCGCCCG	This study
Q67Cys_R	GCTCCTTGCGGCAGAGGACGTCGGCGATCCGCAG	This study
Trp105Cys_F	GAGCTGGCTGTGCATCTTCGCCCCACGGGTGCAG	This study
Trp105Cys_R	GGGCGAAGATGCACAGCCAGCTCGGCACCTTCTG	This study
Thr158Cys_F	CAAGCCGATGTGCCTGTACGTGCGGATGACCTCC	This study
Thr158Cys_R	GCACGTACAGGCACATCGGCTTGCCGTCGACCGG	This study
Ile176Cys_F	GTTCGACCAGTGCGACGAAGCCGGCCTGGTCGGC	This study
Ile176Cys_R	CGGCTTCGTCGCACTGGTCGAACCAGGCCATCAG	This study
W103A_F	GGTGCCGAGCGCGCTGTGGATCTTCGCCCCACGG	This study
W103A_R	AGATCCACAGCGCGCTCGGCACCTTCTGCGCGGG	This study
W105A_F	GAGCTGGCTGGCGATCTTCGCCCCACGGGTGCAG	This study
W105A_R	GGGCGAAGATCGCCAGCCAGCTCGGCACCTTCTG	This study
F107A_F	GCTGTGGATCGCGGCCCCACGGGTGCAGTACCTG	This study

F107A_R	CCCGTGGGGCCGCGATCCACAGCCAGCTCGGCAC	This study
RetSD115_F	GCAGTACCTGGCCTACTACCTGGTGCAGGACGGC	This study
RetSD115_R	CCAGGTAGTAGGCCAGGTACTGCACCCGTGGGGC	This study
RetS-Y91A-F	CCTGGACTACGCCCTGGTGCAGGACGGCCAACTG	This study
RetS-Y91A-R	CCTGCACCAGGGCGTAGTCCAGGTACTGCACCCG	This study
RetS-R136A-F	CCTGTACGTGGCGATGACCTCCAACCATCCGCTG	This study
RetS-R136A-R	TGGAGGTCATCGCCACGTACAGGGTCATCGGCTTGCC	This study
rsmZ-qPCR_F	CGTACAGGGAACACGCAACCCCGA	This study
rsmZ-qPCR_R	AAAAAGGGGCGGGGTATTACCCCG	This study
rpoD-realtimeF	GGGCGAAGAAGAAATGGTC	This study
rpoD-realtimeR	CAGGTGGCGTAGGTGGAGAA	This study

a)

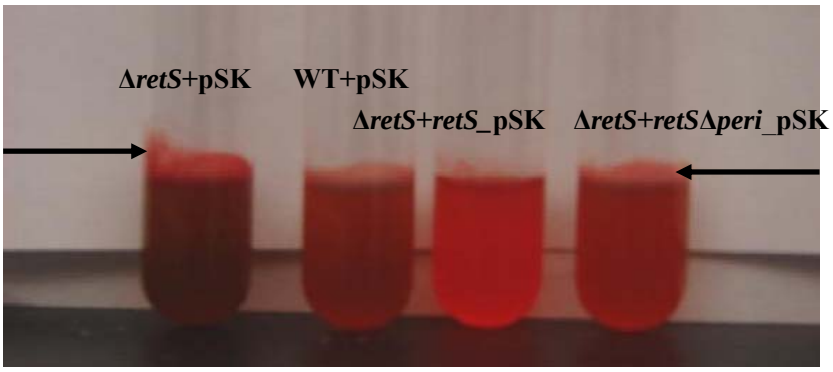
ΔretS+pSK
WT+pSK
ΔretS+retS_pSK
ΔretS+retSΔperi_pSK

b)

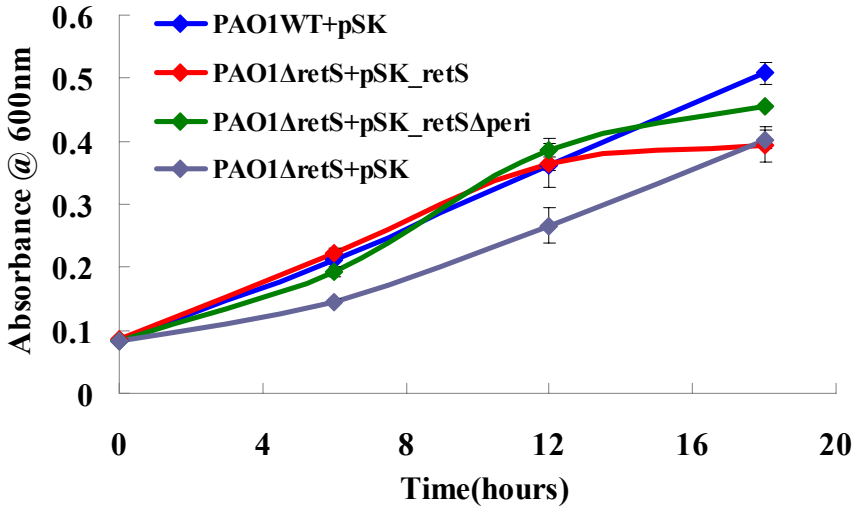
Absorbance @ 600nm
0.6
0.5
0.4
0.3
0.2
0.1
0
PAO1WT+pSK
PAO1ΔretS+pSK_retS
PAO1ΔretS+pSK_retSΔperi
PAO1ΔretS+pSK
0
4
8
12
16
20
Time(hours)

c)

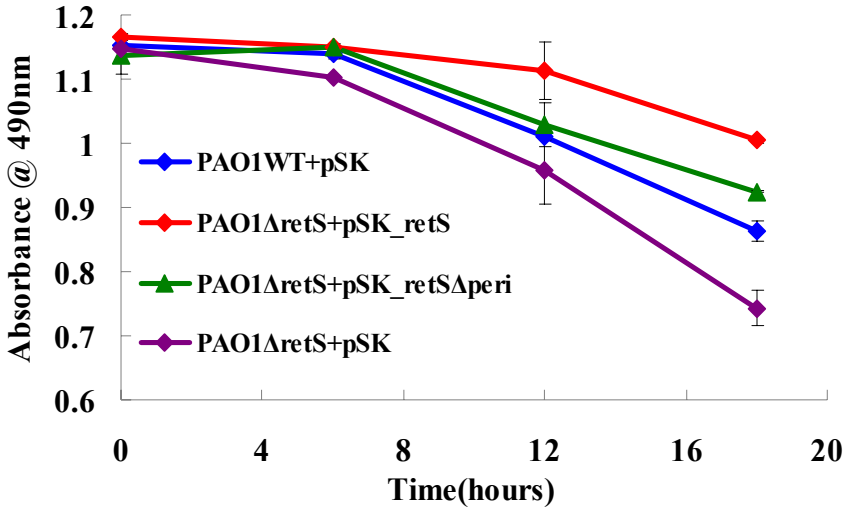
Absorbance @ 490nm
1.2
1.1
1
0.9
0.8
0.7
0.6
PAO1WT+pSK
PAO1ΔretS+pSK_retS
PAO1ΔretS+pSK_retSΔperi
PAO1ΔretS+pSK
0
4
8
12
16
20
Time(hours)

d)

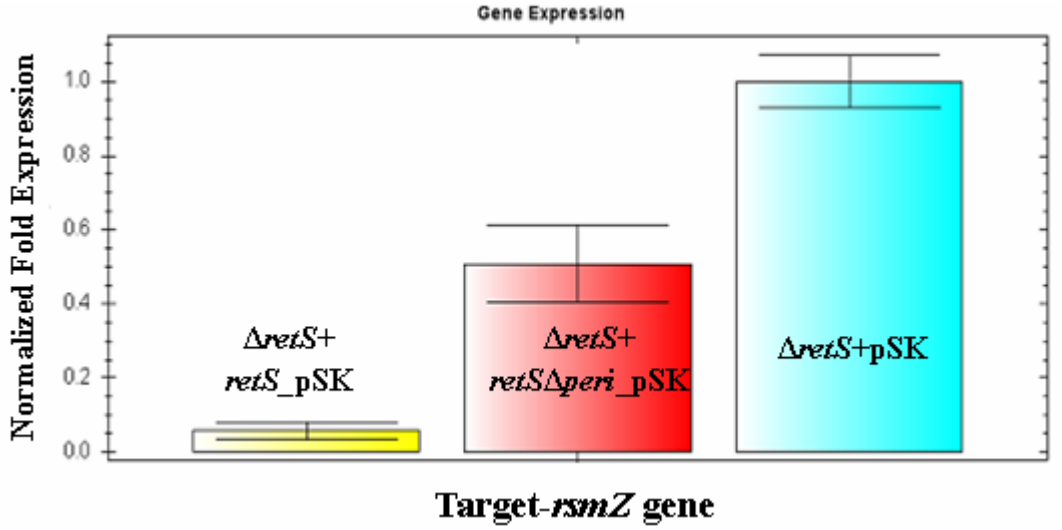

Figure 3.1 Examination of biofilm EPS production and gene expression of target PAO1 strains. (a) Each cell culture supplemented with congo red dye was grown in a glass tube. Biofilm-attachment to the cell tube wall is indicated by the arrows. **(b)** Each planktonic culture in the tube was used to measure the cell density using the absorbance reading at 600nm. **(c)** After 1ml of each planktonic culture was centrifuged, the supernatant was used to detect the unbound congo red dye by absorbance reading at 490nm. **(d)** qPCR experiment results showing RsmZ expression levels of the test mutants.

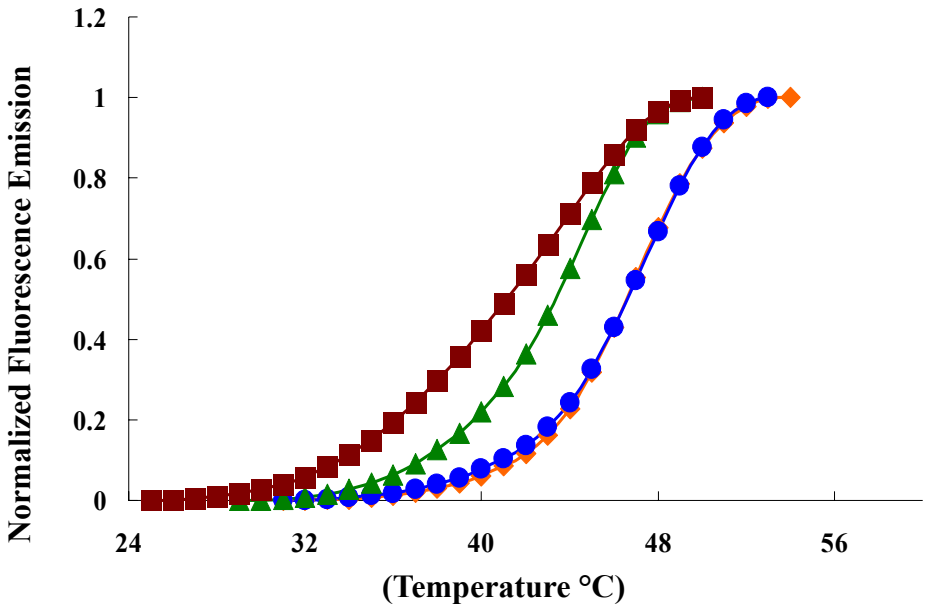

Figure 3.2 Results of the Differential Scanning Fluorimetry (DSF) assay. This assay was aimed at characterizing the ligand binding properties of the RetS periplasmic domain ($RetS_{peri}$) with three carbohydrate samples. **Blue**: 10μM $RetS_{peri}$ without a ligand (control) (Tm: 46.95°C); **Orange**: 10μM $RetS_{peri}$ with 100μM mono-galacturonic acid (Tm: 46.8°C); **Green**: 10μM $RetS_{peri}$ with 100μM polygalacturonic acid (Tm: 43.69°C); **Red**: 10μM $RetS_{peri}$ with a crude biofilm material (Tm: 42.09°C. the sample was unpurifed biofilm material extracted from growth medium of a PSL-overproduction strain). The drop in the melting temperature upon ligand binding suggests a change of the oligomeric state of $RetS_{peri}$.

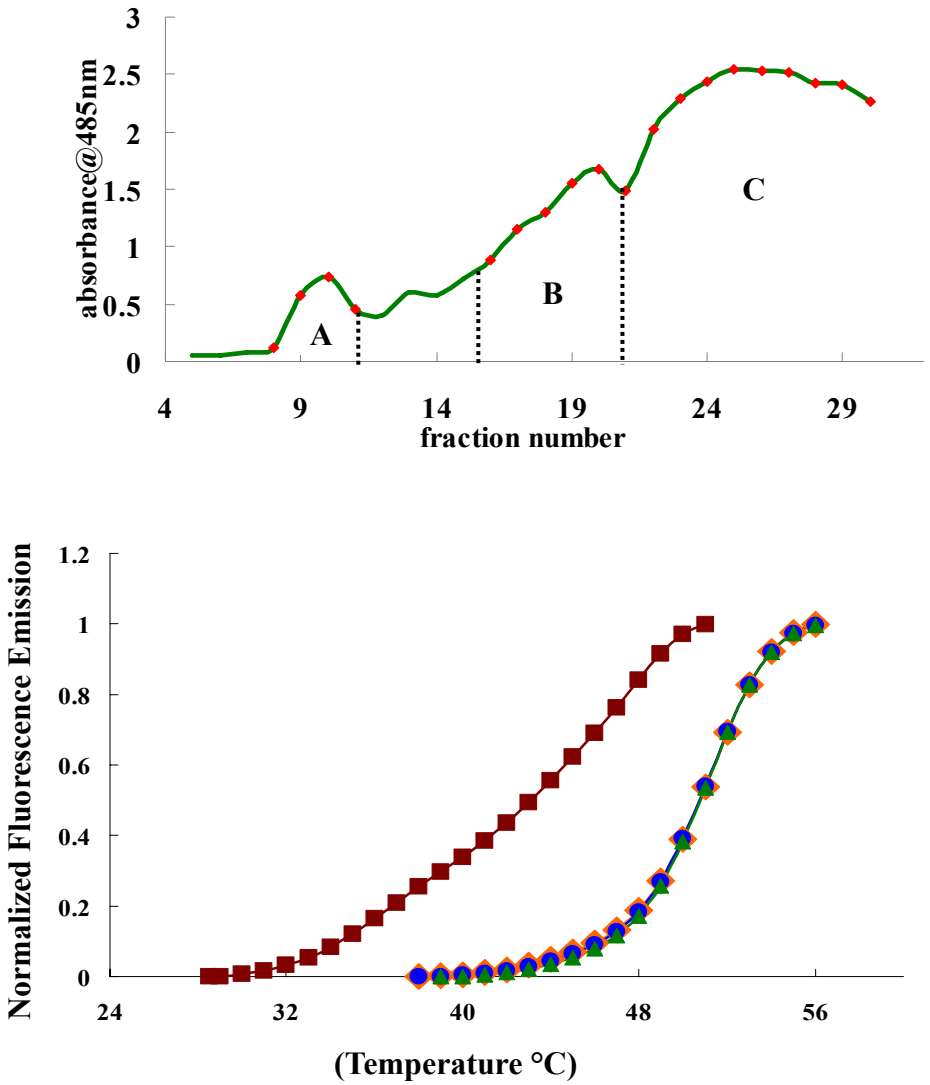

Figure 3.3 Examination of protein-ligand binding for PSL and RetS$_{peri}$. (Top) elution profile of crude carbohydrate extract of the growth medium (3L) of *P. aeruginosa psl*-inducible strain WFPA801 on a Sephadex G-50 column. Fractions B and C contain PSL polysaccharide with ~3–5 and ~1–2 penta-saccharide repeating units respectively. (Bottom) DSF experiments aimed at examining the ligand binding properties of the RetS$_{peri}$ with three fractions. **Blue**: 10μM RetS$_{peri}$ without a ligand for control (Tm: 49.7°C); **Orange/Green**: 10μM RetS$_{peri}$ with 100μM PSL-B/C (equivalent to 100μM mono-mannose) (Tm: 49.8°C); **Red**: RetS$_{peri}$ with 100μM PSL-A (equivalent to 100μM mono-mannose) (Tm: 42°C).

a)

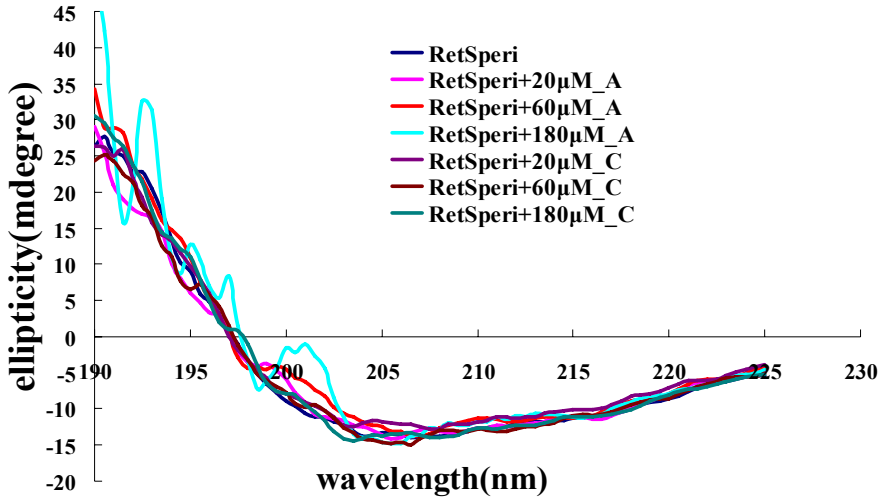

b)

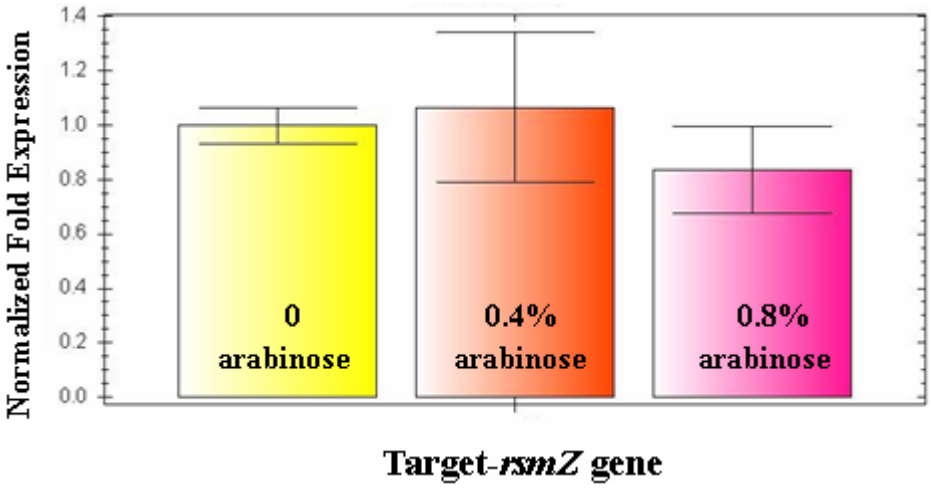

Figure 3.4 Signaling role of PSL overexpression (a) Far-UV circular dichroism (CD) spectra of 10µM $RetS_{peri}$ in the absence (dark blue) and presence of PSL-A (A) or PSL-C (C). The experiments were performed at 4 °C**. (b)** qPCR (real-time PCR) experiment to determine the effect of *psl* overexpression to the rsmZ gene expression level. Cell cultures were supplemented with 0.4% or 0.8% arabinose (zero for control) to achieve different levels of *psl* overexpression. Each culture was inoculated from $O.D._{600nm}$ at 0.05 and allowed to grown at 37 °C for 6 hours before RNA isolation. The *rpoD* gene was used as the reference gene for gene expression normalization.

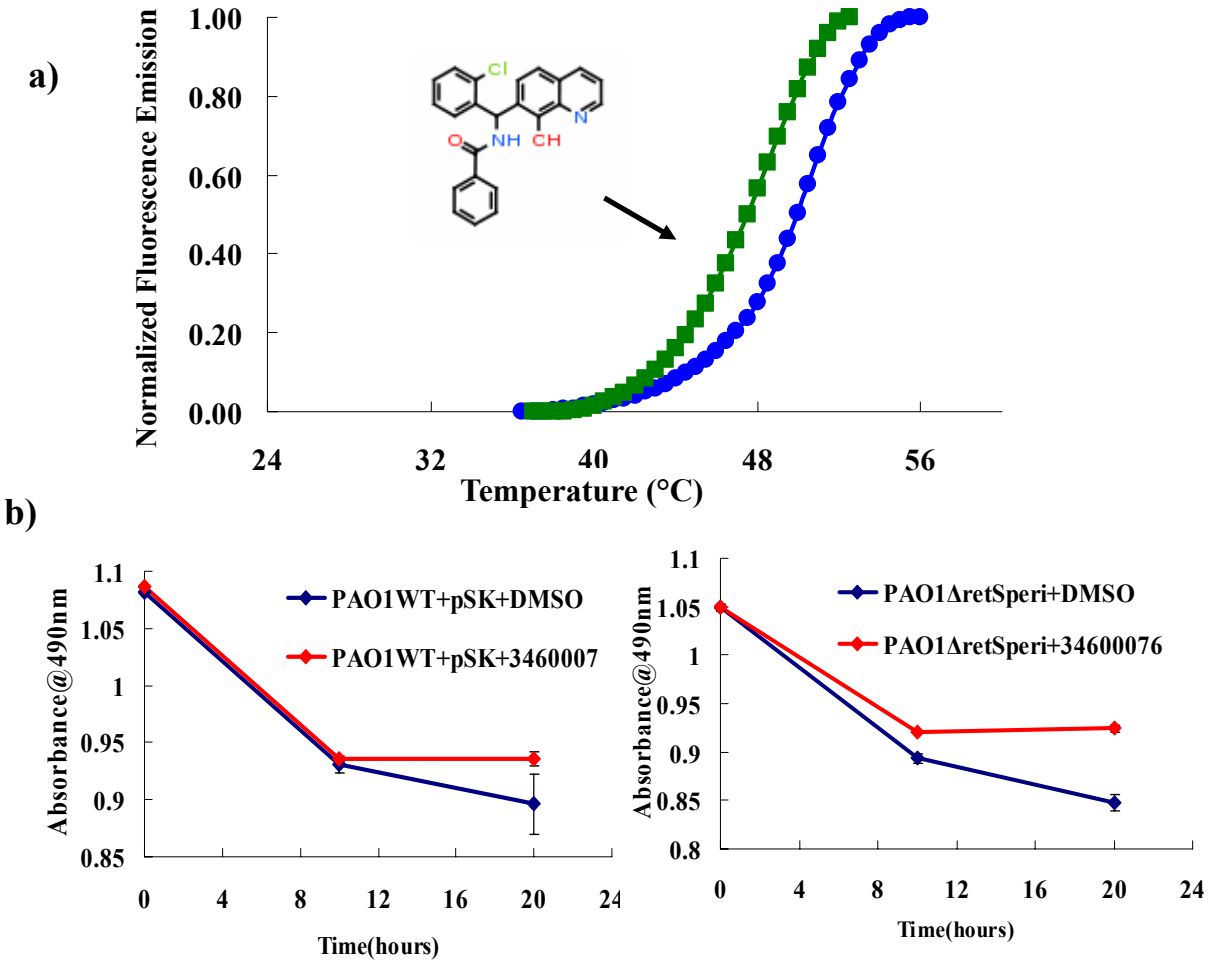

Figure 3.5 Ligand screening aimed at identifying signaling-effective RetS$_{peri}$ ligands using commercial biofilm inhibitors. (a) DSF-based ligand screening using the 21-compounds biofilm-inhibitor library. One compound has been identified that could shift RetS$_{peri}$ (10μM) melting temperature from 48.9°C (Blue: RetS$_{peri}$ with DMSO) to 46.1°C (Green: RetS$_{peri}$ with compound). The formula of this compound is indicated above (compound ID in Chembridge: 34600076). **(b)** Congo red biofilm assay to measure EPS production for target cultures. Wild type PAO1 transformed with empty pSK vector was used as a control. The *retS$_{peri}$* deletion mutant was used to test if the compound has an impact on RetS$_{peri}$ involved signaling. In the experiments, each culture was supplemented with DMSO (control) or 30 μM 34600076 (in DMSO solution).

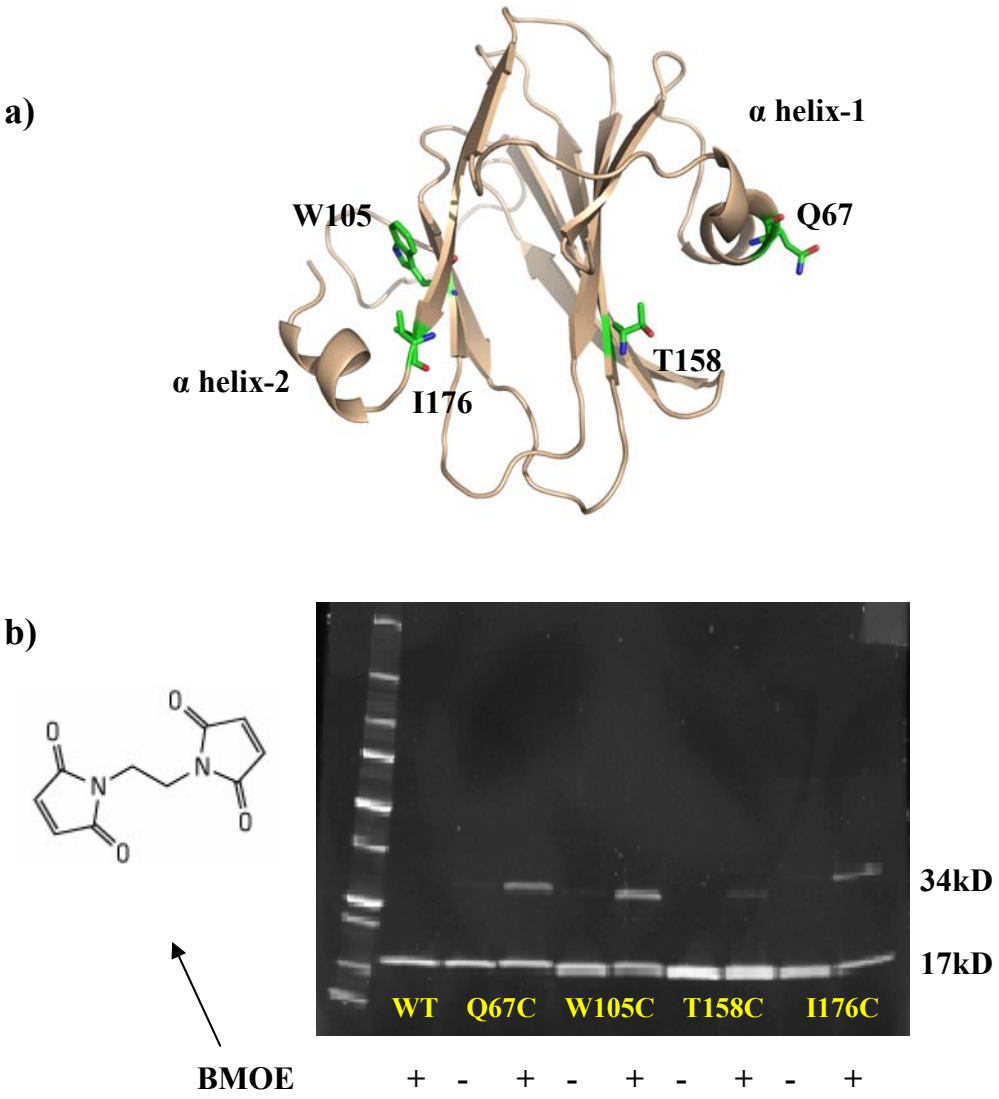

Figure 3.6 *In vitro* cysteine-crosslinking results to probe the RetS$_{peri}$ dimerization interface. (a) PYMOL-generated cartoon representation of the RetS$_{peri}$ structure. The labeled residues close to each putative dimer interface are selected for cysteine introduction sites. (b) each cysteine variant was purified and subjected to crosslinking using the cysteine-cysteine crosslinker BMOE (8Å spacer). The wild type cysteine-less RetS$_{peri}$ was used as a negative control. The crosslinking reactions were incubated at room temperature for 30 minutes and the results were examined by SDS-PAGE. The protein ladder and target protein bands were stained by a fluorescent oriole solution.

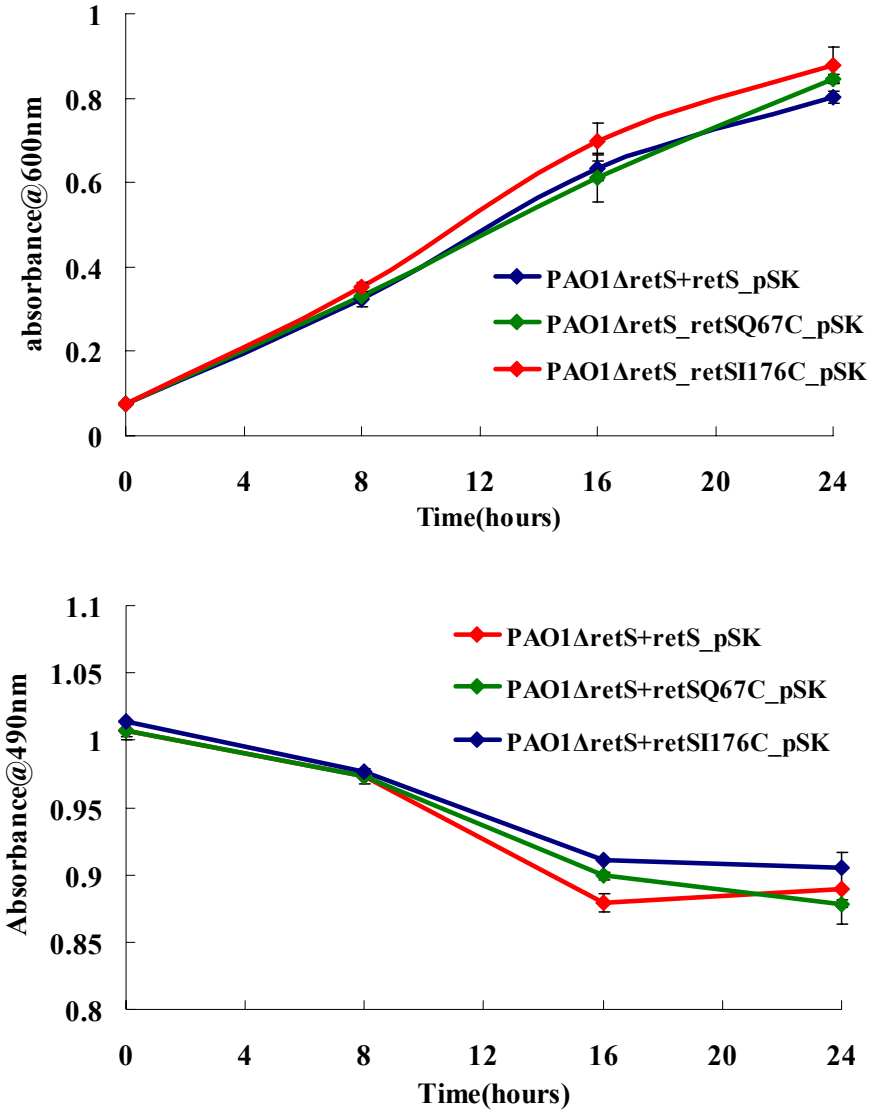

Figure 3.7 Effect of single cysteine introduction into $RetS_{peri}$ on EPS production. PCR based mutagenesis was carried to construct the expression vector carrying corresponding single cysteine mutations. Each RetS variant was expressed in the PAO1 Δ*retS* strain. The complementation strain was used as an experimental control (blue).

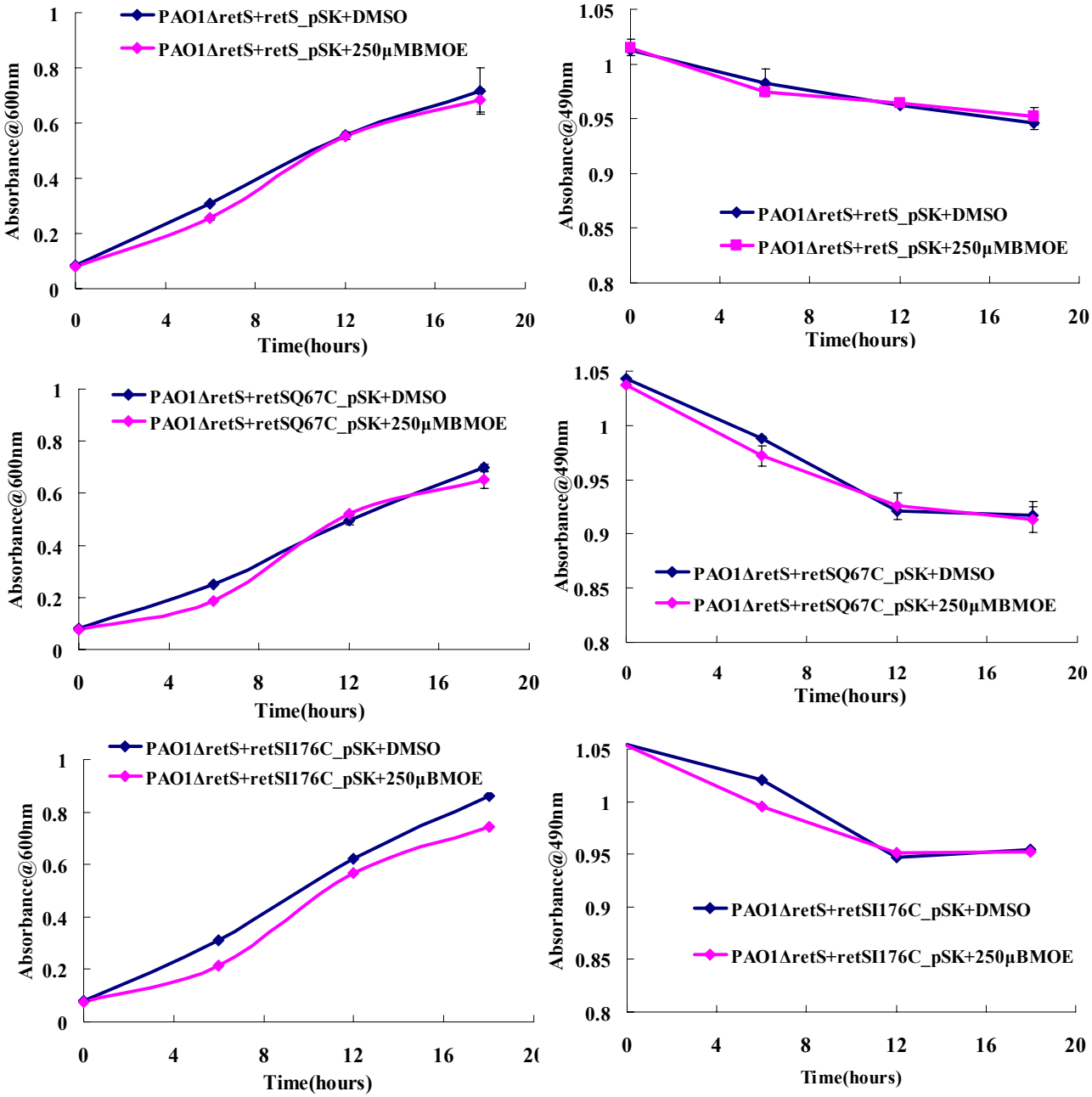

Figure 3.8 Examination of EPS production in single cysteine mutants with cysteine-crosslinker BMOE. The congo red experiments followed standard protocol with the only difference that the membrane-permeable cysteine-cysteine crosslinker BMOE was applied in this assay (DMSO was used for control experiments).

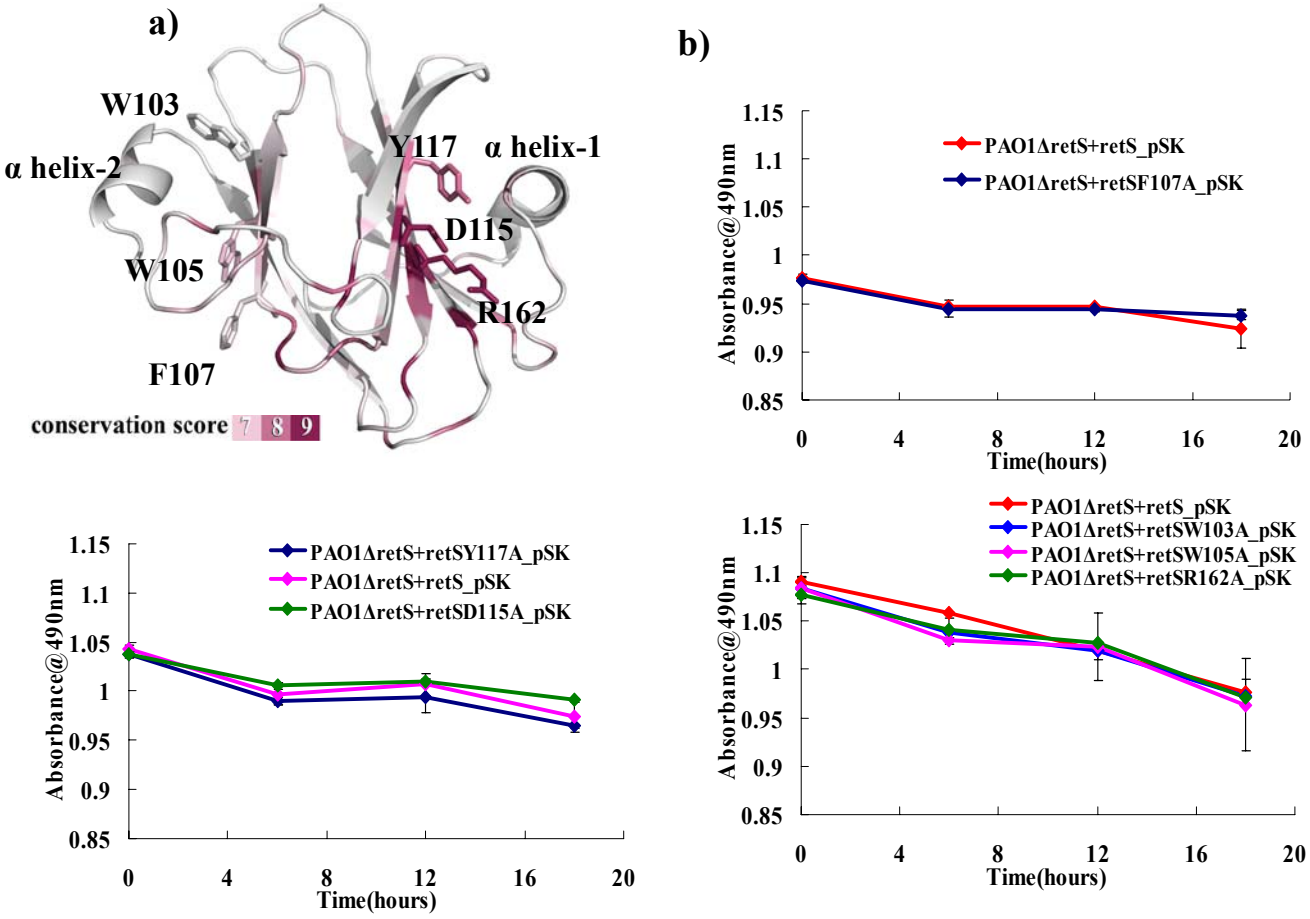

Figure 3.9 *In vivo* mutational analysis targeting the putative RetS$_{peri}$ ligand binding site. (a) The labeled residues represent the two putative ligand binding sites of RetS$_{peri}$. (**b**) Each mutant was tested in the congo red assay. The complementation strain was used as an experimental control. None of these single mutations in RetS$_{peri}$ affected EPS production.

Chapter Four

Study the Functional Role of Cytoplasmic Domains of RetS in Biofilm Formation

ABSTRACT

The current model for RetS-GacS signaling in *P. aeruginosa* posits that RetS does not utilize the conserved two component system (TCS) signaling mechanism to inhibit GacS induced biofilm formation. Instead, RetS is though to form a 1:1 protein complex with GacS, thereby blocking autophosphorylation of the latter protein. Expanding this model, we proposed that ligand binding disrupts the homo-dimerization of $RetS_{peri}$ to assist RetS-GacS hetero-dimerization. However, this RetS-GacS signaling mechanism has never been identified or described in any other two component systems. Moreover, our previous study targeting $RetS_{peri}$ does not support the current hypothesis. Therefore, to uncover the cellular signaling mechanism for RetS, we exmained the cytoplasmic domains of RetS in this chapter to reveal the specific functional role of RetS-GacS complex formation in biofilm formation. Specifically, we sought to determine if the histidine and aspartate residues of RetS that would normally be associated with autophosphorylation and phosphate transfer in signaling kinases are required for EPS production regulation. Moreover, we will attempt to characterize the interaction between RetS and GacS kinase domains *in vitro* with the aim to uncover the structural basis for RetS-GacS signaling.

Introduction

P. aeruginosa utilizes two component systems (TCSs) to switch the gene expression between TTSS and biofilm formation (5, 12). In response to an environmental signal, the histidine kinase (HK) requires the homo-dimerization to achieve "trans"-autophosphorylation at a conserved histidine residue (4). The response regulator (RR) subsequently receives the phosphoryl group at a conserved aspartate residue from its cognate HK. This phosphorylation in turn results in the change of the DNA binding affinity or the enzymatic activity of the RR. A TCSs-involved signal transduction pathway that is responsible for gene expression regulation has been well characterized in *P. aeruginosa* (14). In this pathway, the hybrid sensor kinase RetS inhibits its downstream histidine kinase GacS and in turn represses biofilm formation while upregulating TTSS expression (1, 6, 14).

RetS is an unusual hybrid sensor kinase not only because it possesses a non-typical domain architecture but also because it is proposed to utilize a unique signaling mechanism (6, 9). RetS does not control the *gacS* gene transcription (1, 6). With the discovery that RetS and GacS can physically bind both *in vitro* and *in vivo*, Goodman et. al proposed that RetS and GacS form a 1:1 complex, which causes disruption of the GacS homo-dimer and in turn blocks GacS kinase activity (4, 6). According to this model, we have proposed a hypothesis for the functional role of RetS sensory domain in this particular signaling pathway (11). However, this protein-protein interaction mechanism has not been identified or described in any other TCSs. Besides, we observed an opposite phenotypic change than we would have predicted when the RetS sensory domain ($RetS_{peri}$) was deleted (described in chapter three).

The previous mutational analysis of RetS by Laskowski that the hisitidine residue in the kinase domain and the the aspartate residue in the second respose regulator domain of RetS are involved in TTSS regulation in a biofilm-deficient strain

PA103 (10). On the other hand, Goodman has shown that the conserved phosphorelay residues in RetS do not affect the expression of the small regulatory RNA RsmZ, which is part of RetS/GacS signaling pathway and favors biofilm gene expression (6). To further probe the signaling mechanism, we assessed the functional role of the RetS intrinsic phosphorelay activity in the regulation of the biofilm phenotype, such as exopolysaccharide production (9, 15). To this end, we applied mutational analysis targeting the conserved histidine residue and aspartate residues in the HK and RR domains respectively combined with a biofilm functional assay in this study. Interestingly, only the single mutation on the conserved histidine residue in the RetS HK domain causes a moderate increase of biofilm EPS production. With the fact that RetS is able to inhibit GacS phosphorylation and dephosphorylate phosphorylated GacS (GacS-P) (6), we propose an alternative hypothesis for RetS-GacS signaling: RetS kinase domain acts as a phosphatase to dephosphorylate GacS-P and thus blocks GacS kinase activity. To test this hypothesis, targeting the putative phosphatase activity of RetS kinase domain, a mutational analysis has been carried out in this study (4).

Finally, the stoichiometry of the RetS-GacS complex is an important piece of information for understanding RetS-GacS signaling. It has been demonstrated that RetS HK domain is sufficient for RetS-GacS interaction and inhibition of GacS phosphorylation. Therefore, we seek to determine the complex structure of RetS and GacS kinase domains with the aim to uncover the molecular basis for signaling mechanism between RetS and GacS.

Materials and Methods

Construction of plasmids containing either *retS* or *retS* mutant genes, transformation to *Pseudomonas aeruginosa* and congo red biofilm assay

All the mutants used in this chapter are constructed in same manner as for the mutants used in chapter three. The subsequent congo red biofilm experiments also follow the protocol described in chapter three.

Cloning, expression and purification of the RetS kinase domain and the GacS kinase domain

The domain architectures of both RetS and GacS were predicted using Pfam protein-families database as reference (3). The boundaries of RetS kinase domain (RetSkin) ancomapassing residues 393-649 were marked by the 7th transmembrane helix at the N-terminus and the first response regulator domain at the carboxyterminal end. The N-terminus GacS kinase domain (GacSkin) encompassing amino acids 218-520 is marked by the hydrophilic section of the HAMP domain and the ATPase domain at its corboxy-terminal end (figure 4.1). The following procedures were applied to RetSkin and GacSkin in same manner. The gene fragment coding for each domain (RetS393-649, GacS218-520) was PCR-amplified from *P. aeruginosa* PAO1 genomic DNA. During PCR, a tobacco etch virus (TEV) protease recognition site and the appropriate recombination sites (*attB1* and *attB2*) were added for Gateway cloning (11). Subsequently, each amplicon was recombined into pDONR201 (Invitrogen) to produce the plasmid pDONR201-RetS393-649 and pDONR201-GacS218-520. After verifying the nucleotide sequence via DNA sequencing, each target gene was recombined into the destination vector pDEST-HisMBP to create the expression vector pDEST-HMBP-RetS393-649 and pDEST-HMBP-GacS218-520 (11). Each expression vector is designed to produce RetSkin or GacSkin fused to the carboxy-terminal end of amino-terminally hexahistidine-tagged *E. coli* maltose binding protein (MBP).

RetSkin and GacSkin were expressed and purified in same manner. A single colony of *E. coli* BL21(DE3) CodonPlus RIL cells (Stratagene, La Jolla, CA) containing the expression plasmid were used to inoculate overnight at 37°C in Luria broth (LB) culture containing 100 μg/mL ampicillin and 30 μg/mL chloramphenicol. 75ml overnight culture was then diluted 40-fold into 3L of fresh medium supplemented with 2g/L glucose. When the cell density reached the midlog phase (OD_{600} = 0.6), the temperature was reduced to 27°C and isopropyl-β-D-thiogalacto-pyranoside (IPTG) was added to a final concentration of 1mM. After 4 hours, cells were harvested by centrifugation at 5500*g* for 15 min.

All of the following steps were carried out at 4°C. Cells were resuspended using a buffer containing 50 mM Tris-HCl, 150 mM NaCl, 25 mM imidazole, pH 7.4, 1mM DTT, and 0.3mM phenylmethanesulfonyl fluoride (SIGMA P7626-5G) (buffer A) (5mL of buffer per gram of cell mass). Cells were lyzed through sonication and insoluble debris removed by centrifuging the cell extract at 40,000*g* for 30 min. The supernatant was filtered through a 0.45 μm polyethersulfone membrane and loaded onto to a 30 mL Ni-NTA chromatography column (Qiagen, Valencia, CA) pre-equilibrated in buffer A. The column was washed to baseline with buffer A and eluted with a linear imidazole gradient to 250 mM over nine column volumes. Peak elution fractions were combined and 1.5 mg of His-TEV(S219V)-Arg protease were added to for every 10 mg of total protein to execute the cleavage of His-MBP. The TEV protease-digest reaction mixture was dialyzed overnight into buffer A. After dialysis, the protein solution was filtered and applied to a 40-mL Ni-NTA Superflow column (Qiagen) pre-equilibrated with buffer A. Flow-through fractions containing either RetSkin or GacSkin were pooled. Peak fractions were concentrated and loaded onto a HiPrep 26/60 Superdex^{TM}200 prep grade column (GE Healthcare), pre-equilibrated in a buffer of 25 mM Tris-HCl, 135 mM NaCl, 2mM tris (2-carboxyethyl) phosphine (TCEP) and 2.5% glycerol, pH 7.4 (buffer B). Each

protein was judged to be >95% pure by sodium dodecyl sulfate-polyacrylamide gel electrophoresis (SDS-PAGE).

Circular dichroism experiments to test ATP* (noncleavable ATP analog) binding

Both RetSkin and GacSkin were prepared in buffer B at a concentration of 10μM. Uncleaveable ATP analog (ATP*) was dissolved in pure water to 50mM concentration and titrated into protein samples. The instrument and parameters for circular dichroism experiments were the same as those used in chapter three. Protein buffer backgrounds with or without ATP* were subtracted from the protein spectra to generate the final data.

Crystallization of GacSkin and RetSkin

High-throughput crystallization screening was conducted in the sitting-drop format by combining a solution of either 4mg/ml RetSkin (with or without ATP*) or GacSkin in buffer B with commercially available crystallization matrices at volume ratios of 3:1, 1:1, and 1:3, where the protein solution was maintained at a constant volume of 0.3 μL throughout.

Results and Discussion

The conserved aspartate residues of the RetS response regulator domains are not required for regulating EPS production in PAO1

Mutational analysis in conjunction with the biofilm congo red assay was utilized to assess the functional role of the conserved phosphorelay residues of RetS in biofilm formation regulation. Targeting the conserved histidine residue (His424) in the HK domain and aspartate residues (Asp713, Asp715, Asp858) in two RR domains, single alanine mutations were introduced into the *retS* gene (6). Corresponding RetS variants were expressed in PAO1Δ*retS* in same way as as described in chapter three for wild type RetS. In the subsequently performed congo red biofilm assays was none of the aspartate mutants showed a difference in EPS production compared to the mutant strain complemented with wild-type *retS* (figure 4.2). This result is consistent with the previous study by Goodman showing that mutations on these aspartates did not affect RsmZ expression level in the PAK strain (6). The H424A mutation in the HK domain, on the other hand, caused a slight higher rate of EPS production compared to that of the complementation strain (figure 4.2). This phenotype change is unlikely due to the change of RetS intrinsic phosphorelay activity because the mutations on RR domains do not impact biofilm EPS production. Therefore, this increased EPS production phenotype might be caused by the intrinsic phophatase activity of the HK domain in RetS (4).

Is the phosphatase motif of the RetS kinase domain involved in the regulation of EPS production?

Previous studies have indicated that RetS may not only prevent GacS autophosphorylation but also actively dephosphorylate already phosphorylated GacS (6). Therefore, one potential explanation for the phenotype of the H424A mutant is that this mutation affects the intrinsic phosphatase activity of the HK in RetS (4). Sequence analysis indicates that the RetS kinase domain is a member of the HisKA

subfamily, which is one of the five HK families of sensor kinases, and this HiskA subfamily is characterized by a conserved HE/DXXT/N motif (7). The threonine residue (Thr) has been demonstrated to play an essential role in the phosphatase activity of EnvZ, a histidine kinase in *E. coli* (2). Therefore, to test our hypothesis we mutated corresponding Thr (T428) in RetS and examined effect of this mutation on biofilm formation regulation. To this end the RetS-T428A was expressed in PAO1Δ*retS* mutant followed by congo red biofilm assay. As shown by figure 4.2c, similar to the H424A mutant, the T428A mutant also exhibits a higher rate of EPS production phenotype compared to that of the complementation strain.

This result implies that RetS kinase domain possesses phosphatase activity which has a functional role in EPS production regulation. This result suggests an alternative possibility for the functional role of RetS-GacS binding that it does not block GacS auto-transphosphorylation, but dephosphorylates GacS. This hypothesis is supported by Goodman's data showing that RetS can reduce the phosphorylation level of phosphorylated GacS (GacS-P) (6).We seek to characterize the RetS-GacS interaction with the aim to uncover the molecular basis for RetS-GacS signaling mechanism. It has been demonstrated that the kinase domain of RetS (RetSkin) is sufficient to bind GacSkin and dephosphorylate GacS-P (6). So for subsequent studies, we target to RetSkin and GacSkin, instead of all cytoplasmic domains of these two proteins.

Both purified RetSkin and GacSkin can bind ATP*

Both RetSkin and GacSkin proteins have been successfully purified. As shown by figure 4.1, each construct contains intact ATPase domain and coil-coil region (4, 6). GacSkin also contains part of the HAMP domain. In order to determine if the purification products are properly folded and functional, we examined the ATP binding capability of purified RetSkin and GacSkin. To this end, circular dichroism experiments were applied for protein-ligand binding study. As indicated by figure 4.3, both RetSkin and GacSkin could bind noncleabable ATP (ATP)*. This result also

implies that the absence of a detectable kinase activity of RetS might be due to the deficiency of the ATP hydrolysis but not the ATP binding capability.

Crystallization of RetSkin with and without ATP*

To directly decipher the molecular basis for RetS-GacS signaling, we seek to determine the RetSkin-GacSkin complex structure, which will provide exact information for RetS-GacS interaction pattern. To use end, crystallization and crystallography strategy was applied. Preliminary crystals for both RetSkin with and without ATP* were obtained from condition F7 of the IndexHT screen (Hampton Research). Hit optimization was carried out using the hanging drop vapor diffusion method at room temperature (23°C) (figure 4.4). In the optimized conditions crystals for RetSkin was obtained from drops containing a 3:1 mixture (protein: precipitant) of 10.5 mg/mL protein in buffer B and a crystallization solution composed of 0.2M ammonium sulfate, 0.1M Bis-Tris (pH 6.54) and 25% w/v polyethylene glycol 3350 (figure 4.4).

Conclusion and discussion

The single mutation on the HE/DXXT/N motif causes decreased biofilm EPS production. This result indicates that the potential phosphatase activity of RetS kinase domain might be involved in biofilm formation regulation in *P. aeruginosa*. Most histidine kinases possess both kinase and phosphatase activities. Lacking a detectable kinase activity, RetS kinase domain might exclusively acts as a phosphatase. We have shown in chapter three that deletion of the homo-dimerization domain $RetS_{peri}$, which potentially weakens the RetS homo-dimerization, resulted in increased biofilm EPS production. Hence, it does not support the previous hypothesis that $RetS_{peri}$ regulates hetero-dimerization between RetS and GacS. Instead, an alternative possibility is that $RetS_{peri}$ controls the potential phosphatase activity of RetSkin via sensing environmental signals. We offer an alternative hypothesis for molecular basis of RetS-GacS signaling: RetS-GacS is a hetero-tetramer, which causes

desphophorylation of phosphorylated GacS via a novel mechanism.

Finally, the structure determination for individual RetSkin and GacSkin as well as the RetSkin-GacSkin complex will help us to uncover the mechanism, whereby RetS inhibits the activity of GacS and downstream GacS/GacA signaling.

Acknowledgements

I like to thank the graduate student Jordan Mancl who has been assisting in the RetSkin crystallization optimization. I also want to thank Dr. Webster Santos for kindly allowing us to use the circular dichroism instrument in his lab.

References

1. Andrew L. Goodman, Bridget Kulasekara, Arne Rietsch, Dana Boyd, Roger S. Smith, and Stephen Lory. 2004. A Signaling Network Reciprocally Regulates Genes Associated with Acute Infection and Chronic Persistence in Pseudomonas aeruginosa. Developmental Cell. 7:745–754.
2. Dutta R, Yoshida T, Inouye M. 2000. The Critical Role of the Conserved Thr247 Residue in the Functioning of the Osmosensor EnvZ, a Histidine Kinase/Phosphatase, in Escherichia coli J Biol Chem. 275:38645-53.
3. Finn RD, Mistry J, Tate J, Coggill P, Heger A, Pollington JE, Gavin OL, Gunasekaran P, Ceric G, Forslund K, Holm L, Sonnhammer EL, Eddy SR, Bateman A. 2010. The Pfam protein families database. Nucleic Acids Res. 8:211-22.
4. Gao R, Stock AM 2009. Biological insights from structures of two-component proteins. Annu Rev Microbiol. 63:133-54.
5. Gooderham WJ, Hancock RE. 2009. Regulation of virulence and antibiotic resistance by two-component regulatory systems in Pseudomonas aeruginosa. FEMS Microbiol Rev. 33:279-94.
6. Goodman AL, Merighi M, Hyodo M, Ventre I, Filloux A, Lory S. 2009. Direct interaction between sensor kinase proteins mediates acute and chronic disease phenotypes in a bacterial pathogen. Genes Dev. 23:249-59.
7. Huynh TN, Noriega CE, Stewart V. 2010. Conserved mechanism for sensor phosphatase control of two-component signaling revealed in the nitrate sensor NarX. Proc Natl Acad Sci U S A. 107:21140-5.
8. Jing X, Jaw J, Robinson HH, Schubot FD. 2010. Crystal structure and oligomeric state of the RetS signaling kinase sensory domain. Proteins. 78:1631-40.
9. Ma L-Y, Jackson K, Landry RM, Parsek MR, Wozniak DJ. 2006. Analysis of Pseudomonas aeruginosa conditional Psl variants reveals roles for the Psl polysaccharide in adhesion and maintaining biofilm structure postattachment. J Bacteriol. 188:8213–8221.
10. Michelle A. Laskowski, and Barbara I. Kazmierczak. 2006. Mutational Analysis of RetS, an Unusual Sensor Kinase-Response Regulator Hybrid Required for Pseudomonas aeruginosa Virulence. INFECTION AND IMMUNITY. 74:4462–4473
11. Nallamsetty S, Austin BP, Penrose KJ, Waugh DS. 2005. Gateway vectors for the production of combinatorially-tagged His6-MBP fusion proteins in the cytoplasm and periplasm of Escherichia coli. Protein Sci. 14:2964–2971.
12. Rodrigue, A., Quentin, Y., Lazdunski, A., Mejean, V., and Foglino, M. 2000. Two-component systems in Pseudomonas aeruginosa: why so many? Trends Microbiol. 8:498–504.

13. Shawn Lewenza, et. al. 2005. Construction of a mini-Tn5-luxCDABE mutant library in Pseudomonas aeruginosa PAO1: A toll for identifying differentially regulated genes. Genome Research. 15:583-589.
14. Ventre I, Goodman AL, Vallet-Gely I, Vasseur P, Soscia C, Molin S, Bleves S, Lazdunski A, Lory S, Filloux A. 2006. Multiple sensors control reciprocal expression of Pseudomonas aeruginosa regulatory RNA and virulence genes. Proc Natl Acad Sci U S A. 103:171-6.
15. Wozniak DJ, Wyckoff TJ, Starkey M, Keyser R, Azadi P, O'Toole GA, Parsek MR. 2003. Alginate is not a significant component of the extracellular polysaccharide matrix of PA14 and PAO1 Pseudomonas aeruginosa biofilms. Proc Natl Acad Sci U S A. 100:7907-12.

Table 4.1 Bacterial cells and plasmids

Stain or plasmid	Relevant Information	Source/ Reference
***E. coli* strains:**		
BL21	DE3 CodonPlus RIL cells for protein expression	Stratagene
DH5α	Only used for Gateway cloning procedures	This study
***P. aeruginosa* cells:**		
PAO1	Wild type strain	13
PAO1Δ *retS*	PAO1 *retS* transposon insertion mutant	13
PAO1Δ *retS*+ *retS*_pSK	PAO1 *retS* complementation strain	This study
PAO1Δ*retS*+ *retS*H424A_pSK	PAO1 *retS* complementation strain with alanine mutation on His424	This study
PAO1Δ*retS*+ *retS*D713A_pSK	PAO1 *retS* complementation strain with alanine mutation on Asp713	This study
PAO1Δ*retS*+ *retS*D715A_pSK	PAO1 *retS* complementation strain with alanine mutation on Asp715	This study
PAO1Δ*retS*+ *retS*D858A_pSK	PAO1 *retS* complementation strain with alanine mutation on Asp858	This study
PAO1Δ*retS*+ *retS*T428A_pSK	PAO1 *retS* complementation strain with alanine mutation on Thr428	This study
Plasmids:		
pSK_*retS*	pSK carrying wild type *retS* gene	This study
pSK_*retS*H242A	pSK carrying *reS*H424A	This study
pSK_*retS*D713A	pSK carrying *reS*D713A	This study
pSK_*retS*D715A	pSK carrying *reS*D715A	This study

pSK_*retS*D858A	pSK carrying *reS*D858A	This study
pSK_*retS*T428A	pSK carrying *reS*T428A	This study

Table 4.2 primers (underlined sequences correspond to unique restriction sites utilized for cloning)

Primer	Sequence (5' to 3')	Source/ Reference
retS1006AscI_F	CCAGCCGGCGCGCCTGATCGTTGCCGGGATGATCGT	This study
retSH424A_F	CAAGATCAGCGCCGAGATCCGCACGCCCATGAAC	This study
retSH424A_R	TGCGGATCTCGGCGCTGATCTTGGCCAGGAACTC	This study
retS486_F	ATGACCTCCAACCATCCGCTGATGGCCTGGTTCGACCAGATCGAC	This study
RetSD713_F	GGTCCTGCTCGCCCAGGACATGCCCGGCATGACC	This study
RetSD713_R	GCATGTCCTGGGCGAGCAGGACCACGTCGAAGTA	This study
RetSD715_F	GCTCGACCAGGCCATGCCCGGCATGACCGGCATG	This study
RetSD715_R	TGCCGGGCATGGCCTGGTCGAGCAGGACCACGTC	This study
RetSD858_F	GGTGCTGATGGCCTGCGAGATGCCGGTTCTGGAC	This study
RetSD858_R	GCATCTCGCAGGCCATCAGCACCAGGTCGTACTG	This study
retST428A_F	CGAGATCCGCGCGCCCATGAACGGCGTGCTGGGC	This study
retST428_R	CGTTCATGGGCGCGCGGATCTCGTGGCTGATCTT	This study
-258retS_SacI-F	ATCAGTGCGGAGCTCGTGCTCTGTGCCACCGCCATC	This study
RetSEndEcorRI_R	ATCAGTGAATTCTCAGGAGGGCAGGGCGTCG	This study
RetSkin_393F	GTGGAGAACCTGTACTTCCAGGGTCTGATCCAGCAGCTCAACCTG	This study
RetSkin_649R	GGGGACAACTTTGTACAAGAAAGTTGCTCAGGCGGTGGGGTTCTCCAGCTG	This study
GacSkin_219F	GTGGAGAACCTGTACTTCCAGGGTATGGGCAGCAACGAGCTG	This study
GacSkin_520R	GGGGACAACTTTGTACAAGAAAGTTGCTCAGCCCGGCTCCTCGTTGTCGTC	This study

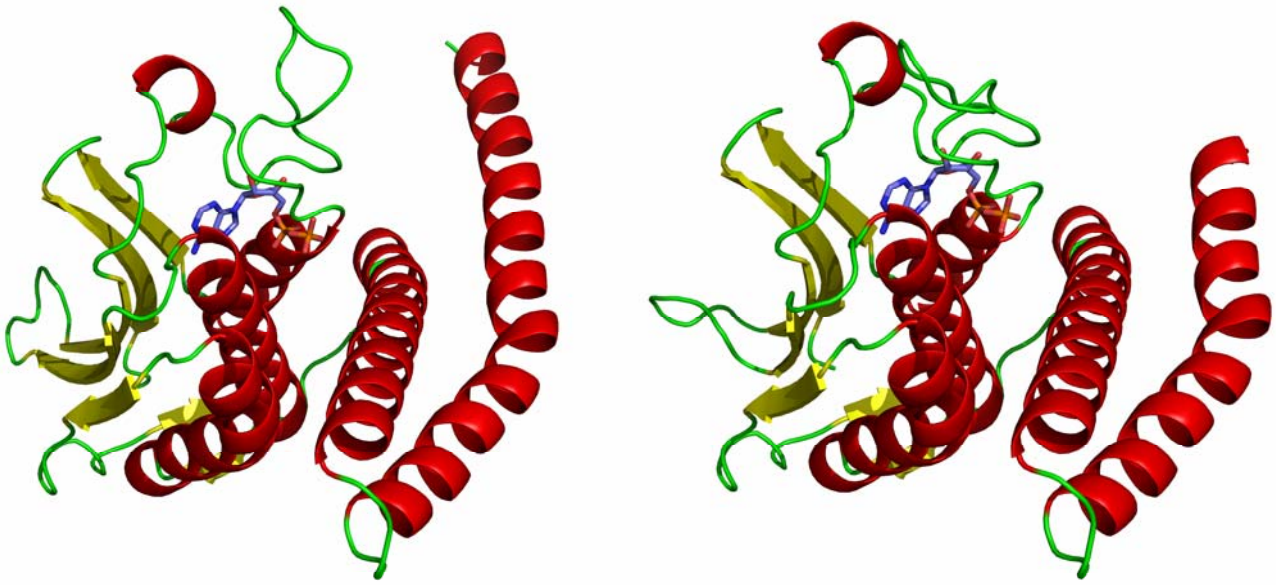

Figure 4.1 Homology models for RetSkin and GacSkin. Cartoon depictions of homology models for RetS kinase domain (**left**) (RetS373-640) and the GacS kinase domain (**right**) (GacS270-511) generated with the SWISS-MODEL server using *Thermotoga maritima* class I histidine kinase HK853 (PDB ID: 3dge) and a tyrosine kinase from *Caulobacter crescentusas* (PDB ID: 4ew8) as the modeling templates, respectively. The putative ATP binding sites of both structures are presented by the ADP residue shown by a stick style in blue color.

a)

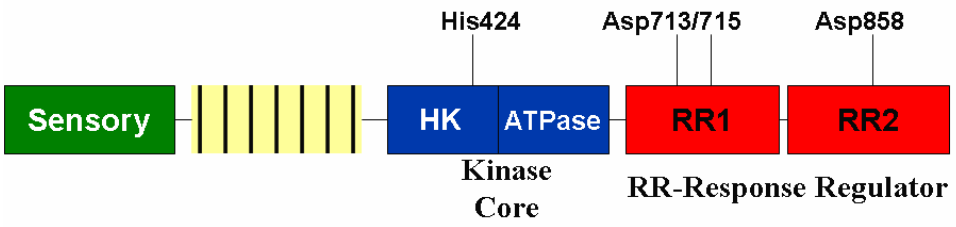

b)

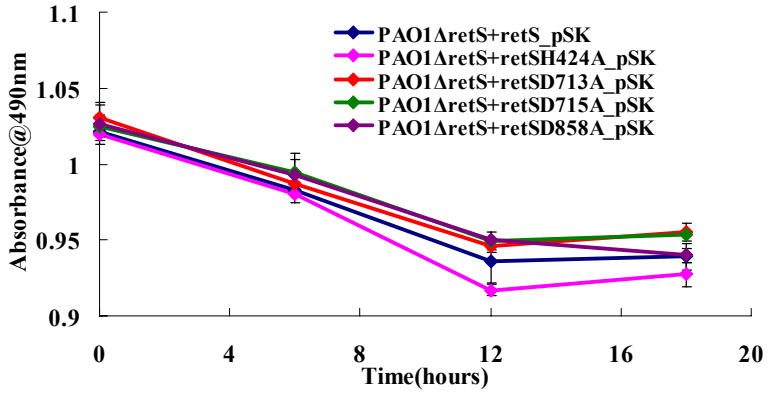

c)

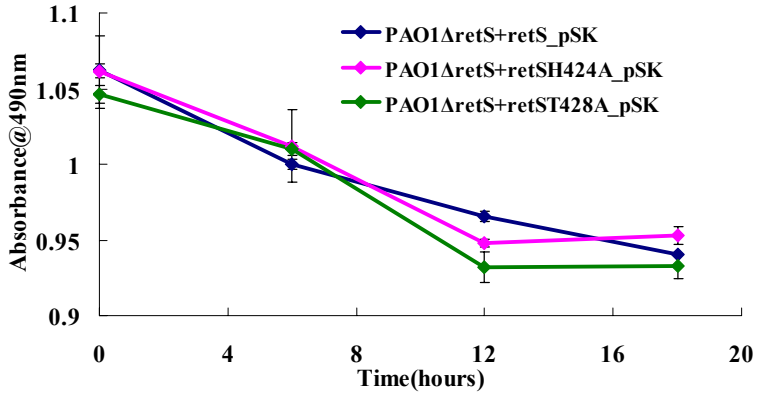

Figure 4.2 The signaling role of phosphorelay residues of RetS in biofilm EPS production regulation. (a) Schematic of the domain architecture of RetS wherein the conserved residues that might be involved in phosphorelay marked. **(b)** To assess the functional role of RetS intrinsic phosphorelay activity in biofilm EPS production regulation a congo red assay analysis was performed on the *retS*-mutant strain transformed with expression plasmids for expressing either wild-type *retS* or the different point mutants *in trans*. **(c)** The examination of the functional role of the putative phosphatase residues H424 and T428 in biofilm EPS production regulation.

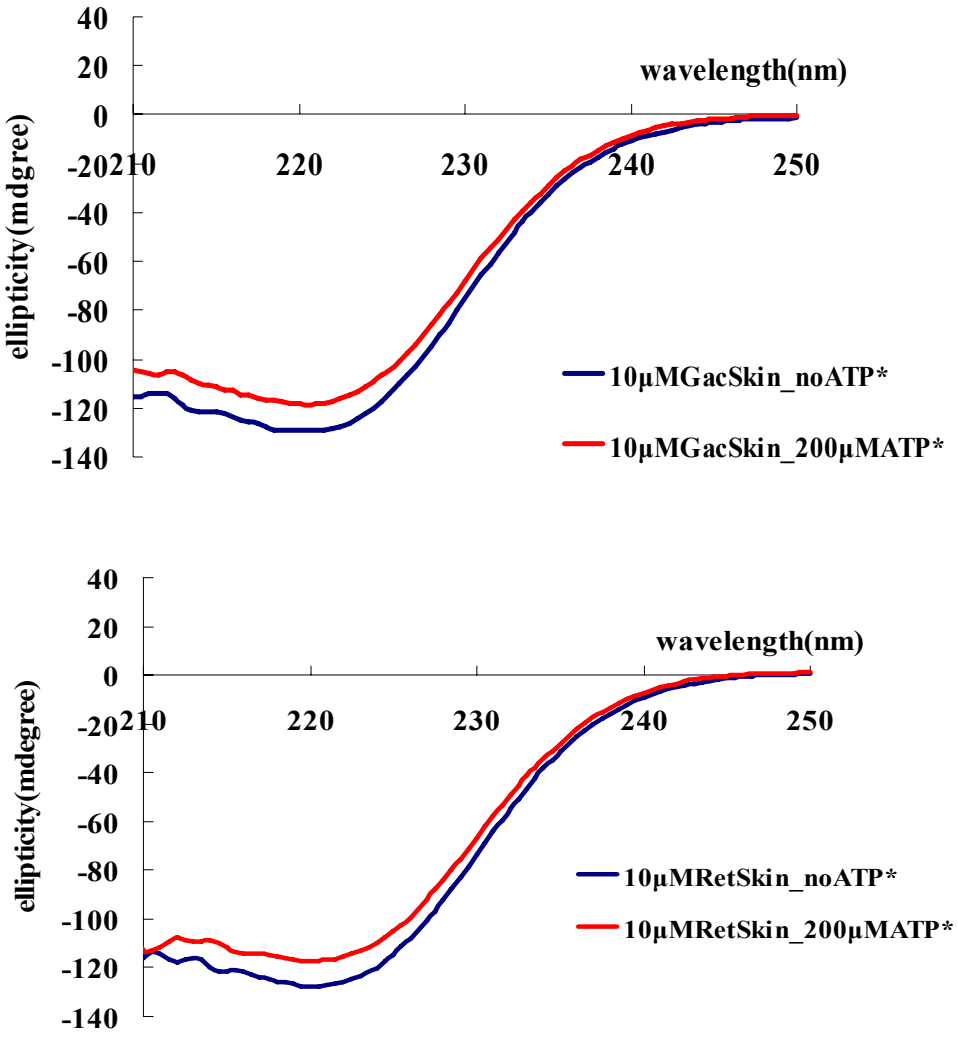

Figure 4.3 Examination of ATP-binding for RetSkin and GacSkin. Far-UV circular dichroism (CD) spectra of 10μM RetSkin or GacSkin in the absence (blue) and presence of ATP* (red) were collected. The experiments were performed at 4 °C.

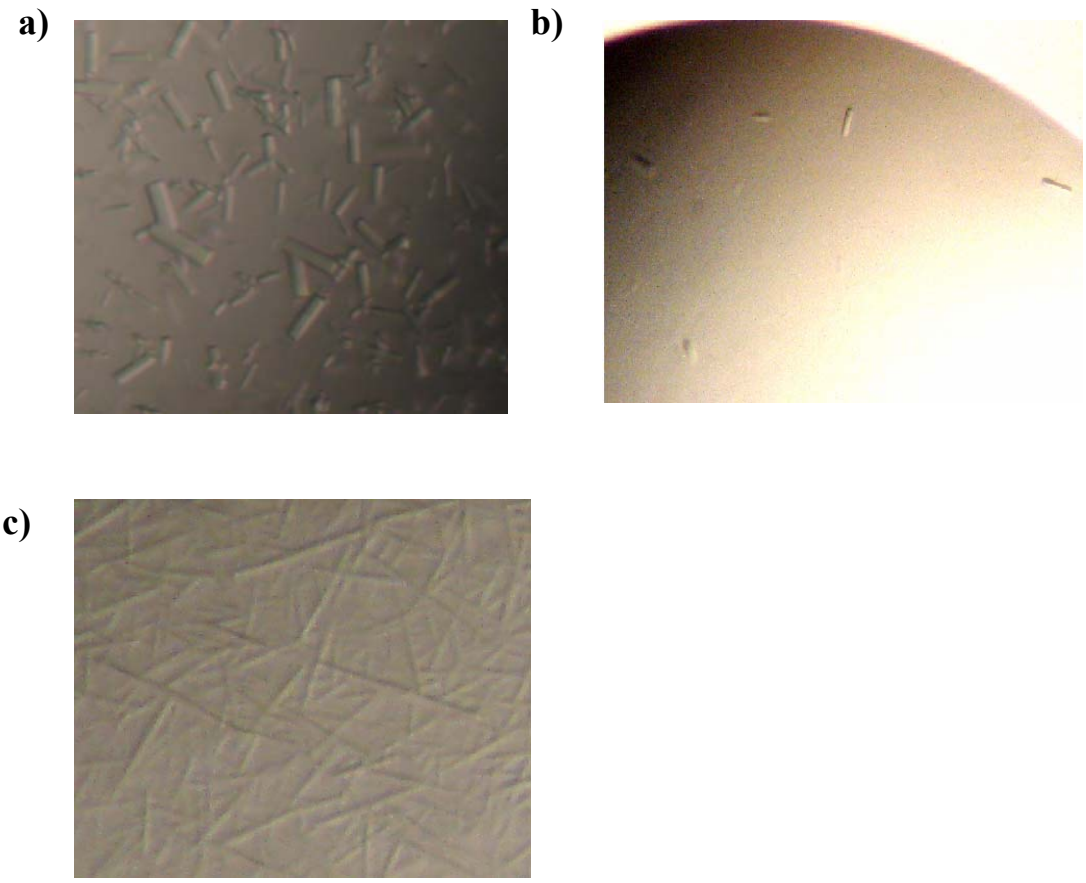

Figure 4.4 Crystallization of RetSkin with and without ATP*. Crystals in **a)** were obtained by sitting-drop crystallization method using 4mg/mL protein with crystallization condition JCSG F7 (0.8M succinate, pH 8.0). Crystals in **b)** and **c)** were produced by hanging-drop using 10mg/mL protein (with 2mM ATP* in **c**) with optimized crystallization condition Index F7 (0.1mM Bis-Tris, pH6.5, 0.25M ammonium sulfate, 25% PEG3350).

Chapter Five

Final Discussion

The chronic infections by *Pseudomonas aeruginosa* are the major cause of high mortality and morbidity among more than 80% cystic fibrosis patients (6). There is a strong interest in looking for effective therapies. The chronic infections by *P. aeruginosa* are strongly associated with biofilm formation, which consists of bacterial cells protected by an exopolysaccharide-rich matrix thus leading to higher levels of resistance to anti-microbial agents compared to the planktonic form of the bactium(9). The ultimate goal of our work is to develop a strategy aimed at repressing biofilm formation-associated gene expression in *Pseudomonas aeruginosa.*

In *P. aeruginosa*, the two-component system (TCS) hybrid sensor kinase RetS significantly represses biofilm formation by interacting with the downstream TCS histidine kinase GacS, which promotes biofilm gene expression (4, 3). Although RetS possesses a conserved TCS domain architecture and conserved phoshorelay residues (3), the signaling mechanism for this protein has been suggested to be unusual (4). We have shown that the mutations in the phosphorelay residues in RetS response regulator (RR) domains do not result in any change to either the biofilm EPS production (chapter four) or biofilm-associated RsmZ expression (4). While data from the Kazmierczak group revealed that the second RR domain of RetS is required for virulence in a mouse model of acute pneumonia, the exact signaling role of RetS RR domains remains unknown.

RetS is an appealing kinase to medical community because it contains a potential drug-target domain ($RetS_{peri}$), which is putatively essential for RetS signaling (2, 8). Unfortunately, all of our attempts to identify signaling-effective ligands for $RetS_{peri}$ have been unsuccessful. Moreover, our experimental results show that single mutations on the putative ligand binding sites of $RetS_{peri}$ had no impact on biofilm EPS production. One explanation for this result is that the natural ligand of $RetS_{peri}$ does not exist in our congo red biofilm assay, implying that either the ligand comes from host human cells infected by *P. aeruginosa* or the availability of the signal for RetS requires the bacterial-host contact. This might explain why overexpression of PSL exopolysaccharide, which is one key component of biofilm matrix in unmucoid *P. aeruginosa* strain (1, 7), did not affect the expression level of the small regulatory

RNA RsmZ (chapter three).

It has been shown that RetS is not capable of autophophorylation. However, this is unlikely caused by the ATP-binding deficiency of RetS kinase domain as shown by chapter four. Whether the unsuccessful detection of RetS kinase activity is due to ATP-hydrolysis deficiency or the absence of RetS sensory domain in the reported phosphorylation experiments is unclear (2, 4). Based on the novel RetS-GacS signaling model, two different groups including ours proposed the same hypothesis for the signaling role of $RetS_{peri}$. Subsequently, we have developed experimental strategies to test these hypotheses. However, as described in chapter three, the impact of deleting of $RetS_{peri}$ on biofilm EPS production was opposite to what we had expected (4). Introducing single cysteine residues that were able to enhance *in vitro* $RetS_{peri}$ homo-dimerization did also not produce changes in the EPS production phenotype. Therefore, we question the veracity of the current model for the RetS-GacS signaling mechanism. In addition, along with the data showing that RetS (or RetS kinase domain-RetSkin) block GacS (or GacS kinase domain-GacSkin) autophosphorylation, Goodman with colleagues have also shown that RetS or RetSkin was able to dephosphorylate the phosphorylation-state GacS or GacSkin (4). Hence, considering the RetSkin has an intrinsic phosphatase activity (2, 5), we hypothesize in chapter four that RetSkin serves as a phosphatase for GacSkin when the RetS-GacS complex forms. It has been described that the equilibrium between the kinase activity and the phosphatase activity is tuned by signal sensing on sensor kinases (2). This notion might explain the slightly faster biofilm EPS production in the putatively phosphatase-deficient mutants considering a $RetS_{peri}$ ligand is probably absent in our congo red assay. This possibility leads to an alternative hypothesis for $RetS_{peri}$ signaling role that is proposed in chapter four. This hypothesis can be used to explain why deletion of $RetS_{peri}$ resulted in an increased biofilm-EPS production phenotype (chapter three).

Finally, according to this alternative hypothesis, dephosphorylation of GacS by RetS does not require the disruption of GacS homo-dimerization. Future experiments will examine the oligmeric state of RetS-GacS complex to test this model. This work

will be enhanced by ongoing structure-determination studies aimed at understanding the molecular basis for the RetS-GacS interactions and revealing the unique structural features of the RetS kinase domain.

References

1. Byrd MS, Sadovskaya I, Vinogradov E, Lu H, Sprinkle AB, Richardson SH, Ma L, Ralston B, Parsek MR, Anderson EM, Lam JS, Wozniak DJ. 2009. Genetic and biochemical analyses of the Pseudomonas aeruginosa Psl exopolysaccharide reveal overlapping roles for polysaccharide synthesis enzymes in Psl and LPS production. Mol Microbiol. 73:622-38.
2. Gao R, Stock AM. 2009. Biological insights from structures of two-component proteins. Annu Rev Microbiol. 63:133-54.
3. Goodman AL, Kulasekara B, Rietsch A, Boyd D, Smith RS, Lory S. 2004. A signaling network reciprocally regulates genes associated with acute infection and chronic persistence in Pseudomonas aeruginosa. Dev Cell. 7:745–754.
4. Goodman AL, Merighi M, Hyodo M, Ventre I, Filloux A, Lory S. 2009. Direct interaction between sensor kinase proteins mediates acute and chronic disease phenotypes in a bacterial pathogen. Genes Dev. 23:249-59.
5. Huynh TN, Noriega CE, Stewart V. 2010. Conserved mechanism for sensor phosphatase control of two-component signaling revealed in the nitrate sensor NarX. Proc Natl Acad Sci U S A. 107:21140-5.
6. Lyczak, J. B., C. L. Cannon, and G. B. Pier. 2000. Establishment of Pseudomonas aeruginosa infection: lessons from a versatile opportunist. Microbes Infect. 2:1051–1060.
7. Ma L-Y, Jackson K, Landry RM, Parsek MR, Wozniak DJ. 2006. Analysis of Pseudomonas aeruginosa conditional Psl variants reveals roles for the Psl polysaccharide in adhesion and maintaining biofilm structure postattachment. J Bacteriol. 188:8213–8221.
8. Michelle A. Laskowski, and Barbara I. Kazmierczak. 2006. Mutational Analysis of RetS, an Unusual Sensor Kinase-Response Regulator Hybrid Required for Pseudomonas aeruginosa Virulence. INFECTION AND IMMUNITY. 74:4462–4473.
9. Schooling SR, Beveridge TJ. 2006. Membrane vesicles: an overlooked component of the matrices of biofilms. Journal of Bacteriology. 188:5945–5957.

Part II

The catalytic domain of the germination-specific lytic transglycosylase SleB from *Bacillus anthracis* displays a unique active site topology

Xing Jing[1], Howard R. Robinson[2], Jared D. Heffron[3], David L. Popham[1], and Florian D. Schubot[1.] 2012. Proteins Journal. 80(10):2469-75

[1] Virginia Tech, Department of Biological Sciences, Life Sciences, Blacksburg, Virginia 24061

[2] Biology Department, Brookhaven National Laboratory, Upton, New York 11973-5000

[3] USAMRIID, Bacteriology Division, Frederick, Maryland 21702-5011

Keywords: SleB; CwlJ; *Bacillus anthracis*; spore;germination; lytic transglycosylase; muramic-δ-lactam; peptidoglycan; cortex peptidoglycan

Abstract

Bacillus anthracis produces metabolically inactive spores. Germination of these spores requires germination-specific lytic enzymes (GSLEs) that degrade the unique cortex peptidoglycan to permit resumption of metabolic activity and outgrowth. We report the first crystal structure of the catalytic domain of a GSLE, SleB. The structure revealed a transglycosylase fold with unique active site topology and permitted identification of the catalytic glutamate residue. Moreover, the structure provided insights into the molecular basis for the specificity of the enzyme for muramic-δ-lactam-containing cortex peptidoglycan. The protein also contains a metal-binding site that is positioned directly at the entrance of the substrate-binding cleft.

Abbreviations:

Cwlj, cell wall hydrolase j; DTT, dithiothreitol; EGTA, ethylene glycol tetraacetic acid; GSLEs, germination-specific lytic enzymes; MAD, multiple wavelength anomalous dispersion; MBP, maltose-binding protein; NAG, *N*-acetylglucosamine; NAM, *N*-acetylmuramic acid; Ni-NTA, nickel–nitrilotriacetic acid; PG, peptidoglycan; SleB, spore cortex lytic enzyme B; $SleB_{CAT}$, catalytic domain of SleB.

Introduction

Bacterial endospores can survive in a metabolically dormant state for many years and exhibit extreme resistance to a wide range of killing agents (24). Dormancy and most resistance properties are dependent on the relative dehydration of the spore core (cytoplasm), and this dehydration is dependent on the presence of the spore cortex peptidoglycan (PG) wall surrounding the core (24). When spores sense a favorable growth environment and initiate germination, they must degrade the cortex PG as an essential step to allow full core rehydration and a resumption of metabolism (21, 23). The germination-specific lytic enzymes (GSLEs) responsible for cortex degradation are produced during spore formation and are held in a highly stable yet inactive state during spore dormancy. The mechanism by which GSLEs are held inactive, their mechanism of activation, and the molecular basis for their specificity for the cortex PG are of basic as well as applied interest. Treatments that activate GSLEs result in a loss of spore resistance properties (14). A method of triggering highly efficient and synchronous activation of GSLEs would therefore greatly simplify spore decontamination measures, which is relevant for clinical spaces, food preparation facilities, and anti-bioweapon development.

The GSLE SleB has been shown to play a key role in the germination of spores of several *Bacillus* species (2, 10, 18), and *sleB* genes are highly conserved across the *Bacillus* genus as well as in some *Clostridium* species (20). SleB is produced within the developing spore with a signal peptide that is cleaved following SleB translocation across the spore membrane (17, 18, 19). SleB then remains inactive within the same spore compartment as the cortex PG and is activated during germination. Active SleB functions as a lytic transglycosylase to depolymerize the cortex PG (2, 10). SleB and other GSLEs exhibit specificity for PG containing the modified sugar muramic-δ-lactam (4, 5, 21), which is found only within spore cortex PG (26).

In addition to its catalytic domain (pfam07486) (13), SleB possesses an N-terminal PG-binding domain (pfam01471) (11, 18, 19), which increases its affinity

for PG and its rate of PG cleavage although it is not required for either role (11). Interestingly, a second GSLE, CwlJ, possesses significant sequence similarity with the catalytic domain of SleB but lacks the PG-binding domain (13).

To begin characterization of SleB substrate recognition and cleavage factors, we have determined the crystal structure of the catalytic domain of *Bacillus anthracis* SleB ($SleB_{CAT}$) to a resolution of 1.9 Å. Although it shares some features with other transglycosylases, $SleB_{CAT}$ displays a unique binding cleft topology reflective of its unusual specificity for muramic-δ-lactam-containing PG. The structure also revealed the catalytic glutamate residue and led to the unexpected discovery of a metal binding site, which is conspicuously positioned at the entrance of the substrate-binding pocket.

Materials and Methods

Expression and purification of SleB and $SleB_{CAT}$

The expression vectors and protocols used for full-length SleB and $SleB_{CAT}$ were identical to those used in a previous study (11) with minor modifications. Protein expression was induced at 20°C rather than 10°C. Cells were resuspended in 5 mL buffer A (50 mM Tris-HCl, 150 mM NaCl, 25 mM imidazole, pH 7.4), 1 m*M* dithiothreitol (DTT), and 0.3 m*M* phenylmethanesulfonyl fluoride (Sigma) per gram cells. Cell lysis via sonication was followed by centrifugation at 40,000*g* for 30 min. The supernatant was filtered through a 0.45-μm polyethersulfone membrane and loaded onto to a 30-mL nickel–nitrilotriacetic acid (Ni-NTA) Superflow column (Qiagen) pre-equilibrated in buffer A. The column was washed with buffer A and eluted with a linear imidazole gradient to 250 mM. Cleavage of the HisMBP fusion proteins was achieved by adding a variant of Tobacco Etch Virus protease, His-TEV(S219V)-Arg (1.5 mg TEV/10 mg of total protein) to the pooled peak fractions. The reaction mixture was dialyzed overnight into buffer A. Subsequently, the protein solution was filtered and applied to a 40-mL Ni-NTA Superflow column (Qiagen) pre-equilibrated with buffer A. Flow-through fractions containing the SleB or $SleB_{CAT}$ were dialyzed overnight into 50 mM Tris, 50 mM NaCl, pH 7.5, and 2 mM DTT with 2.5% glycerol (buffer B). The sample was then applied to a 10-mL Heparin column (GE Healthcare) pre-equilibrated with buffer B and was eluted with a linear gradient to 0.5M NaCl. Peak fractions were concentrated and loaded onto a HiPrep 26/60 Superdex™200 prep grade column (GE Healthcare) pre-equilibrated in a buffer of 25 mMTris-HCl, 150 mM NaCl, 2 mM *tris*(2-carboxyethyl)phosphine, and 2.5% glycerol, pH 7.4 (buffer C). The protein was judged to be >95% pure by sodium dodecyl sulfate-polyacrylamide gel electrophoresis.

Cloning, expression, and purification of selenomethionine-substituted $SleB_{CAT}$ and $SleB_{CAT}^{L143M}$

As the single methionine in the native sequence of $SleB_{CAT}$ proved insufficient for structure solution, a second methionine was introduced in position 143 via

site-directed mutagenesis using the following primers: 5′-TGATATTCAGAT GATGGCAAACGCAGTATATGGA-3′ and 5′-CGTTTGCCA TCATCTGAATATCATTTTGAGAATA-3′. After sequencing, the modified plasmid was transformed into *Escherichia coli* BL21 (DE3) CodonPlus RIL cells (Stratagene, La Jolla, CA) for protein expression.

To prepare selenomethionine-substituted $SleB_{CAT}$ or $SleB_{CAT}^{L143M}$, cells obtained from a 1 L of mid-log phase culture (prepared as described above) were washed twice in 100 mL of M9 selenomethionine growth media (Medicilon). The cells were resuspended in 100 mL of M9 selenomethionine growth media and used to inoculate four 1-L cultures containing M9 selenomethionine growth media and antibiotics. These cultures were grown with agitation at 37°C until the OD_{600nm} reading reached 0.5. Protein expression and purification followed the same procedures as described above.

Crystallization of native $SleB_{CAT}$ and $SleB_{cat}^{L143M}$

Crystallization screening in the sitting-drop format produced an initial hit from condition F7 of the IndexHT screen (Hampton Research). Hit optimization was carried out using the hanging drop vapor diffusion method at room temperature (23°C). Diffraction quality crystals for both native $SleB_{CAT}$ and SeMet-$SleB_{CAT}^{L143M}$ were obtained from droplets containing a 1:1 mixture of 2.5 mg/mL protein and a crystallization solution composed of 0.2M ammonium sulfate, 0.1M Bis-Tris (pH 5.8) and 15% w/v polyethylene glycol 3350.

Data collection, structure solution, and refinement

Crystals were loop-mounted after they had been soaked in a cryosolution consisting of crystallization stock solution supplemented with either 10 or 12.5% glycerol, and subsequently flash-frozen in liquid nitrogen. All data sets were collected at beamline X-29A of Brookhaven National Laboratory using an ADSC Q315 CCD detector. The CCP4 program suite (15) was used for data processing.

Multiple wavelength anomalous dispersion (MAD) data collection (12) of the $SleB_{CAT}^{L143M}$ variant crystal yielded excellent electron density maps used for model

building. Selenium atom search, initial phase calculation, density modification, and automated model building were all completed in the PHENIX program suite (1). Iterative cycles of manual model adjustment using COOT followed by refinement in PHENIX converged to produce the final structures. Detailed statistics for data collection, experimental phasing, and model refinement are summarized in table 6.1. The model quality was validated using Procheck (16). The coordinates for the two molecules in the asymmetric unit have been deposited with the Protein Data Bank (pdb code 4FET).

Construction of active site mutant and assay of SleB function

To create the *sleB E151A* allele in which the catalytic glutamate is changed to an alanine, PCR-based site-directed mutagenesis was carried out using the following primers: 5′CTCATG GCAAACGCAGTATACGGAGCGTCTCGTGG TG3′ and 5′CACCACGAGACGCTCCGTATACTGCGTTT GCCATGAG3′. The alteration was made to the *sleB* gene in plasmid pDPV346 (10). The resulting plasmid pDPV430 was introduced into strain DPBa74 (9) to test if the altered protein allows completion of spore germination. Spores were plated in the presence and absence of lysozyme as described previously (9).

Results

Structure solution and overall fold of $SleB_{CAT}$

Following an unsuccessful attempt to crystallize the full-length SleB, we focused on the structure of the catalytic domain encompassing residues 125–253 of the enzyme. We were unable to solve the structure by molecular replacement and therefore a MAD phasing strategy was employed. Ultimately, data collected from crystals of the selenomethionine-substituted $SleB_{CAT}^{L143M}$ variant permitted modeling of the two virtually identical molecules in the asymmetric unit. Cartoon and solvent accessible surface representations of one molecule are shown in figure 6.1. The completed models made it immediately obvious why molecular replacement had not been successful: While there is a good structural correspondence between the $SleB_{CAT}$ and the structures of other transglycosylases for a core region encompassing helices H1, H2, and H5, the overall structure of $SleB_{CAT}$ is distinct, particularly with respect to the topology of the active site. H1 contains the conserved catalytic residue, which is positioned at one end of the active site cleft by the other two core helices. In addition, the large H2 helix also forms the floor of this cleft. Beyond this minimal structural conservation, a search of the protein data bank for related structures produced only a single protein with more extensive structural homology to $SleB_{CAT}$ belonging to the *E. coli* lytic PG transglycosylase YceG (pdb code 2R1F). The root-mean-square-deviation for the backbones of the 47 overlapping amino acids was 2.5 Å (figure 6.2). $SleB_{CAT}$ has an approximately globular shape, measuring ~46, 36, and 30 Å along its three longest perpendicular axes. Although primarily an α-helical protein, a large portion of the active site is formed by a three-stranded antiparallel β-sheet, also preserved in YceG. The 15 Å-deep active site cleft measures about 27 Å end-to-end; its width varying between 10 and 13Å over the length of the cleft.

Identification of the catalytic glutamate residue of SleB and CwlJ

The active site clefts of PG transglycosylases contain five or more subsites for binding ring-shaped carbohydrate moieties. For instance, the bacteriophage φKZ

enzyme gp144 contains five subsites −4 to +1 and cleavage occurs between the *N*-acetylmuramic acid (NAM) and the NAG moieties bound in sites −1 and +1 (7). The mechanism whereby lytic transglycosylases catalyze the generation of the characteristic 1,6-anhydromuramic acid product is not fully understood. According to the currently held model, the cleavage reaction requires a single glutamate and the *N*-acetyl group of the NAM moiety bound to the −1 subsite (7, 22). Cleavage is initiated by the *N*-acetyl oxygen, which carries out a nucleophilic attack on the C1-atom of the NAM group. The glutamate is believed to stabilize the first transition state of the reaction by donating a proton to the forming hydroxyl group of the departing NAG moiety. The glutamate is also thought to stabilize the second transition state when the C6-hydroxyl of the terminal NAM moiety displaces the *N*-acetyl oxygen at the C1 position to give the final product (figure 6.2).

The low degree of sequence similarity between SleB and other lytic transglycosylases where the catalytic glutamate had already been identified prevented the determination of the catalytic residue of SleB until now. However, the functionally similar enzymes display a higher degree of conservation at the tertiary structure level. Therefore, a least-square superposition of the $SleB_{CAT}$ structure with Slt-70 (25), bacteriophage φKZ lytic transglycosylase gp144 (7) and the to-date unpublished but pdb-deposited structure of a lytic transglycosylase YceG from *E.coli* precisely overlaid residue E151 of SleB with glutamates in the other enzymes. In all cases, this residue is strictly conserved and positioned near one end of the large substrate-binding cleft at the very end of a large helix. The essential role of this positionally conserved glutamate in catalysis has been confirmed for both gp144 and Slt-70 (7, 25). A second glutamate, E-155 in $SleB_{CAT}$, is also conserved among SleB-type enzymes and is positioned in a loop region that marks the edge of the binding cleft, suggesting that this residue might form part of the +1 site required for NAG binding.

We created a version of *sleB* in which the catalytic E-151 was changed to an alanine and tested for SleB function in allowing completion of germination. Spores lacking *cwlJ1* and *sleB* are unable to complete germination and form colonies

(10) (table 6.2). Complementation with a plasmid bearing *sleB* restores function, but the same plasmid bearing *sleB E151A* did not. The ability of a limited application of external lysozyme to rescue these spores' colony-forming ability indicates that their germination defect is in cortex degradation.

In addition to SleB, *B. anthracis* produces a second GSLE specific for the cleavage of cortex PG, CwlJ1 (10). Functionally redundant with SleB, this enzyme possesses no PG-binding domain but its catalytic domain displays 40% sequence identity with SleB. CwlJ1 features a close succession of three glutamate residues in the region that likely contains the catalytic amino acid, making its identification complicated. However, the close similarity of CwlJ1 and SleB sequences allowed the construction of a homology model of CwlJ1, which in turn enabled us to predict that E21 mediates catalysis in this enzyme, whereas E23 and E25 are likely involved in NAG binding in the +1 site.

Conserved and unique features of the PG-binding cleft of $SleB_{CAT}$

$SleB_{CAT}$ displays a number of unique structural features beyond the conserved positions of a core of three helices. The structure most similar to $SleB_{CAT}$ is that of the YceG enzyme from *E. coli*. Therefore, we focused our analysis of the carbohydrate-binding cleft on a comparison of these two proteins. As *E. coli* does not produce muramic-δ-lactam-containing PG, this comparison was particularly helpful with discerning between universally conserved features of the $SleB_{CAT}$ active site and features that are potentially reflective of the unique substrate specificity of SleB. Characteristic of carbohydrate-binding sites, the binding clefts of both enzymes are lined with a number of aromatic amino acids. figure 6.3a shows the superposition of $SleB_{CAT}$ and *E. coli* YceG. figure 6.3c shows the side chains of residues that are structurally conserved. $SleB_{CAT}$ residues F190 and F232 of the *E. coli* enzyme are also included because their side chains occupy a very similar space in the pocket although they are not related at the primary structure level. Similarities in the folds of the two proteins and in the topologies of the binding clefts are particularly pronounced near the catalytic residues. This is consistent with the fact that the substrates of the two enzymes do not differ in the regions that bind to subsites −2, −1, and +1. A

fascinating aspect about GSLEs is the question of how these enzymes achieve specificity for the muramic-δ-lactam moiety that binds in the −3 site. Figure 6.3d is an extension of figure 6.3c to now include the side chains of residues that are present in $SleB_{CAT}$ but not in the *E. coli* enzyme. Intriguingly, these residues are clustered around a relatively small part of the binding pocket. To determine if this region of SleB is responsible for muramic-δ-lactam recognition, we attempted to cocrystallize $SleB_{CAT}$ with a tetrasaccharide muropeptide containing muramic-δ-lactam (Muropeptide Q, Tetrasaccharide-Ala in Ref (10)), which was similar to a SleB product. As this was unsuccessful, we examined the ligand-binding modes in the complexes of the related bacteriophage gp144 enzyme with chitotetraose and of *E. coli* transglycosylase SLT70 in complex with the inhibitor Bulgecin A. In both cases, the ligands are bound in an extended orientation (figure 6.3b). Especially, the relative positions of the two rings bound to the −2 and −1 sites are very similar. In this extended conformation, the ring of the chitotetraose that is bound to the −3 site of gp144 is positioned about 11 Å away from the carboxylate group of the catalytic glutamate. If we assume that SleB binds substrate to subsites −2 and −1 as observed in the other two enzymes, then the approximate position of the unique −3 site can be inferred. This approach suggests that SleB residues F176, P187, R188, W236, and perhaps even S234 form the −3 subsite that is all residues located in structurally unique regions of SleB. Consistent with the hypothesis that F176, P187, and W236 play a role in the binding of muramic-δ-lactam, the three residues are not only conserved among SleB homologues but also in CwlJ where F48, P62, and W114 occupy the corresponding positions in the sequence (Supporting Information File S3). It should be noted that there is a group of closely related SleB-type proteins, typified by *B. subtilis* YkvT, which should not specifically function in the degradation of cortex PG (5), but the above-listed residues are conserved here as well. Therefore, it is possible that these residues are necessary but not sufficient for the exclusive specificity of SleB for muramic-δ-lactam. In addition, the specificity might be fine-tuned by the next tier of amino acids that acts as scaffolding for the active site and ensures proper positioning of backbone and side chain atoms.

The entrance of the $SleB_{CAT}$ substrate binding cleft is shaped by a metal-binding site

A surprising feature of the *SleB CAT* structure was the discovery of a bound metal ion near the putative −4 subsite of the binding cleft. The metal ion is octahedrally coordinated by five backbone carbonyl groups of residues from a loop region that bridges helices H2 and H3 and the side-chain oxygen of asparagine N178. The six ligand atoms are all positioned about 2.4 Å away from the ion. This distance is characteristic for complexes of either Ca^{2+} or Na^{1+} ion, whereas Mg^{2+} was dismissed based on the observation that it forms shorter bonds of around 2.1 Å (8). The addition of the calcium-chelating agent EGTA to a previously described *in vitro* assay (11) had no significant impact on SleB activity. Moreover, modeling a calcium ion into the $SleB_{CAT}$ structure produced negative density in the F_o–F_c map, which indicates that either the site is only partially occupied or that the actual ion has fewer electrons. Finally, when EGTA was included during crystallization, this had no impact on the height of the electron density peak, leading us to conclude that calcium was not bound to this site. Therefore, although a metal analysis showed slightly elevated calcium levels in the protein sample compared to the reference buffer, we concluded that the observed ion is most likely a Na^{+1}. The conspicuous position of the metal binding site at the entrance of the substrate binding pocket is intriguing; however, the biological role of the metal ion remains to be explored.

Discussion

The presented crystal structure of the SleB catalytic domain places this enzyme within the Slt family of (PF01464) lytic transglycosylases. Although other lytic enzymes have been shown to be promiscuous, cleaving both cortex and conventional PG, SleB requires the presence of the muramic-δ-lactam structure for its activity and does not act on regular PG. Therefore, testing our predictions concerning the muramic-δ-lactam-binding pocket may not be easy because mutations in this region could not only cause a loss of specificity for muramic-δ-lactam but also produce an enzyme that is inactive on all substrates. Additional structural studies of SleB–substrate complexes might be able to clarify this unique substrate specificity.

Acknowledgements

Funding for data collected at beamline 29 NSLS is provided by DOE/DER and NIH/NCRR.

References

1. Adams PD, Afonine PV, Bunkoczi G, Chen VB, Davis IW, Echols N, Headd JJ, Hung LW, Kapral GJ, Grosse-Kunstleve RW, McCoy AJ, Moriarty NW, Oeffner R, Read RJ, Richardson DC, Richardson JS, Terwilliger TC, Zwart PH. 2010. PHENIX: a comprehensive Python-based system for macromolecular structure solution. Acta Crystallogr D Biol Crystallogr. 66:213–221.
2. Boland FM, Atrih A, Chirakkal H, Foster SJ, Moir A. 2000. Complete spore-cortex hydrolysis during germination of Bacillus subtilis 168 requires SleB and YpeB. Microbiology. 146:57–64.
3. Brunger AT. 1992. Free R value: a novel statistical quantity for assessing the accuracy of crystal structures. Nature. 355:472–475.
4. Chen Y, Fukuoka S, Makino S. 2000. A novel spore peptidoglycan hydrolase of Bacillus cereus: biochemical characterization and nucleotide sequence of the corresponding gene, sleL. J Bacteriol. 182:1499–1506.
5. Chirakkal H, O'Rourke M, Atrih A, Foster SJ, Moir A. 2002. Analysis of spore cortex lytic enzymes and related proteins in Bacillus subtilisendospore germination. Microbiology. 148:2383–2392.
6. Emsley P, Lohkamp B, Scott WG, Cowtan K. 2010. Features and development of Coot. Acta Crystallogr D Biol Crystallogr. 66:486–501.
7. Fokine A, Miroshnikov KA, Shneider MM, Mesyanzhinov VV, Rossmann MG. 2008. Structure of the bacteriophage phi KZ lytic transglycosylase gp144. J Biol Chem. 283:7242–7250.
8. Harding MM. Small revisions to predicted distances around metal sites in proteins. 2006. Acta Crystallogr D Biol Crystallogr. 62:678–682.
9. Heffron JD, Lambert EA, Sherry N, Popham DL. 2010. Contributions of four cortex lytic enzymes to germination of Bacillus anthracisspores. J Bacteriol. 192:763–770.
10. Heffron JD, Orsburn B, Popham DL. 2009. Roles of germination-specific lytic enzymes CwlJ and SleB in Bacillus anthracis. J Bacteriol. 191:2237–2247.
11. Heffron JD, Sherry N, Popham DL. 2011. In vitro studies of peptidoglycan binding and hydrolysis by the Bacillus anthracis germination-specific lytic enzyme SleB. J Bacteriol. 193:125–131.
12. Hendrickson WA, Horton JR, LeMaster DM. 1990. Selenomethionyl proteins produced for analysis by multiwavelength anomalous diffraction (MAD): a vehicle for direct determination of three-dimensional structure. EMBO J. 9:1665–1672.
13. Ishikawa S, Yamane K, Sekiguchi J. 1998. Regulation and characterization of a newly deduced cell wall hydrolase gene (cwlJ) which affects germination of Bacillus subtilis spores. J Bacteriol. 180:1375–1380.
14. Koshikawa T, Beaman TC, Pankratz HS, Nakashio S, Corner TR, Gerhardt P. 1984. Resistance, germination, and permeability correlates of Bacillus

megaterium spores successively divested of integument layers. J Bacteriol. 159:624–632.
15. Laboratory SD. COLLABORATIVE COMPUTATIONAL PROJECT, NUMBER 4. 1994. The CCP4 Suite: Programs for Protein Crystallography. Acta Cryst D. 50:760–763.
16. Laskowski RA, Macarthur MW, Moss DS, Thornton JM. 1993. Procheck-a program to check the stereochemical quality of protein structures. J Appl Crystallogr. 26:283–291.
17. Moriyama R, Fukuoka H, Miyata S, Kudoh S, Hattori A, Kozuka S, Yasuda Y, Tochikubo K, Makino S. 1999. Expression of a germination-specific amidase, SleB, of Bacilli in the forespore compartment of sporulating cells and its localization on the exterior side of the cortex in dormant spores. J Bacteriol. 181:2373–2378.
18. Moriyama R, Hattori A, Miyata S, Kudoh S, Makino S. 1996. A gene (sleB) encoding a spore cortex-lytic enzyme from Bacillus subtilis and response of the enzyme to L-alanine-mediated germination. J Bacteriol. 178:6059–6063.
19. Moriyama R, Kudoh S, Miyata S, Nonobe S, Hattori A, Makino S. 1996. A germination-specific spore cortex-lytic enzyme from Bacillus cereus spores: cloning and sequencing of the gene and molecular characterization of the enzyme. J Bacteriol. 178:5330–5332.
20. Popham DL, Heffron JD, Lambert EA. 2012. Degradation of spore peptidoglycan during germination. In: Abel-Santos E, editor. Bacterial spores: current research and applications. Norwich, UK: Caister Academic Press.
21. Popham DL, Helin J, Costello CE, Setlow P. 1996. Muramic lactam in peptidoglycan of Bacillus subtilis spores is required for spore outgrowth but not for spore dehydration or heat resistance. Proc Natl Acad Sci USA. 93:15405–15410.
22. Scheurwater E, Reid CW, Clarke AJ. 2008. Lytic transglycosylases: bacterial space-making autolysins. Int J Biochem Cell Biol. 40:586–591.
23. Setlow B, Melly E, Setlow P. 2001. Properties of spores of Bacillus subtilis blocked at an intermediate stage in spore germination. J Bacteriol. 183:4894–4899.
24. Setlow P. 2006. Spores of Bacillus subtilis: their resistance to and killing by radiation, heat and chemicals. J Appl Microbiol. 101:514–525.
25. Thunnissen AM, Rozeboom HJ, Kalk KH, Dijkstra BW. 1995. Structure of the 70-kDa soluble lytic transglycosylase complexed with bulgecin A. Implications for the enzymatic mechanism. Biochemistry. 34:12729–12737.
26. Warth AD, Strominger JL. 1969. Structure of the peptidoglycan of bacterial spores: occurrence of the lactam of muramic acid. Proc Natl Acad Sci USA. 64:528–535.

Table 6.1 Data Collection and Refinement Statistics for the SeMet-SleB$_{CAT}$ ^{L143M} Crystal Structure

(A) Data collection statistics			
Space group		$P22_12_1$	
molecules/asymmetric unit		2	
Cell parameters (Å)		a = 53.9, b = 64.5, c = 84.0	
Wavelength (Å)	0.9792	0.9611	0.9794
Resolution (Å)	30.34–1.9 (1.9–2.0)	30–1.9 (1.9–2.0)	30–2.0 (2.0–2.11)
Completeness (%) (last shell)[a]	99.3 (100)	99.2 (98.3)	99.1 (98.6)
Redundancy	12.8 (13.9)	12.5 (12.1)	11.9 (11.5)
I/σ	19.4 (5.0)	23.3 (4.6)	22.5 (4.6)
R_{merge} (%)[b]	9.1 (51.5)	6.8 (55.3)	7.2 (54.1)
No. of unique reflections	23,743	23,899	23,892
No. of measured reflections	849,540	1,025,839	1,079,414
(B) Refinement statistics			
Resolution range (Å)		33.22–1.91	
R (%)[c]/ R_{free} (%)[d]		20.51/24.87	
rms bonds (Å)/ rms angles (°)		0.02/2	
Number of protein atoms		1896	
Number of water atoms		319	
Overall mean B-factor value (Å^2)		13.95	
Wilson plot B-value		13.45	
Ramachandran analysis (%)			
Most favored		95	
Allowed		5	
Disallowed		0	

a. The values in parentheses relate to the highest resolution shell.

b. $R_{merge} = \Sigma |I - \langle I \rangle| / \Sigma I$, where I is the observed intensity and ‹I› is the average intensity obtained from multiple observations of symmetry-related reflections after the rejection of significant outliers.

c. $R = \Sigma ||Fo| - |Fc|| / \Sigma |Fo|$, where F_o and F_c are the observed and calculated structure factors, respectively.

d. R_{free} defined by Brunger (3).

Table 6.2. Failure of *sleBE151A* to complement for germination function

cfu/ml/OD600[a]

Strain	Genotype	-lysozyme	+lysozyme
DPBA61	*cwlJ1*	$2x10^8$	$8x10^7$
DPBA74	*cwlJ1 sleB*	$2x10^5$	$4x10^7$
DPBA145	*cwlJ1 sleB*/pDPV346 *sleB*	$1x10^8$	$6x10^7$
DPBA151	*cwlJ1 sleB*/pDPV430 $sleB_{E151A}$	$2x10^5$	$4x10^7$

a- Spores were plated onto BHI medium with and without 1 μg/ml of lysozyme.

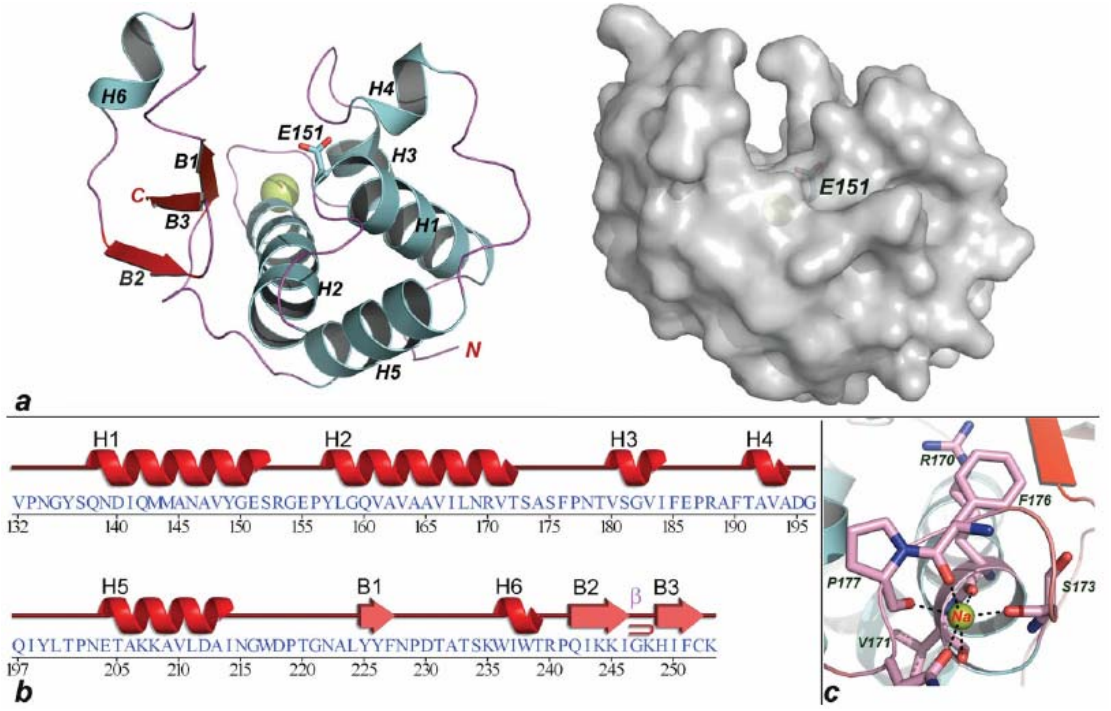

Figure 6.1 Crystal structure of $SleB_{CAT}$. (a) Cartoon and surface depictions of the $SleB_{CAT}$ structure. The sodium ion is shown as a yellow sphere and the side chain of the catalytic glutamate is shown in the stick format. (b) Summary of correlation between $SleB_{CAT}$ sequence and secondary structure topology. (c) Schematic presentation of the metal-binding site formed by residues from a loop region encompassing amino acids 170–178.

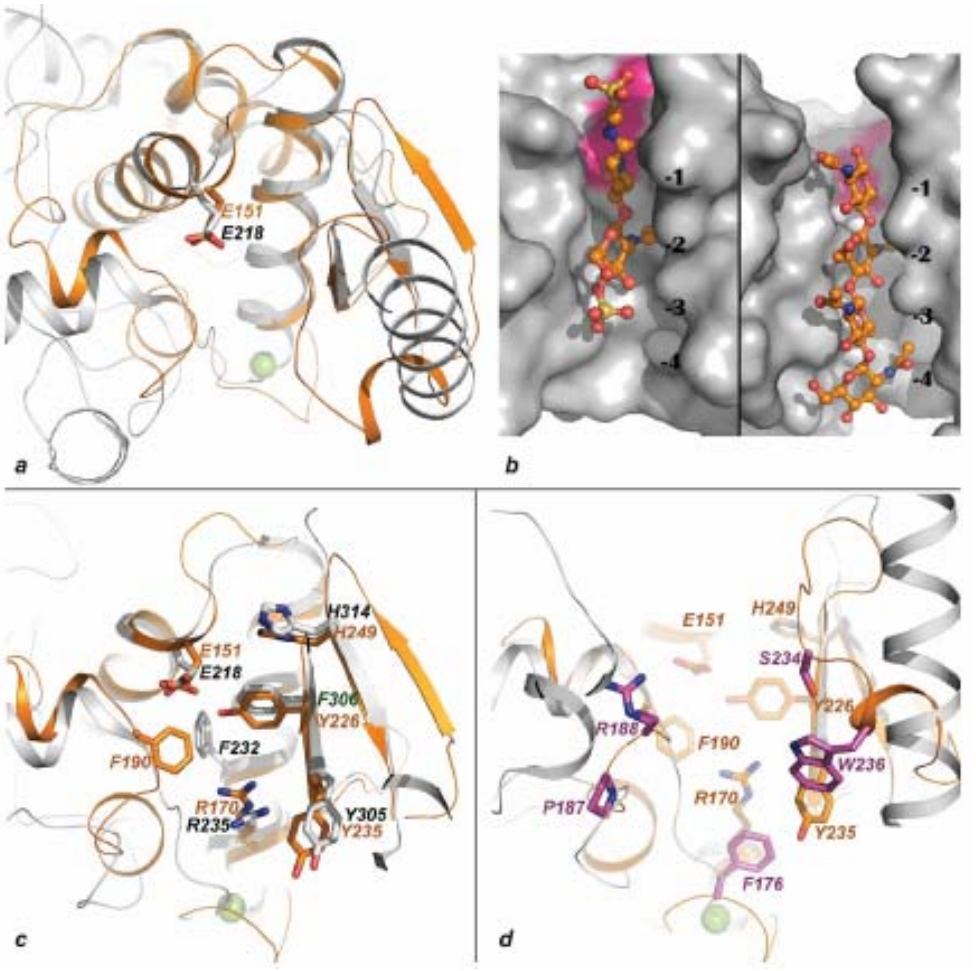

Figure 6.2 Mapping of conserved and unique features of the SleB$_{CAT}$-active site. (a) Superposition of SleB (orange) and YceG (gray, pdb code 2R1F). (b) Close-up view of the Slt-70-bulgecin (left) and gp144-chitotetraose (right) complexes showing the extended binding modes of the ligands. (c) Superposition of SleB (orange) and YceG (gray) backbones showing the side chains of structurally conserved residues from both protein. (d) Superposition of SleB (orange) and YceG (gray) showing the side chains of SleB residues that are structurally conserved with YceG in orange and those that are unique to SleB in magenta.